APPLYING MATHEMATICAL MODELS OF HUMAN CIRCADIAN RHYTHMS FOR EXPERIMENTAL DESIGN AND DATA ANALYSIS

by

Nora E. H. Stack

A thesis submitted to the Faculty and the Board of Trustees of the Colorado School of Mines in partial fulfillment of the requirements for the degree of Doctor of Philosophy (Computational and Applied Mathematics).

Golden, Colorado

Date _____

Signed: _____
Nora E. H. Stack

Signed: _____
Dr. Cecilia Diniz Behn
Thesis Advisor

Golden, Colorado

Date _____

Signed: _____
Dr. Gregory Fasshauer
Professor and Head
Department of Applied Mathematics and Statistics

ABSTRACT

The adult human circadian pacemaker has an intrinsic period just over 24 h that entrains to a 24 h day by environmental cues such as light, eating, and exercise. Dynamic phenomenological mathematical models of the human circadian pacemaker have been developed to simulate the pacemaker's response to light. These models have been widely used for applications such as minimizing jet lag and optimizing experimental protocol design. This thesis is focused on applying mathematical models to account for the interindividual differences that are inherently present in humans and therefore also in circadian data. We optimized an experimental protocol to ensure robust performance across individuals with varying intrinsic circadian periods. Next, we developed novel MCMC-based methodology to use phase shift data to determine the mean intrinsic circadian period of a group of study participants. Finally, we investigated parameter sensitivity of a circadian pacemaker model and applied this knowledge to an adolescent data set where distinct behavior within the cohort was observed. This thesis highlights the utility of human circadian pacemaker models in a variety of contexts and establishes new insights into properties of these models and their influence on behavior.

TABLE OF CONTENTS

LIST OF FIGURES

LIST OF TABLES

LIST OF SYMBOLS

General Nomenclature

Time dependent light input . . . . . $I(t)$

Drive rate, rate of activation induced by I . . . . . $\alpha(I)$

Percentage of elements in their used state . . . . . n

Output Drive . . . . . $\hat{B}$

Sensitivity Modulation . . . . . B

Rate constant . . . . . α_0

Power constant . . . . . p

Light constant . . . . . I_0

Backwards regeneration constant . . . . . β

Rate of the cumulative drive . . . . . G

Sensitivity modulation constant . . . . . s_1

Sensitivity modulation constant . . . . . s_2

Oscillator stiffness . . . . . μ

Intrinsic oscillator period . . . . . τ

Constant for the incorporation of Aschoff's rule . . . . . k

Constant relating light intensity to brightness C

Modulation index . . . . . m

Chapters 3, 4, and 5

Endogenous body temperature X

Complementary variable . . . . . X_c

Chapter 2

Endogenous circadian rhythm X

Complementary variable . . . . . X_c

LIST OF ABBREVIATIONS

suprachiasmatic nucleus . . . . . SCN

forced desynchrony . . . . . FD

phase response curve . . . . . PRC

light-dark (light:dark) . . . . . LD

Markov Chain Monte Carlo . . . . . MCMC

quantity of interest . . . . . QoI

minimum core body temperature . . . . . CBT_{min}

constant routine . . . . . CR

ACKNOWLEDGMENTS

I would like to express my gratitude to my advisor Cecilia Diniz Behn. Thank you for believing in me and teaching me about so much more than just math. I would also like to thank the faculty and students of the Applied Math and Statistics Department for their support. Finally, I would like to thank my friends and family who have always encouraged and supported me.

I would also like to thank our collaborators Victoria Booth, Stephanie Crowley, Mary Carskadon, David Barker, Monique LeBourgeois, Jamie Zeitzer, Charles Czeisler, and Paul Diaz. This work was supported by NSF DMS 1412571 (CDB), Childrens Hospital Colorado/-Colorado School of Mines Collaborative Pilot Award (CDB and Dr. Stacey Simon, Co-PIs), and NIH ROIHD087707 (ML).

For my family.

CHAPTER 1

INTRODUCTION

1.1 The Human Circadian Rhythm

Sleep is a complex process consisting of interactions between neuronal populations, the homeostatic drive, and the circadian rhythm which has an estimated intrinsic period of $\sim$ 24.2 h in adults [1–4]. Each of these processes has its own unique job in the human body. The Suprachiasmatic Nucleus (SCN) is the master circadian pacemaker [5], consisting of a group of $\sim$20,000 neurons located in the hypothalamus [5, 6]. Many physiological processes are under circadian regulation. Measures such as core body temperature and melatonin secretion can be used as experimental measures of the circadian rhythm [5]. Additionally, circadian rhythms influence other bodily functions such as eating, digestion, and hormone regulations [6].

The neurons in the SCN respond to environmental cues like light and exercise to entrain the human sleep/wake schedule to 24 hours [6, 7]. Specifically, the SCN receives light information through the eye, which then activates neurons that convert photons into electrical signals that then travel to the SCN [8]. In particular, light affects circadian phase and amplitude [9]. Experiencing light at different times during the day can produce phase advances or delays and alter amplitude. The properties and behavior of the human circadian pacemaker influence many aspects of life such as jet lag, shift work, school start times, and light therapy treatments.

1.2 Mathematical Models

1.2.1 Mathematical Models of Human Circadian Rhythms

There are many ways to model the human circadian rhythm or drive such as a static phenomenological model, SCN nueron models, molecular/protein models, and dynamic circadian pacemaker models [3, 10–17]. Multiple types of models of the circadian drive are used

for various types of applications because of their differences in temporal and spatial scales.

Static phenomenological models were developed based on observed circadian behavior that do not incorporate the light as a function of time. For examples the simpliest form of these models is the Two Process Model which represents the circadian rhythm as a sine wave. The Two Process model contains Process S and Process C [10, 18]. Process S describes homeostatic pressure, sleep need, while Process C is the circadian drive. Process S exponentially increases during wake until it reaches an upper threshold and exponentially decreases during sleep until it reaches a lower threshold. The oscillating thresholds, often described with sine waves, are Process C [10, 18]. These types of models incorporate different features of sleep-wake dynamics and circadian oscillation but are not able to capture the behavior under variable light conditions.

Another approach to modeling the circadian rhythm is to focus on SCN period 1 (per1) neurons. In 2009, Belle and colleagues derived a model based on data and theory that simulated the behavior of the firing rate of SCN neurons that contain the per1 gene [19]. They did this by implementing a Hodgkin-Huxley type model [20] to simulate the electrophysiological behavior of SCN neurons. In 2013, Diekman and colleagues extended the work by Belle and colleagues by incorporating intracellular calcium dynamics, L-type calcium current, and K_{ca} current [21]. Additionally, they incorporated a model of gene regulation based on the Goodwin oscillator [22] to investigate the dynamics between the intracellular clock and hyperexcitation.

Another category of models of the circadian rhythm is molecular/protein models. These models consider the circadian clock within a cell in the SCN and the interactions between genes and proteins within that cell. Specifically, the interactions between period proteins (PER) and other proteins or molecules give rise to a negative feedback loop therefore producing oscillation [13, 23]. An extension of this type of model was presented by Hannay in his PhD dissertation [24]. Hannay and colleagues derived a macroscopic model of the human circadian pacemaker by starting from a model which described the phase of a clock cell in

the SCN and expanded this to a model of weakly coupled system of clock neurons and to a two population model of neurons in the ventral and dorsal phase clusters. These models produced similar results to a dynamic phenomenological circadian pacemaker model by Forger and colleagues [14]. This work suggests that although the Forger model is a phenomenological model, it produces qualitatively similar results when compared to models derived from neuronal behavior and interactions.

1.2.2 Dynamic Phenomenological Circadian Pacemaker Models

The models implemented in this thesis can be characterized as dynamic phenomenological circadian pacemaker models based on modified van der Pol oscillators. These models incorporate parameters derived from physical experiments as well as observed circadian behavior.

This type of model was first proposed by Kronauer and colleagues in 1982 [25]; the model simulated the relationship between core body temperature and sleep-wake rhythm and incorporated the effect of a periodic zeitgeber, an environmental cue that synchronizes the circadian rhythm (e.g., light), on the circadian system. Since then, many different iterations of a modified van der Pol oscillator that incorporates the effects of a zeitgeber (light) have been developed.

In 1990 [26], 1996 [27], and 1998 [16] models were developed to incorporate the effect of a time dependent light function. In these models, the drive of light onto the circadian pacemaker was represented by a single equation. This type of model enabled researchers to incorporate different light schedules into their simulations. For example, in the model by Klerman and colleagues the human circadian pacemaker is simulated by a second order modified van der Pol oscillator where one variable representsendogenous circadian rhythm and the other is a complementary variable [27]. For this model light enters the system in a drive in a brightness function that is incorporated into the modified van der Pol oscillator. This model enabled researchers to implement various light schedules but did not account for certain circadian features found in humans such as Aschoff's rule which states that period

is shortened with increasing light intensities in diurnal organisms [28].

From Kronauer's 1990 model, several variations have been established. To more accurately capture human photonic sensitivity, in 1999 Kronauer and colleagues developed a model that incorporated a Process L (for light processing) and a Process P (for the pacemaker) [17]. In this model, light enters the system in Process L and is ultimately converted with a sensitivity modulation function that is passed to Process P. Within Process L, two processes are present, a prompt response system and a maintained drive system. The prompt response system produces large prompt response values when light is turned on which quickly decays over time. The maintained drive system shows no prompt response to light. These systems are similar to behavior seen in the action of light on photopigments of retinal photoreceptors (prompt response) and the postsynaptic ionic channels opened by neurotransmitter molecules (maintained drive) [17]. Process P is a modified van der Pol oscillator that does not affect Process L. In Process P, the second-order dynamical system represents endogenous core body temperature and plasma melatonin rhythm. Process P also incorporates Aschoff's rule [28].

Another of these variations is a model by Forger and colleagues which we will refer to as the Forger model [14]. This model incorporates Process L and Process P but reduces the order of the equations in Process P from degree seven, as in Jewett et al. and Kronauer et al., to degree three [15, 17]. Although the order of the equations is lessened, simulations of two human experimental studies with the Forger model were as accurate, if not more accurate, than the Jewett et al. and Kronauer et al. models when compared to data from those studies. In the Forger model, the variables in Process P represent endogenous core body temperature and an associated complementary variable.

In this thesis, the models by Forger and colleagues [14] and Klerman and colleagues [27] will be discussed in detail. These models have been used to designexperimental laboratory protocols [27] and investigate jet lag [29].

1.3 Experimental Protocols

1.3.1 Extended Day and Ultradian Forced Desynchrony Protocols

To estimate certain circadian features, it is necessary to desynchronize the circadian and rest-activity cycles. Initially, assessments of intrinsic periods were completed in temporal isolation [30]. Subjects self-selected light, which therefore influenced the circadian clock that affected their assessments. To estimate circadian features accurately and assess intrinsic period, a class of forced desynchony (FD) protocols was developed [4]. These protocols are primarily used to estimate intrinsic circadian period.

The human intrinsic circadian period is an important aspect of the circadian system. Estimates of intrinsic periods in healthy adults have found that the intrinsic period is approximately 24.2 h [4]. Additionally, it has been found that the intrinsic circadian period may vary with age, sex, and race/ethnicity [31–33]. There are still many unknowns about the circadian period, particularly about the evolution (or lack thereof) of the circadian period over the course of the human lifetime. There have been some estimates of intrinsic periods in adolescents [34, 35] but some demographic groups cannot participate in FD protocols (e.g., children).

Historically, extended day forced desynchony protocols were implemented to estimate the intrinsic circadian period. These protocols require study participants to experience a light-dark (LD) cycle that is longer than the 24 h day and outside of the range of entrainment. A 28 h LD cycle is typically implemented for extended day FD protocols. The 28 h extended day FD protocol has a LD cycle with 18.66 h of light and 9.33 h of darkness. Therefore, extended day FD protocols distribute light across both the 24 h day as well as the circadian day. In 1996, Klerman and colleagues used a mathematical model of the human circadian pacemaker to optimize the implementation of these protocols for experimental studies [27]. Two of their main conclusions about extended day FD protocols were that the light intensities during the protocol should be dim (10 lux) and that the in-lab portion of the protocol needed to be at least 20 days long. This work led to protocols that produced more accurate estimates of

intrinsic period.

Recently, ultradian FD protocols have become popular. These protocols implement a short LD cycle to which humans cannot entrain. For example, protocols can be ultrashort 1 h cycles with 40 m of light and a 20 m of darkness [36] or a 4 h LD cycle with 2.5 h of light and 1.5 h of darkness have been completed [37]. It is thought that these protocols require less time in the lab than the extended day FD protocols but no formal analysis or optimization of these methods has been completed prior to the work presented in this thesis. Additionally, ultradian FD protocols have been used to generate phase response curves [37, 38].

Both the extended day and ultradian FD protocols are useful protocols to gain information about intrinsic periods as well as other circadian features such as phase response curves and sleep propensity.

1.3.2 Illuminance-Response Curves

The effects of light on the circadian system vary with time of day [39, 40], light intensity [41–43], duration [39, 44], and wavelength [45]. Illuminance-response curves are used to characterize the response of the circadian system to different light intensities [41–43]. These protocols are timed so that each participant receives a specific light intensity for 6.5 h in the early biological night [41, 43] or 5 h of light on three consecutive days in the late biological night [42]. The light intensities vary from very dim to very bright.

In 2000, Zeitzer and colleagues found that the human circadian pacemaker was much more sensitive to light during the early biological night than previously thought [41]. They used fit logistic curves to melatonin phase shift data and melatonin suppression data. These fits predicted that the half-maximal phase-delaying response was ∼50-130 lux which is in the range of ambient room lighting. This work provided insights into the effects of light in the early biological night.

Next, Zeitzer and colleagues investigated the effects of varying light intensities during the late biological night [42]. Logistic curves were fit to melatonin phase shift and melatonin suppression data separately. In this study they found that the half-maximum phase-advancing

response was ∼50-160 lux. Thus the circadian system is highly sensitive to light during the late biological night as well as the early biological night.

In 2007, Duffy and colleagues investigated the effects of evening light in older adults ($\geq$ 65 years old) [43]. The study participants in the previous two studies were healthy adults so results from this study were compared to the illuminance repsonse curves of healthy adults. They found that older adults were less sensitive to moderate light intensities than the younger adults in the Zeitzer study [41].

These types of studies seek to characterize the response of the circadian system to different light intensities, varying from dim light to very bright lights. These studies have shown that the circadian pacemaker is much more sensitive to light than previously thought and that there are changes to this sensitivity that occur with aging.

1.3.3 Phase Response Curves (PRCs)

Phase Response Curves (PRCs) characterize the effect of bright light on the circadian system at different times of day. Contrary to the illuminance-response curves, each participant in a PRC study receives the same light intensity but at different times throughout the circadian day. PRC studies have used various light intensities, durations, cycles, and types of light to investigate properties of the pacemaker [39, 40, 44, 46–48]. Human phase response curves protocols have also been designed to assess the effect of melatonin on the circadian system [49–51]. Most PRC protocols utilize Constant Routines (CRs), long periods in dim light, to assess markers of circadian phase (e.g., core body temperature, plasma melatonin) but some researchers have used mathematical methods to unmask the endogenous rhythm. Phase shifts are computed from the difference between these circadian markers assessed prior to the exposure to bright light and after exposure to bring light. For these protocols, participants are given doses of melatonin. These following studies discussed are PRCs to light conducted with healthy adult participants.

In 1989, Czeisler and colleagues conducted a three cycle PRC study with 5 h of bright light (7000 to 12000 lux) and compared their results to fourteen control trials without a

bright light stimulus [46]. Body temperature, plasma cortisol, and urine output were used as a marker of circadian phase. They discovered that the effect of light on the circadian pacemaker varied depending on the circadian phase at which the stimulus occurred.

Minors and colleagues developed a human PRC protocol to a single 3 h bright light pulse (9000 lux) and a PRC protocol over 3 consecutive cycles of 3 h of bright light in 1991 [44]. Phase shifts were assessed using body temperature. Unlike all of the other PRC protocols discussed in this section, these experiments did not implement a CR and instead used two mathematical methods to unmask the endogenous rhythm. They found that larger phase shifts were produced with three cycles than one cycle.

In 1994, Jewett and colleagues conducted studies to produce one and three cycle PRCs [39]. Bright light exposure was 5 h (three cycle) and 4.0 to 6.2 h (one cycle) at 7000-12000 lux. Core body temperature was used to determine phase shifts. Additionally, they conducted a two cycle protocol to assess changes in amplitude. They concluded that the human circadian system was not a phase-only oscillator, meaning that both phase and amplitude must be considered to accurately characterize the human response to light.

In 2003, Khlasa and colleagues conducted a PRC study with 6.7 h of bright light (10,000 lux at fixed gaze alternated with 5000-9000 lux free gaze every 6 minutes) [40]. Core body temperature, plasma melatonin, and salivary melatonin samples were collected. Their study produced a PRC of 43 participants derived in highly controlled conditions.

In 2012, St Hilaire and colleagues devised a PRC protocol with 1 h of bright white light ($\sim$ 8000 lux) [47]. Phase shifts were measured from plasma melatonin. They found that 1 h of bright white light produced phase shifts of up to $\sim$2 h. Although their bright light duration was only 15% of the light duration used by Khalsa and colleagues, their response was 40% of that from the 6.7 h protocol.

In 2012, Rüger and colleagues created a PRC study to incorporate exposure to short-wavelength blue light [48]. The participants were exposed to 6.5 h of blue light. Compared to the PRC derived from 6.7 h of bright white light by Khalsa and colleagues, this PRC

achieved ∼75% of their resetting response.

PRCs characterize the response of the circadian system over the circadian day under many different conditions. Studies have varied light intensity, light duration, cycle number, and wavelength. Understanding the circadian pacemaker's response to light has implications for applications from jet lag to light therapy.

1.4 Structure of Thesis

In this thesis, the underlying theme is the inherent interindividual differences present in humans and therefore in circadian data. We utilized knowledge about human physiology and circadian data to optimize an experimental laboratory protocol design, learn estimate average group intrinsic period from existing phase shift data using Markov chain Monte Carlo methods, and examine parameter sensitivity within a mathematical model of the adult human circadian pacemaker to better understand distinct adolescent behavior. The numerics for all of the projects were implemented in MATLAB.

Historically, estimates of the human intrinsic period have been estimated using protocols called extended day forced desynchrony protocols that have a long light:dark cycle (e.g. 28 h) and need to be implemented for at least 20 day in the lab. Recently, so-called ultradian forced desynchrony protocols have become popular. These protocols have short light:dark cycles (e.g. 4 h) and are implemented for only a few days in the lab. In chapter 2 we will discuss the optimization of ultradian forced desynchrony protocols to accurately estimate intrinsic periods over a range of known intrinsic periods. We investigated light:dark cycle duration, light intensity (lux), phase onset, and study duration. This work provided recommendations for implementing ultradian forced desynchrony protocols to minimize error in estimating intrinsic period and provided estimates of error for existing ultradian studies.

In Chapter 3, to estimate the group intrinsic period of a a study cohort, we implemented a Markov chain Monte Carlo (MCMC) algorithm on synthetic and experimental illuminance-response curve data. Synthetic phase shift data was simulated from known intrinsic period values; this enabled comparisons between known intrinsic periods and estimated parameter

values from MCMC. Next, we applied this methodology to experimental illuminance-response curve data from 23 healthy adults. This work established a framework for estimating average group intrinsic period using illuminance-response curve data.

Parameter sensitivity of Phase Response Curves (PRCs) and potential parameters that simulate adolescent behavior from an experimental protocol are investigated in Chapter 4. The sensitivity of PRC metrics to parameters was investigated by varying parameters by 10% and monitoring the resulting changes to the metrics. These insights were then applied to adolescent data. These data were clustered using k-means clustering into groups that had quantitatively different behavior. The parameters identified in the parameter sensitivity analysis were then used to determine parameter combinations that simulated different adolescent behavior from the data.

Finally, in Chapter 5 a brief summary of the projects is presented as well as some future extensions of the projects previously presented.

CHAPTER 2

A MODEL-BASED APPROACH TO OPTIMIZING ULTRADIAN FORCED DESYNCHRONY PROTOCOLS FOR HUMAN CIRCADIAN RESEARCH

Published in *Journal of Biological Rhythms*, Volume: 32 issue: 5, pages: 485-498.

 DOI: 10.1177/0748730417730488. [52].

Nora Stack, MS,[*] David Barker, PhD,[†] Mary Carskadon, PhD,[†,‡] and Cecilia Diniz Behn, PhD[*,§,] [1]

[*]Department of Applied Mathematics and Statistics, Colorado School of Mines, Golden, CO, USA, [†]Sleep for Science Research Laboratory, Department of Psychiatry and Human Behavior, Alpert Medical School of Brown University, Providence, RI, USA, [‡]Centre for Sleep Research, University of South Australia, Adelaide, South Australia, Australia, and [§]Division of Endocrinology, Department of Pediatrics, University of Colorado Anschutz Medical Campus, Aurora, CO, USA

2.1 Abstract

The human circadian system regulates internal 24h rhythmicity and plays an important role in many aspects of human health. To investigate properties of the human circadian pacemaker such as intrinsic period and light sensitivity, experimental researchers have developed forced desynchrony (FD) protocols in which manipulations of the light-dark (LD) cycle are used to desynchronize the intrinsic circadian rhythm from the rest- activity cycle. FD protocols have typically been based on exposure to long LD cycles, but recently, ultradian FD protocols with short LD cycles have been proposed as a new methodology for assessing intrinsic circadian period. However, the effects of ultradian FD protocol design, including

[1]To whom all correspondence should be addressed: Cecilia Diniz Behn, Department of Applied Mathematics & Statistics, Colorado School of Mines, 1015 14th Street, Golden, CO 80401, USA; e-mail: cdinizbe@mines.edu.

light intensity or study duration, on estimates of intrinsic circadian period have not, to our knowledge, been systematically studied. To address this gap, we applied a light-sensitive, dynamic mathematical model of the human circadian pacemaker to simulate ultradian FD protocols and analyze the effects of protocol design on estimates of intrinsic circadian period. We found that optimal estimates were obtained using protocols with low light intensities, at least 10 days of exposure to ultradian cycling, and an LD cycle duration that produced uniform light exposure across all circadian phases. Our results establish a theoretical framework for ultradian FD protocols that can be used to provide insights into data obtained under existing protocols and to optimize protocols for future experiments.

2.2 Introduction

The human circadian pacemaker in the suprachiasmatic nucleus (SCN) maintains an ∼24-h intrinsic rhythm, entrains to the exactly 24-h day based on light and other environmental inputs, and coordinates circadian rhythms throughout the body [4, 53]. The intrinsic period (τ) has been estimated to range from 23.8 to 25h in healthy, adult humans [54], and τ may vary on the basis of sex, age, and race/ethnicity [31–33, 55]. Variability in τ may underlie differences in individual responses to both normal, entrained conditions and to challenges to the circadian system, and there is an increasing appreciation for the role that circadian rhythms play in many different aspects of health, including metabolism, cardiovascular function, and immune function [36, 56–61]. Furthermore, interventions that consider and/or target the circadian system have been developed for treatment in acute situations such as intensive care units [62, 63] and in everyday life. These interventions have included direct environmental modifications, such as changes to ambient lighting or light therapy, as well as policy changes that indirectly impact the the circadian system, e.g., delaying school start times for adolescents [64, 65]. To optimally exploit circadian biology to improve health outcomes, improved understanding of the human circadian system in individuals, groups, and disease states is vital.

Typically, experiments to assess features of human circadian rhythms are very time and resource intensive, often requiring participants to stay in highly controlled laboratory conditions for extended periods of time. Since light is a major influence on the circadian clock, consideration of light conditions is essential for circadian research. To investigate properties of the human circadian clock such as intrinsic period (τ) and light sensitivity, experimental researchers have developed forced desynchrony (FD) protocols in which manipulations of the light-dark (LD) cycle are used to desynchronize the intrinsic circadian rhythm from the rest-activity cycle. To achieve this desynchronization, at least three different experimental paradigms have been described: temporal isolation, extended day FD, and ultradian FD [37]. In temporal isolation conditions, such as the early circadian experiments conducted in caves or bunkers [30, 66], participants were isolated from external time cues, but they were able to self-select the timing of wake and sleep, thereby influencing the timing of their exposure to light. By contrast, under extended day or ultradian FD protocols, participants are scheduled to regular LD cycles with periods longer or shorter, respectively, than the range of entrainment of the intrinsic pacemaker [4, 37, 54, 67]. Previous work has established that the human circadian pacemaker cannot entrain to LD cycles shorter than 21h or longer than 26h, although the exact relationship between the circadian pacemaker and its limits of entrainment depend on factors such as the intrinsic period of the oscillator and light intensity during light exposure [27, 68–70].

Extended day FD protocols, typically involving a 28h LD cycle, represent a well-established methodology for conducting controlled laboratory studies of the human circadian system [4]. These protocols have been applied to probe both the properties of the system and the underlying circadian rhythmicity of measures such as the propensity for sleep [4, 32, 34, 54, 55, 69, 71, 72]. To optimize the design of extended day FD protocols, Klerman and colleagues (1996) applied a mathematical model of the human circadian pacemaker to simulate protocols under different experimental conditions including variable light intensities and study durations. Their results determined optimal conditions for estimating the intrinsic period

using extended day FD protocols and established a theoretical framework for interpretation of data collected using these methods.

Desychronization of sleep and circadian rhythms can also be induced by exposure to LD cycles with periods shorter than 21h. Historically, 20h LD cycles have been used [67, 73], but recently, investigators have developed ultradian FD protocols that use very short (typically 1.5-5 h) LD cycles [31, 33, 36, 37, 51, 74–76]. These ultradian FD protocols are less resource intensive and require less time in the lab compared with extended FD protocols. However, to our knowledge, the effects of protocol design on experimental outcomes such as estimated intrinsic periods have not been formally quantified in ultradian FD protocols. For example, it is not known if estimates of intrinsic period obtained under ultradian FD protocols will depend on light intensity or study duration [37]. Furthermore, some ultradian FD protocols, such as those with a 4h LD cycle, have not been designed to distribute sleep/wake behavior and/or light exposure equally across all circadian phases. This non-uniformity may make such protocols more susceptible to protocol effects compared to extended day FD protocols.

Although FD protocols could be optimized through systematic experimentation, this approach would be extremely resource-intensive. Alternatively, we used a light-sensitive, dynamic mathematical model of the human circadian pacemaker to simulate ultradian FD protocols and analyze protocol effects on estimates of intrinsic circadian period obtained from simulated data. We considered a range of light intensities, LD periods, and study durations to optimize protocol design for assessing physiologically relevant intrinsic circadian periods. Our results establish a theoretical framework for ultradian FD protocols that can be used to provide insights into data obtained under existing protocols and to optimize protocols for future experiments.

2.3 Methods

2.3.1 Human circadian pacemaker model

To model the human circadian pacemaker, we implemented an established dynamic modeling formalism based on a modified van der Pol oscillator [26, 27]. This model captures key

attributes of the human circadian pacemaker: it is intrinsically oscillatory, and it can be entrained by a periodic light stimulus. Furthermore, the model has been calibrated to human data sets to appropriately represent the pacemakers dynamic response to light of varying durations and intensities, and it was used to investigate features of extended day FD protocols (PRCs; [27]).

The human circadian pacemaker model is governed by the following equations [27]:

$$\frac{12}{\pi}X' = X_c + 0.13\left[X - \frac{4}{3}\frac{X^3}{X_0^2}\right] + B \tag{2.1}$$

$$\frac{12}{\pi}X_c = -\left[\frac{24}{\tau}\right]^2 X + \frac{BX_c}{3} \tag{2.2}$$

where X represents the endogenous circadian rhythm (maintaining a fixed phase relationship with core body temperature, a marker of the circadian clock) and X_c is a recovery variable. The term $B = (1 - mX)CI^{1/3}$ represents sensitivity modulation of light input to the oscillator. The model has 5 parameters: $C = 0.018$ $1/(\text{lux}^{1/3})$, $m = 1/3$, $X_0 = 0.832$, light intensity I (lux), and intrinsic clock period τ (h). The parameters I and τ are varied to represent protocol-dependent light conditions and individual physiology, respectively. To investigate model dependence in our simulation results, we also simulated ultradian FD protocols using an alternative model of the human circadian pacemaker that incorporates light preprocessing [14]. Additional details regarding the alternative model are available in the Supplementary Online Material.

Model equations were implemented in MATLAB (Mathworks, Natick, MA) and solved numerically using the built-in MATLAB solver **ode45** with a relative error tolerance of 1e-9 and an absolute error tolerance of 1e-10. For the variable X, local minima that occurred 20 to 30 h apart were used to determine the phase of the oscillator and to compute phase shifts. The built-in MATLAB Signal Processing Toolbox function **findpeaks** was used to detect minima of X.

2.3.2 Simulating ultradian LD protocols and estimating intrinsic circadian period

We systematically investigated the effects of LD period, light intensity, intrinsic period, and study length on the observed period, τ_{obs}, where τ_{obs} is the estimate of τ obtained from the simulated ultradian FD protocol. The structure of the simulated protocols was based on the structure of published ultradian LD protocols [37, 51] and included an at-home schedule and an in-lab schedule consisting of an adaptation night, baseline night, phase assessment, and period of ultradian LD cycling (Figure 2.1). All simulated protocols began with a 14-d at-home schedule in which light intensity was set to 0 lux from 2200 to 0800 h and 150 lux at all other times. The adaptation night and baseline night represent a participants transition to the in-lab setting. During this transition, the same timing of LD exposure was maintained, but light intensity during the light period was reduced to 30 lux. During the phase assessment, dim light conditions of 10 lux were imposed from 1800 to 0000 h and 0500 to 1200 h with a period of 0 lux from 0000 to 0500 h. Following the period of phase assessment, a schedule of 4h LD cycling was initiated and continued for at least 33 d. To assess the sensitivity to phase of ultradian LD cycle onset, we simulated protocols with LD cycling initiated at the standard phase (at 1200 h following the phase assessment), 1h before the standard phase, and 1h after the standard phase.

We simulated ultradian LD cycling involving 4, 5, or 7h LD cycles. The proportion of light and dark in each cycle was held constant across protocols, resulting in 2.5 h L: 1.5 h D; 3.125 h L: 1.875 h D; and 4.375 h L: 2.625 h D for the 4, 5, and 7h LD cycles, respectively. These LD cycle durations were chosen to represent published ultradian FD protocols [37, 51] as well as exploratory protocols that used relatively short LD periods, maintained the same proportion of light and dark as the 4h LD cycle, and involved cycle durations that did not evenly divide the 24h period of the entrained oscillator. The number of ultradian cycles per 24h day was determined by the duration of the LD cycle.

We simulated protocols with light intensities of 10, 50, 100, 150, 500, 750, and 1000 lux; intrinsic periods from 23.8 to 25.0 h; and study durations of 3 to 33 days. Light intensities represent a range typically encountered in daily life, and specific intensities were chosen for comparison to previous work [27] and published ultradian FD protocols [37, 51]. Intrinsic periods were selected to represent the physiological range of τ reported for adult humans [54]. Study duration describes the number of 24h days of ultradian LD cycle exposure measured from 1200 to 1200 h following the phase assessment; study durations were chosen for comparison with published ultradian and extended day FD protocols [27, 37, 51]. In addition, we simulated several protocols for study durations of 100 days to verify that increasing study duration beyond 33 days did not affect estimates of intrinsic circadian period. To determine the effect of constant light on the period of the circadian oscillator, we also simulated a protocol with constant 10 lux light exposure.

For each protocol, the observed circadian period, τ_{obs}, was estimated on day d, denoted $\tau_{obs,d}$, for $3 \leq d \leq 33$. We computed $\tau_{obs,d}$ to be the slope of the regression line after the first $d+1$ minima of X beginning with the minimum during the phase assessment and including minima through d days of ultradian LD cycling. Minima were constrained to occur 20 to 30h apart.

2.3.3 Quantifying estimates of τ_{obs}

To quantify the robustness of τ_{obs} across days, we fixed $\tau = 24.2$h and computed the regression line based on thirty-three 24h days of ultradian cycling to determine $\tau_{obs,33}$, a stable estimate of intrinsic circadian period. Then we compared the maximum, minimum, and average deviations of individual circadian minima on study days d, $3 \leq d \leq 33$, from the computed regression line.

To quantify the accuracy of τ_{obs} as a function of study duration, light intensity, and LD cycle duration, we systematically varied these protocol parameters, estimated τ_{obs}, and compared estimates to the known intrinsic period τ. To further examine the role of study duration on the accuracy of τ_{obs}, we defined a worst-case deviation of $\tau_{obs,d}$ from τ for $\tau_{obs,d}$

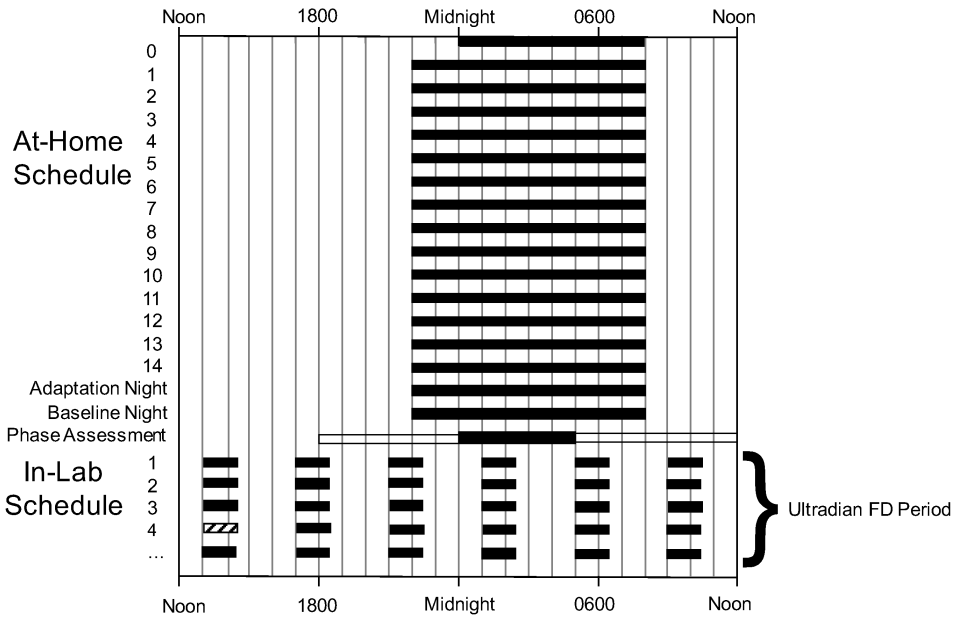

Figure 2.1: Comprehensive schematic for simulated ultradian FD protocol with 4h LD cycle. Protocol includes a 14 day At-Home portion and an In-Lab portion consisting of an Adaptation Night, a Baseline Night, a Phase Assessment, and then exposure to ultradian LD cycling. Black bars denote periods with a light intensity of 0 lux. Light intensities at all other times depend on the part of the protocol: the At-Home schedule involves light conditions of 0 lux from 22:00-8:00 and 150 lux at all other times; the Adaptation Night and Baseline Night involve light conditions of 0 lux from 22:00-8:00 and 30 lux at all other times; the Phase Assessment requires dim light of 10 lux from 12:00-00:00 and 5:00-12:00 with 0 lux from 00:00-5:00; and the Ultradian FD Period involves 4h LD cycles with 2.5 hours of light (variable light intensities depending on protocol) and 1.5 hours of 0 lux. The hatched bar denotes the ultradian cycle after which estimates of circadian period are computed.

of study duration d with $3 \leq d \leq 33$: *deviation on day* $d = max_{k=d}^{33}|\tau_{obs,k} - \tau|$. We computed the worst-case deviation for $\tau = 24.2$h, $I = 10$ lux, and protocols using 4, 5, or 7h LD cycle durations with different phases of ultradian LD cycle onset, and we determined the maximum deviation over the 3 phases of protocol onset previously described.

To summarize the effect of LD cycle duration on the deviations of τ_{obs} from the intrinsic period τ and the sensitivity of τ_{obs} to the phase of ultradian LD cycle onset, we estimated τ_{obs} on study day 4 and study day 10 for intrinsic periods τ ranging from 23.5 to 25 h under 4, 5, or 7h LD cycles with different phases of LD cycle onset. Study days 4 and 10 were selected to reflect a typical study duration of 3 days of ultradian LD exposure and a study duration that produces a stable value of τ_{obs}, respectively.

2.3.4 Assessing the distribution of light exposure over the circadian cycle

For ultradian FD protocols with 4, 5, or 7h LD cycles, we quantified the distribution of light exposure associated with running ultradian cycling over 4 or 10 days of 24 h. We partitioned the 24h day into 0.1h bins and determined the light exposure for each bin with fixed light intensity I. Data were averaged in bins of one hour and normalized by the number of 24h days simulated.

2.4 Results

To investigate the effects of protocol parameters on estimated circadian periods, we used a mathematical model of the human circadian pacemaker to simulate ultradian FD protocols with varying LD cycles, light intensities, and study durations. For each simulated protocol, the timing of the minimum of the simulated circadian oscillation was determined, and the progression of the minimum over each 24-h cycle indicated that the oscillator was unable to entrain to any of the ultradian cycles. For $\tau = 24.2$h, the timing of the minimum of the simulated circadian oscillation showed the expected rightward progression under a protocol involving 4 (Figure 2.2), 5 (Suppl. Fig. 1), or 7h (Suppl. Fig. 2) LD cycles. We computed τ_{obs} to be the slope of the linear regression on the minima as described in the Methods

section.

2.4.1 Accuracy of τ_{obs} depends on light intensity and study duration

For all protocols, $\tau_{obs,33}$ provided a stable estimate of τ and deviated less than 0.05 h from the known τ. The daily progression of the minimum of X was approximately constant at a light intensity of 10 lux, suggesting that the use of low light levels during the protocol minimizes variability around the regression line. To quantify the robustness of τ_{obs} under different light intensities, we computed the maximum, minimum, and mean deviation of individual circadian minima from the regression line computed on study day 33. For each simulation, we fixed $\tau = 24.2$ h and computed τ_{obs} under an ultradian FD protocol with light intensity specified to be 10, 50, 100, 150, 750, or 1000 lux. For a protocol with 4h LD cycle, maximum, minimum, and mean deviations generally decreased with light intensity (Figure 2.3). Similar results were observed for protocols with 5 (Suppl. Fig. S3) or 7h (Suppl. Fig. S4) LD cycles. For protocols with 4, 5, or 7h LD cycles, the maximum deviation of individual circadian minima from the regression line was less than 0.2h for a light intensity of 10 lux, and maximum deviations were bounded above by 0.9h across all simulated light intensities.

To investigate the effect of protocol duration and light intensity on τ_{obs}, we simulated protocols with variable numbers of study days and light intensities using a model circadian pacemaker with τ ranging from 23.8 to 25h. We report results for $\tau = 23.8$, 24.2, 24.6, and 25.0h. We found that estimates of intrinsic period under ultradian FD protocols with 4 (Figure 2.4), 5 (Suppl. Fig. S5), and 7h (Suppl. Fig. S6) LD cycles depended on the intrinsic period τ, light intensity I, and the number of study days. Although intrinsic period affected the accuracy of estimates of τ_{obs}, we did not detect a systematic effect of τ on τ_{obs}. High light intensities were associated with greater deviations of τ_{obs} from τ, and the light intensity dependence of τ_{obs} was most pronounced for $\tau_{obs,d}$ with short study durations d. As study duration increased, τ_{obs} generally converged to a value near τ for all protocols. To further quantify the convergence of τ_{obs} to τ as a function of study duration, we computed

an average worst-case deviation of $\tau_{obs,d}$ from τ under typical dim light conditions. We found that $\tau_{obs,d}$ converged within a neighborhood of ± 0.07h of τ by study day 10 for all LD cycles (Figure 2.5). Across different intrinsic periods, the rate of convergence was fastest for the protocol with a 7h LD cycle; under these conditions, $\tau_{obs,d}$ converged within a neighborhood of ± 0.05h of τ by study day 10.

Based on this evidence that $\tau_{obs,10}$ stably estimated τ, we quantified the robustness of $\tau_{obs,10}$ relative to $\tau_{obs,d}$ for $11 \leq d \leq 33$ by computing the maximum deviation of individual minima on study days 11 to 33 from the regression line associated with $\tau_{obs,10}$. We found that this maximum deviation was less than 0.07 for protocols with 4, 5, or 7h LD cycles and for all light intensities (data not shown). At 10 lux, the maximum deviation was less than 0.04 h for the protocols with 4 or 5h LD cycles and less than 0.02 for the protocol with the 7h LD cycle.

For $\tau = 24.2$h, we simulated a protocol of constant 0 and 10 lux light conditions and found minimal effect on the estimated period period of the original model with $\tau_{obs,33} = 24.2314$h at 0 lux and $\tau_{obs,33} = 24.2346$h at 10 lux.

2.4.2 Accuracy of τ_{obs} depends on LD cycle duration and resulting pattern of light exposure

To investigate the dependence of the observed circadian period on LD cycle duration, we compared estimates of $\tau_{obs,3}$ and $\tau_{obs,10}$ computed for ultradian FD protocols with 4, 5, or 7h LD cycle durations for τ ranging from 23.8 to 25h. In addition, we considered the sensitivity of τ_{obs} to the phase of LD cycle onset by simulating the protocols with the onset of the ultradian LD cycles offset by 1h shifts. We found that the deviation of observed period from τ varied with the phase of protocol onset for all protocols, though relative differences depended on τ (Figure 2.6). For 4, 5, and 7h LD cycles, $\tau_{obs,3}$ and $\tau_{obs,10}$ generally overestimated τ independent of phase of protocol onset, although there were values of τ for which $\tau_{obs,3}$ provided underestimates. This phase dependence was attenuated for $\tau_{obs,10}$ compared with $\tau_{obs,3}$. In addition, variability of $\tau_{obs,3}$ and $\tau_{obs,10}$ with phase of LD cycle

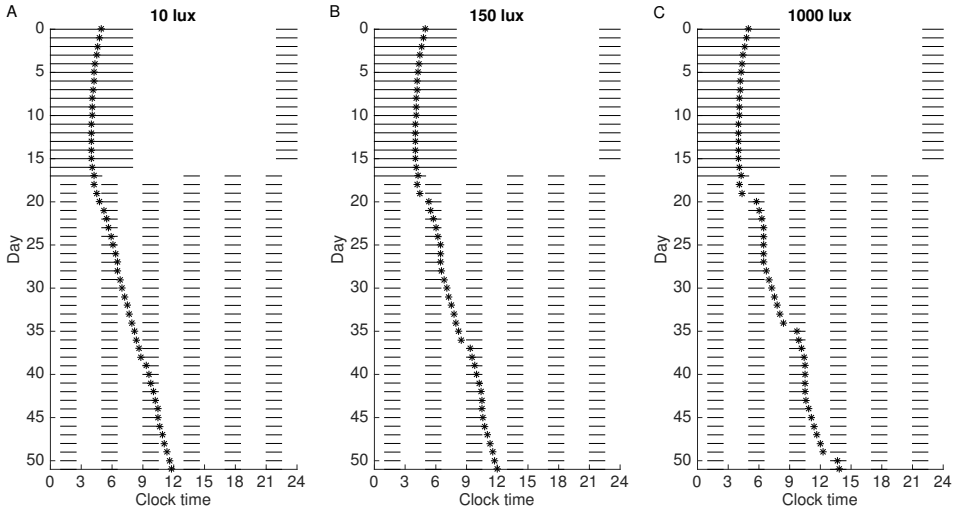

Figure 2.2: Minimums of X are used to estimate intrinsic period. Daily minimums of X (*) are plotted with respect to clock time across the entire simulated ultradian FD protocol with 4h LD cycle. During LD cycles, light levels are fixed to 10 (A), 150 (B), and 1000 lux (C). Black lines indicate times with light intensity set to 0 lux. For all simulations, intrinsic period τ=24.2h, so the minimums of X drift to the right after the ultradian FD period is initiated. The slope of the line through these minima provides an estimate for the intrinsic period.

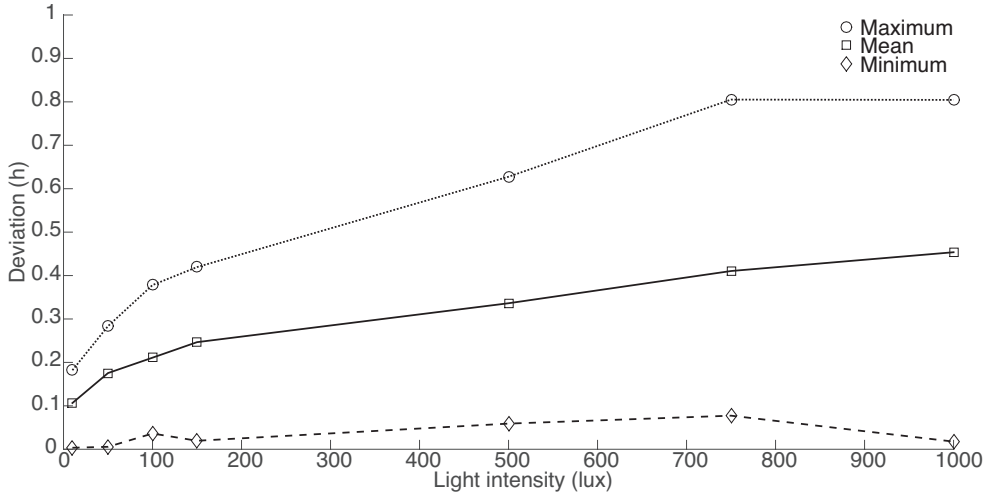

Figure 2.3: Robustness of τ_{obs} was reduced at high light intensities. The deviations of the minimums of X from the regression line computed on study day 33 under 4h LD cycling generally decrease with light intensity. The maximum, mean, and minimum deviation of the X minima from the regression line were computed for light intensities of 10, 50, 100, 150, 500, 750, and 1000 lux. For all simulations, intrinsic period τ=24.2h.

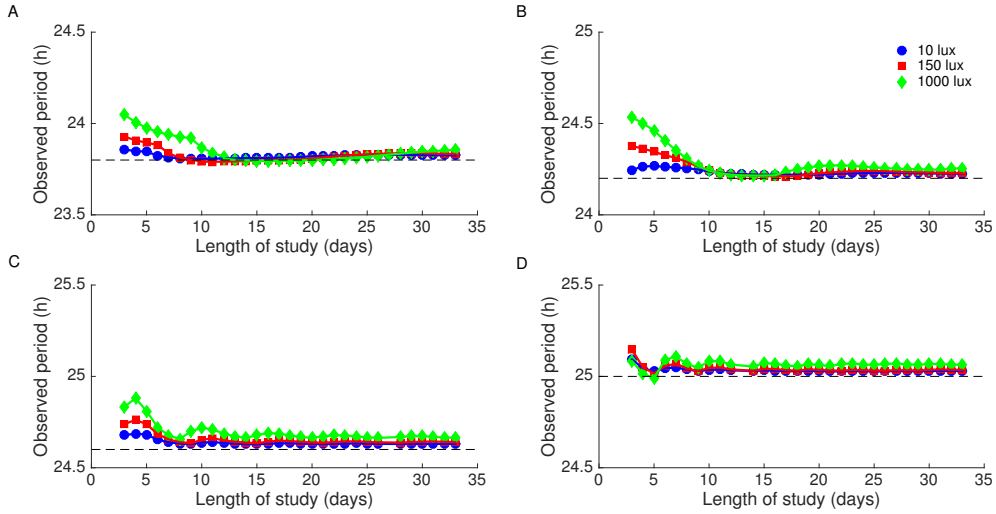

Figure 2.4: Estimates of intrinsic period improve with longer studies and lower light levels independent of intrinsic period τ. For τ= 23.8 (A), 24.2 (B), 24.6 (C), and 25.0h (D), higher light intensities were associated with greater deviations of τ_{obs} from τ. For all simulations, τ_{obs} generally converged within a neighborhood of the intrinsic period with sufficiently long exposure to 4h LD cycling with light intensities of 10, 150, or 1000 lux.

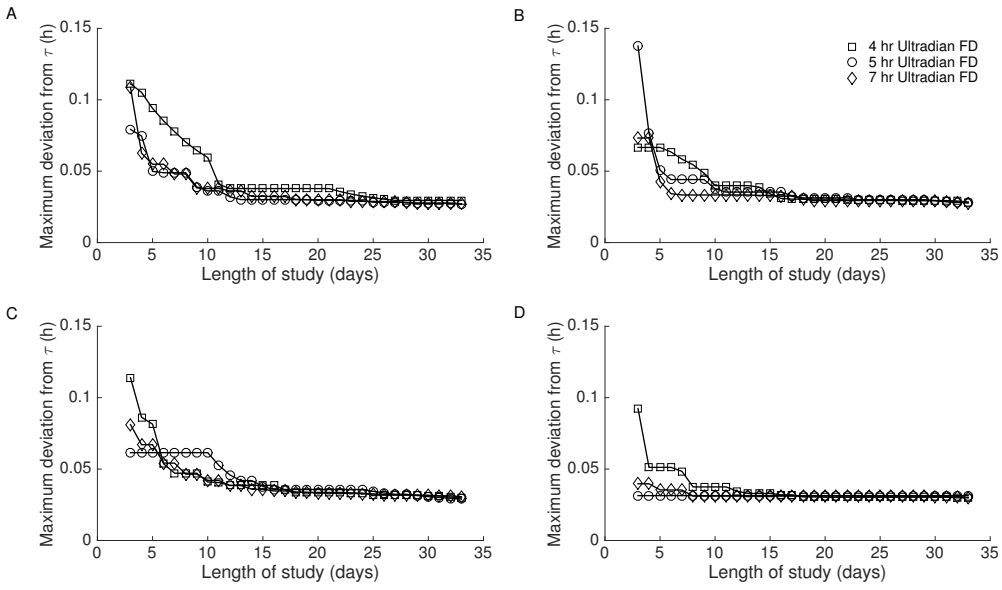

Figure 2.5: Circadian periods estimated using ultradian FD protocols with 4, 5, and 7h LD cycles and a light intensity of 10 lux converge to the intrinsic period. For τ= 23.8 (A), 24.2 (B), 24.6 (C), and 25.0h (D), the maximum deviation of τ_{obs} computed on day d and maximized over phase of protocol onset was within 0.07h of the intrinsic period for $d \geq 10$ and within 0.05h of the intrinsic period for $d \geq 13$.

onset was minimized for protocols with 7h LD cycles compared with 4 or 5h LD cycles across intrinsic periods. For $\tau_{obs,10}$, the deviation of observed period from intrinsic period was < 0.1h for all protocols and all values of τ and < 0.05h for the ultradian FD protocol with 7h LD cycle durations.

We hypothesized that the decreased sensitivity to onset phase in the ultradian protocol with 7h LD cycles compared with protocols with 4 or 5h LD cycles was caused by protocol-associated differences in the timing of light exposure. To test this hypothesis, we computed light exposure at each clock time across the 24h day for each protocol (Figure 2.7). We found that patterns of light exposure associated with 4h LD cycles were less uniform than those associated with 7h LD cycles, and this difference was more pronounced in the 3 day protocol compared with the 10 day protocol.

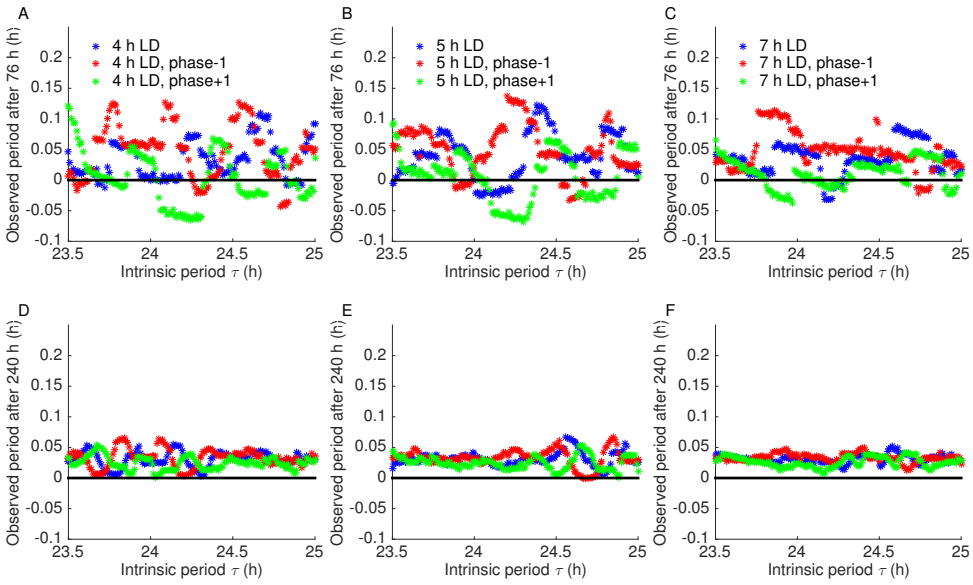

Figure 2.6: Circadian periods estimated using ultradian FD protocols with 4, 5, and 7h LD cycles depended on phase of protocol onset and generally overestimated true circadian period. Shifting the phase of ultradian cycling onset to begin one hour earlier or later than the baseline phase of protocol onset revealed that protocols with LD cycles of 4 (A, D) or 5h (B, E) were more sensitive to the phase of protocol onset compared to the protocol with 7h LD cycles (C, F). Both the phase-dependence and the variability in τ_{obs} were decreased with a study duration of 10 days (D, E, F) compared to estimates with a study duration of 3 days (A, B, C).

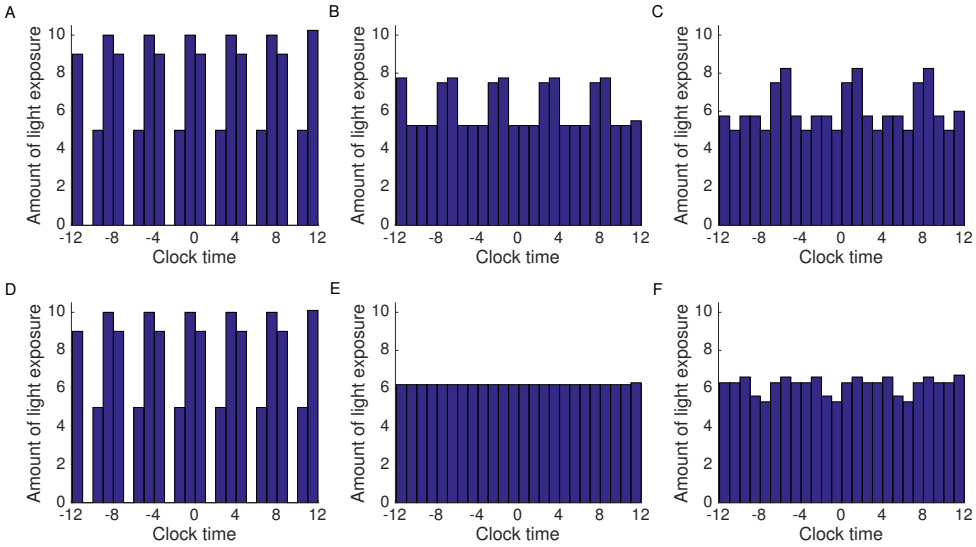

Figure 2.7: Relative light exposure varies for ultradian FD protocols with LD cycles of different durations. Histogram of relative light exposure for an ultradian protocol with 4 (A, D) or 5h (B, E) LD cycles shows less uniform light exposure compared to protocols with 7h LD cycles (C, F). Variability in light exposure was decreased with a study duration of 10 days (D, E, F) compared to variability observed in a study duration of 3 days (A, B, C).

2.4.3 Model dependence observed in τ_{obs} but not in protocol design features

Since simulation results depend on the choice of human circadian pacemaker model, we duplicated all simulations using an alternative pacemaker model to investigate the potential model dependence of our results. We found that the conclusions regarding ultradian FD protocol design were consistent with simulation results from both models. Specifically, accuracy of τ_{obs} was maximized for low (e.g., 10 lux) light intensities, study durations of at least 10 days, and LD cycle durations of 7h (Suppl. Fig. S7 and S8). Computing τ_{obs} using the alternative pacemaker model typically resulted in underestimates of τ independent of phase of protocol onset (Suppl. Fig. S8). Furthermore, the deviations of $\tau_{obs,10}$ from τ were greater using the alternative model compared with the original model. Simulating a protocol of constant 10 lux light conditions with the alternative model resulted in a decreased estimated period compared with the estimated period associated with 0 lux conditions: $\tau_{obs,33}$

= 24.1975 h at 0 lux and $\tau_{obs,33}$ = 24.1176 h at 10 lux.

2.5 Discussion

2.5.1 Summary and interpretation of results

Intrinsic circadian period, τ, represents a key characteristic of the human circadian system, and current extended FD experimental protocols used to obtain estimate τ are highly resource intensive. Ultradian FD protocols offer a promising alternative, but less is known about the optimal design of these protocols for obtaining accurate estimates of intrinsic circadian period. Using a light-sensitive, dynamic model of the human circadian pacemaker, we simulated ultradian FD protocols and analyzed the effects of light intensities, LD periods, study durations, and intrinsic period on estimated intrinsic circadian period, τ_{obs}. We found that optimal estimates were obtained for protocols when light intensities (e.g., 10-15 lux). The estimate of observed period was improved and sensitivity to phase of protocol onset was reduced for protocols using 5 or 7h LD cycle durations compared to 4h LD cycle durations. Although the rate of convergence of τ_{obs} toτ varied for different intrinsic periods, exposure to ultradian LD cycles for 10 24h days produced a stable estimate of observed period within 0.07h of the intrinsic period with improved accuracy for protocols with 7h LD cycles.

A key feature of extended day FD protocols is a pattern of light scheduling that results in uniform light exposure over all circadian phases. This scheduling ensures uniform sampling of the circadian pacemaker's phase response curve (PRC) to light, and it minimizes the biased PRC sampling that may occur under free-running protocols in which participants are able to self-select light exposure. However, in an ultradian FD protocol with a 4h LD cycle, light occurs at the same clock times across the protocol. This results in a pattern of light exposure that is not uniform over the entire circadian cycle, particularly when study durations are short. For this model, the published PRC to one 5h pulse of light of 150 lux suggests that non-uniform light exposure will result in biased sampling of phase advance and delay regions of the PRC, thereby affecting the estimate of observed period [27]. Furthermore, the phases at which increased light exposure occurs will depend on the phase at which the protocol is

initiated, thereby increasing the sensitivity of τ_{obs} to protocol effects. This suggests that, for the same individual under the same protocol with a 4h LD cycle, slight variations in internal circadian phase at protocol onset may produce different estimates τ_{obs} due to shifted patterns of light exposure acting differentially on the PRC to light. Such sensitivity to the phase of protocol onset could also account for increased variability in τ_{obs} across a study cohort consistent with observations in our data. Sensitivity to phase of protocol onset is minimized in ultradian FD protocols with 7h LD cycles and study durations of at least 10 days.

Implementation of ultradian FD protocols has varied across labs. Our results suggest that the accuracy of intrinsic period estimates using published ultradian FD protocols may vary as a function of τ, study duration, phase of protocol initiation, and light intensity. Since the ability to control for factors such as τ and phase of protocol initiation is limited, ultradian FD protocols must be designed to provide reliable estimates despite variability in these factors. Consistent with best practices predicted by our simulation results, published ultradian FD protocols have typically involved low light intensities. However, other protocol features, such as the common use of 4h LD cycles and study durations of 3-4 days, are not consistent with predicted optimal protocol design. Given the potential constraints on accuracy of τ_{obs}, caution is warranted when interpreting estimates of intrinsic periods obtained using ultradian FD protocols that do not conform to predicted best practices.

2.5.2 Alternative design of ultradian FD protocols

In this study, we focused on simulations of ultradian FD protocols with light intensities and light:dark ratios similar to those in published extended day or ultradian FD protocols. In addition, we considered effects of study durations and LD cycle durations on estimates of intrinsic circadian period. Our results suggest that LD cycle durations of 5h or 7h provide improved estimates of τ_{obs} compared to 4h LD cycle durations due to more uniform light exposure across the 24h day and the underlying circadian cycle. The regular pattern of light exposure associated with the 4h LD cycle over the 24h day would also occur with an LD

cycle of any duration that even divides 24h, e.g., 2, 3, 6, 8 or 12h LD cycles. Design of future ultradian FD protocols should consider implementing LD cycles of durations that do not evenly divide 24h in order to ensure a more uniform distribution of light across the 24h day.

In this study, we chose to preserve the 2.5:1.5 light:dark ratio when we varied LD cycle duration since this light:dark ratio allowed proportions of active/inactive time similar to those experienced in a typical day. However, future work could consider the effects of varying light: dark ratios within an LD cycle of fixed duration.

2.5.3 Comparison with extended day FD protocols

In previous work, Klerman and colleagues (1996) used this circadian pacemaker model to simulate extended day FD protocols and the effects of protocol design on estimates of intrinsic circadian period. They found that observed period depended on light intensity, LD period, and intrinsic period. Their results suggested that estimates of τ using 28h FD protocols initially overestimated τ and τ_{obs} approached τ when the protocol included at least 3 beat periods (approximately twenty-five 24h days) with a light intensity not to exceed 10 lux. They did not report specific magnitudes of the deviations they observed, although they indicated that the deviation of the observed period from the intrinsic period was considerable at high light intensities.

Consistent with their conclusions, we found that under ultradian FD protocols, τ_{obs} typically overestimated τ if study durations were not sufficiently long, and optimal results were obtained under low light intensities. Our results also demonstrated that initial estimates of τ_{obs} using ultradian FD protocols were closer to actual intrinsic periods and converged more quickly to intrinsic periods compared with estimates of τ_{obs} using extended day FD protocols. In addition, the robustness of estimates of τ_{obs}, measured as deviations of individual circadian minima from the regression line, was improved in the ultradian FD protocol compared with the extended day FD protocol. These differences highlight an advantage of ultradian FD protocols: the use of shorter LD cycles reduces the perturbation experienced

by the circadian system under the FD protocol. Since this perturbation is particularly pronounced for 28h FD protocols with short study durations due to highly nonuniform light exposure, much longer study lengths are required to obtain accurate estimates of τ_{obs} with 28h protocols compared with ultradian FD protocols.

In our simulations, ultradian FD protocols with 4, 5, or 7h LD cycles, produced estimates of τ_{obs} within 0.05h of τ with 10 days of exposure to ultradian LD cycling.

2.5.4 Model dependence in protocol effects

A primary limitation of this study is the constraint imposed by the assumptions inherent in the circadian pacemaker model. To facilitate comparison with previous work, this study applied the same human circadian pacemaker model that was used to evaluate protocol effects in extended day FD protocols [27]. However, other models of the human circadian pacemaker have been proposed [14, 15, 25, 77], and differences among models may affect simulation outcomes. Most significantly, differences in the models response to light, including the PRCs to light of different durations and intensities, may produce different predicted relationships between estimated period and intrinsic period under similar experimental conditions [25].

To address the issue of model dependence, we duplicated all simulations using an alternative mathematical model of the human circadian pacemaker [14]. We found that simulations produced by the alternative model supported our previous conclusions regarding light intensity, study duration, and LD cycle duration for optimal design of ultradian FD protocols for estimating intrinsic circadian period. However, our results also suggested that, particularly under conditions in which τ_{obs} had not yet converged to τ, individual estimates of τ_{obs} demonstrated model dependence. Furthermore, simulations of the original and alternative models resulted in respective over- or underestimation of τ by τ_{obs}. Model dependence in estimates of τ_{obs} is probably caused by differences in light processing between models. In particular, the model proposed by Forger and colleagues [14] includes an implementation of Aschoff's rule, a theory that higher light intensities are associated with shorter circadian periods in diurnal organisms [28]. Using a constant dim light protocol, we confirmed that

this implementation of Aschoff's rule resulted in a light intensity-dependence of circadian period in the alternative model that was not present in the original model. In addition to producing differential responses to light stimuli between the two models, the implementation of Aschoffs rule complicates the interpretation of the deviation of τ_{obs} from τ in the alternative model since τ varies as a function of light exposure.

Although these preliminary investigations of model dependence did not alter our conclusions regarding the optimal design of ultradian FD protocols for estimating intrinsic circadian period, the evidence for model dependence in individual estimates of τ_{obs} suggests that more work is needed to develop robust methods to relate actual intrinsic circadian period to estimates of circadian period based on an individuals response to an ultradian FD protocol. Such methods would have great utility for refining interpretation of existing data sets and enabling comparisons among data collected under different protocols.

2.6 Conclusions and Implications

In summary, ultradian FD protocols represent a promising experimental paradigm for addressing key questions in circadian research. In particular, the relative resource- and time-effective features of ultradian FD protocols underscore their utility for studies that require larger numbers of participants or address research questions in pediatric or other populations in which compliance with the time requirements of an extended day FD protocol are particularly challenging. Simulations of a human circadian pacemaker model support the use of well-designed ultradian FD protocols for estimating intrinsic circadian period. In addition, our results highlight the utility of mathematical modeling for optimizing circadian protocols and establish a theoretical framework that provides insights into data obtained under existing protocols and enables design of optimal protocols for future experiments.

2.7 Acknowledgments

This study was supported by the National Science Foundation grant DMS 1412571 (to C.D.B.) and National Institute of Mental Health grant MH076969 (M.A.C.).

2.8 Conflict of Interest Statement

The author(s) have no potential conflicts of interest with respect to the research, authorship, and/or publication of this article.‘

2.9 Note

Supplementary material is available on the journals website at http://jbr.sagepub.com/supplemental. This work was performed at the Colorado School of Mines.

CHAPTER 3

ESTIMATING GROUP INTRINSIC PERIOD FROM ILLUMINANCE-RESPONSE CURVE DATA

Paper in preparation.

Nora Stack MS[*], Jamie Zeitzer PhD[†,‡], Charles Czeisler PhD,MD[•], Cecilia Diniz Behn PhD[*,§2]

[*] Department of Applied Mathematics and Statistics, Colorado School of Mines, Golden, CO, USA. [†] Department of Psychiatry and Behavioral Sciences, Stanford University, Stanford, CA, USA. [‡] Mental Illness Research Education and Clinical Center, VA Palo Alto Health Care System, Palo Alto, CA, USA. [•]Department of Neurobiology, Harvard Medical School, Boston, MA, USA. [§] Division of Endocrinology, Department of Pediatrics, University of Colorado Anschutz Medical Campus, Aurora, CO, USA.

3.1 Abstract

The human circadian pacemaker entrains to the 24 h day, but interindividual differences in properties of the pacemaker, such as intrinsic period, affect many aspects of daily life including chronotype. These properties also mediate responses to challenges to the circadian system, like shift work and jet lag, and efficacy of therapeutic interventions like light therapy. Robust characterization of circadian properties requires desynchronization of the circadian system from the rest-activity cycle, and these forced desynchrony protocols are very time- and resource-intensive. This has limited the ability to characterize circadian properties across individuals and demographic groups. By contrast, circadian protocols designed to derive the relationship between light intensity and phase shift, which is inherently affected by intrinsic period, may be applied more broadly. We exploited this relationship by applying a

[2]To whom all correspondence should be addressed: Cecilia Diniz Behn, Department of Applied Mathematics & Statistics, Colorado School of Mines, 1015 14th Street, Golden, CO 80401, USA; e-mail: cdinizbe@mines.edu.

mathematical model of the human circadian pacemaker with a Markov-Chain Monte Carlo parameter estimation algorithm to illuminance-response curve data to estimate the mean intrinsic period of the group of participants contributing to the curve. We first validated this methodology using simulated illuminance-response curve data where the intrinsic period was known. Over a normal range of intrinsic periods, this method accurately estimated the average intrinsic period of the group. We also applied the method to previously published experimental data describing the illuminance-response curve for a group of healthy adult participants. We estimated the study participants' average intrinsic period to be 24.26 and 24.27 hours using uniform and normal priors, respectively, consistent with estimates of the average intrinsic period of healthy adults. Our results establish an approach to estimate a mean group intrinsic period from illuminance-response curve data, thereby facilitating characterization of intrinsic period across a broader range of participant populations than could be studied using forced desynchrony protocols. Future applications of this approach may improve understanding of demographic differences in intrinsic circadian period.

3.2 Introduction

Molecular clocks maintain an $\sim$24 hour rhythm in the firing rate of neurons in the suprachiasmatic nucleus (SCN) [19, 29, 78]. The collective activity of these neurons gives rise to a circadian rhythm that acts as a pacemaker to coordinate biological rhythms throughout the body [1]. The properties of this pacemaker, including its intrinsic period and amplitude, affect an individuals ability to overcome jet lag [79], tolerate shift work [79], and respond to circadian- based therapeutic interventions such as light therapy [80]. Furthermore, circadian properties may inform societal constructs such as appropriate work hours [81] and school start times [82–84].

Forced desynchrony (FD) protocols represent the gold-standard methodology for assessing an individuals intrinsic circadian period. In these protocols, circadian rhythmicity is desynchronized from sleep/wake behavior by imposing a regular light:dark (LD) cycle that is outside the range of entrainment of the circadian pacemaker. A marker of free-running

circadian period, usually salivary or plasma melatonin or core body temperature, is used to estimate the pacemakers intrinsic period, τ [4, 34]. Using FD protocols, τ has been estimated to be 24.18 $\pm$ 0.04h (mean $\pm$ SEM) in healthy young men [4], but the intrinsic period can vary based on many different factors including age, sex, and race/ethnicity [31–34, 76]. The range of intrinsic periods observed in healthy adults has been estimated to be 23.5 h to 24.9 h [31, 32].

FD protocols are highly time- and resource-intensive with accurate assessments requiring an extended day FD protocol of at least 20 days [27] or an ultradian FD protocol of at least 10 days [52]. These constraints limit the applicability of FD protocols and may prevent experimental assessment of τ in populations such as young children or individuals diagnosed with conditions that could be exacerbated by induced desynchrony of sleep and circadian rhythms. Indeed, assessment of τ is rarely performed when it is not a primary outcome of an experiment. However, τ likely affects other measures of the circadian system such as phase response curves (PRCs) to light [40, 44, 75] PRCs to other behavioral [85] or pharmacological factors [49, 51], and illuminance dose-response curves [41, 43]. In PRCs and illuminance-response curves, each point typically corresponds to a different participant. Therefore, the data collectively reflect the intrinsic periods of all of the participants in the group. In this study, we sought to exploit this τ-dependence to develop methodology to mine circadian measures that depend on τ for novel information about the average intrinsic period of the group.

To relate experimental data to properties of the human circadian pacemaker, we used a mathematical model developed by Forger and colleagues [14]. This human circadian pacemaker model, based on a modified van der Pol oscillator, incorporates many key features of circadian pacemaker dynamics including phase and amplitude responses to light and Aschoffs rule, the observation that higher light intensities produce shorter circadian periods in diurnal species [14, 28]. Furthermore, the intrinsic period, τ, is an explicit parameter of this circadian pacemaker model and represents the period of the pacemaker observed in total

darkness. Under typical 24-h light:dark (LD) cycles, the oscillator is entrained to the LD cycle and produces an exactly 24-h period. The carefully calibrated light responses of this model have contributed to its widespread use to investigate and simulate many different circadian characteristics [29, 52, 86, 87].

Using this model in conjunction with Markov Chain Monte Carlo (MCMC) parameter estimation methods, we aimed to develop methodology to estimate τ from illuminance-response curve data. To validate this approach, results were first obtained for synthetic data for which τ values were known. We simulated phase shift data by implementing a published illuminance-response curve protocol [41] using this human circadian pacemaker model [14] with known τ values. By applying MCMC parameter estimation to the simulated data, we calculated a posterior distribution of intrinsic periods to compare with the known τ values used to generate the synthetic data. We also applied this method to previously published experimental data [41] to determine the group intrinsic periods of participants in an experimental illuminance-response curve study involving healthy adults.

3.3 Methods

3.3.1 Human Circadian Pacemaker Model

A mathematical model of the human circadian pacemaker developed by Forger and colleagues was used to perform all simulations. The model is a modified van der Pol oscillator that consists of Process P and Process L [14]. Process P describes the oscillator representing the circadian pacemaker, and Process L represents the processing of external light and includes a phase-dependent sensitivity modulation. The equations associated with the two components of the model are as follows:

Process P

$$\frac{dX}{dt} = \frac{\pi}{12}\left(x_c + B\right)$$

$$\frac{dX_c}{dt} = \frac{\pi}{12}\left[\mu\left(x_c - \frac{4x_c^3}{3}\right) - x\left[\left(\frac{24}{0.99669\tau}\right)^2 + kB\right]\right].$$

Process L

$$\alpha(I) = \alpha_0 \left(\frac{I^p}{I_0^p} \right)$$

$$\frac{dn}{dt} = 60[\alpha(I)(1-n) - \beta n]$$

$$\hat{B} = G(1-n)\alpha(I)$$

Sensitivity Modulation

$$B = \hat{B}(1 - 0.4x)(1 - 0.4x_c).$$

External light, $I(t)$, enters the system through equation $\alpha(I)$ which represents the drive rate. The variable n models phototransduction, and both n and $\alpha(I)$ contribute to the output drive $\hat{B}$ which then feeds into the sensitivity modulation B. The sensitivity modulation dictates how light from Process L interacts with Process P, thereby introducing phase-dependence into the light effect. In Process P, X represents endogenous circadian body temperature and X_c is a complementary variable. Therefore, minimums of X correspond to minimum core body temperature (CBT_{min}), an experimental a marker of circadian phase.

Kronauer and colleagues established baseline parameters of this circadian pacemaker model, including τ, α_0, and β, by fitting the model to experimental data collected from healthy adults [14, 17]. The intrinsic circadian period, τ, represents the intrinsic period of the circadian oscillator in constant darkness, and the model incorporates the effects of Aschoffs rule on the circadian system such that the period of the oscillation decreases with increasing light exposure. Standard published parameter values [14, 17, 88], summarized in Table A.1 in Appendix A, were used for all simulations with the exception of the intrinsic period, τ, which was allowed to vary.

3.3.2 Experimental illuminance-response curve protocol

The illuminance-response curve protocol design and the experimental data used as a test case for the method were previously published in a study by Zeitzer and colleagues designed to quantify the sensitivity of the human circadian pacemaker to nocturnal light [41]. In this study, 23 healthy adults ages 18-44 participated in the 9-day in-lab protocol. During the nocturnal light exposure, each participant was exposed to a different light intensity. Phase delay and percent melatonin suppression were measured in order to construct illuminance-response curves of these measures.

The study protocol was as follows: for two weeks prior to the 9-day illuminance- response curve, protocol participants maintained a consistent 16:8 LD schedule (Figure 3.1). Following three baseline days in the lab, they underwent an $\sim$ 50 h constant routine at 15 lux where initial phase of the circadian system was assessed in the lab using minimum core body temperature (CBT_{min}). Study participants then experienced 8 h of darkness followed by 16 h of light centered about a 6.5 h light pulse. Each participant experienced a different light intensity ranging from 2.56 lux to 9106 lux. Exact constant routine duration was chosen so that the light pulse began 6.75 h before predicted CBT_{min} and ended 0.25 h before CBT_{min}. During the remainder of the 16 h, the participants experienced dim light ($<$ 15 lux). Following another 8 h of darkness, they underwent another $\sim$ 30 h constant routine to find CBT_{min} and allow calculation of the phase shift in melatonin rhythm induced by the light exposure. Participants then slept for 8 h and were discharged upon waking on day 9.

3.3.3 Simulating the experimental illuminance-response curve protocol

The simulated protocol was designed to mimic the experimental protocol described in the previous subsection. Before beginning the simulated illuminance-response curve protocol, the model simulated circadian phase for two weeks on a consistent 16:8 h LD schedule with a light level of 150 lux from 0800 to 0000 and a light level of 0 lux from 0000 to 0800. During the simulated in-lab portion of the protocol, light during the light period of the

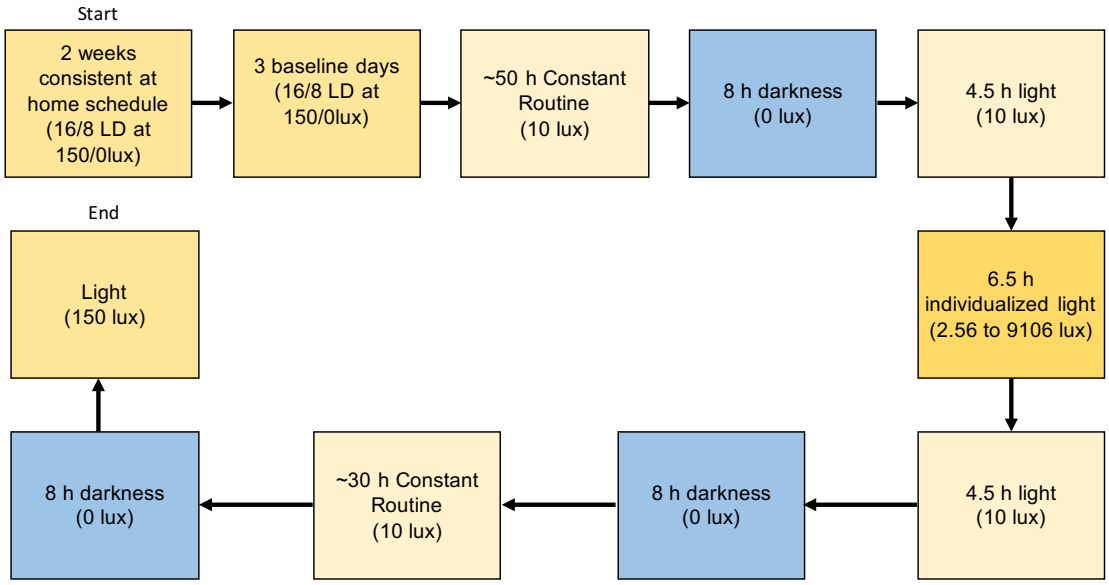

Figure 3.1: A schematic of the illuminance-response curve protocol with light intensities. Two weeks of a consistent schedule at home are followed by three baseline days in the lab. Then participants undergo an $\sim$ 50 h constant routine, an 8 h period of darkness, and a 16 h period of light. During the light period, the participant is exposed to a specific light intensity for 6.5 h (varied per person from 2.56 to 9106 lux). This exposure is timed to begin 6.75 h before CBT_{min} and to end 0.25 h before CBT_{min}. The rest of the wake period is spent in dim light. The light exposure is followed by 8 h of darkness, an $\sim$ 30 h constant routine, and another 8 h of darkness to end the protocol.

baseline days was set to 150 lux; dim light was set to 10 lux for the synthetic data and set to each participant's measured light intensity (< 15 lux) for experimental data; individual light intensity was set to a value in the range of 2.56 lux to 9106 lux for the experimental light exposure; and dark periods were set to 0 lux (Figure 3.1). To determine the appropriate duration of the constant routine in the simulated protocol, we first simulated the two weeks prior to the experiment and a 56-h constant routine. Based on these results, we determined CBT_{min} and calculated the constant routine duration necessary to time the light pulse to begin 6.75 h before CBT_{min} and end 0.25 h before CBT_{min}. Using this newly calculated constant routine duration to ensure accurate timing of light exposure, we simulated the full protocol with appropriate nocturnal light exposure and computed light-induced phase shifts as the difference between CBT_{min} during the first constant routine and CBT_{min} during the second constant routine.

Model equations were implemented in MATLAB (Mathworks, Natick, MA) and solved numerically using the built-in MATLAB solver **ode45** with a relative error tolerance of $1e^{-9}$ and an absolute error tolerance of $1e^{-10}$. The built-in MATLAB Signal Processing Toolbox function **findpeaks** was used to detect minima of X to compute phase shifts.

3.3.4 Markov Chain Monte Carlo algorithm and simulations

We implemented a Markov Chain Monte Carlo (MCMC) method to estimate τ for a given illuminance-response curve using the Metropolis algorithm. The goal of MCMC is to determine the posterior distribution, the probability of the parameter(s) given data $P(\mu|D)$, using Bayes Theorem which states

$$P(\mu|D) \propto P(D|\mu) * P(\mu)$$

for parameter(s) μ and data D. $P(\mu)$ is called the prior distribution and may include assumptions about what the distribution of the parameter(s) is likely to be. For the application of MCMC to illuminance-response data to determine intrinsic period τ, Bayes theorem is:

$$P(\tau|\mathbf{PS}) \propto P(\mathbf{PS}|\tau) * P(\tau)$$

where **PS** is a vector of phase shifts. Phase shift data (**PS**) were simulated using the same light intensities as the experimental data. Each data point was assumed to be normally distributed with a mean of the measured phase shift and a 0.5 h standard deviation. The Metropolis algorithm was implemented in MATLAB and completed 10,000 iterations per MCMC run. MCMC runs were started from different initial chain values (23.8, 24.1, and 24.7 h) to verify that the starting point of the chain did not affect the estimated distributions. All densities are presented with a 5% burn-in, i.e., the first 500 iterations are not included in the analyses and metrics.

3.3.5 MCMC and illuminance-response curve test cases

To validate the MCMC approach, we produced synthetic data sets with phase shifts using model simulations in which the generative single τ or multiple τs were known. Two different cases of synthetic data were considered. The first test case was the single τ illuminance-response curve where all data points on the illuminance-response curve were generated using one τ value. We simulated single τ illuminance-response curves for $\tau = 23.7$, 24.2, 24.6, and 24.9 h. We also considered multi-τ illuminance-response curves where synthetic data were generated using τs drawn from normal distributions with means of 23.7, 24.2, and 24.6 h and various standard deviations. The single τ illuminance-response curves represent an idealized case in which all phase shifts reflect the same τ. By contrast, the multi-τ illuminance-response curves are representative of experimentally-generated illuminance-response curves in which each point represents the phase shift of a different individual.

To generate synthetic data using known τs, the circadian pacemaker model simulated the experimental illuminance-response curve protocol across the range of light intensities. Phase shifts were calculated for each illuminance level and then used to specify the phase shift data for the Metropolis algorithm. A standard deviation of 0.5 h was added to the simulated phase shift data. For all runs with simulated illuminance- response curve data the prior was selected to be $U(23.5, 25)$ to reflect the range of τs found for healthy adults [31, 32]. After the algorithm completed 10,000 iterations, the known τ value or distribution was compared

to the results from the algorithm with a 5% burn-in.

Using previously published light intensities and phase shifts [41], we used this MCMC method to estimate the distribution of the group intrinsic period of the 23 healthy adults who participated in the protocol. Each data point was assumed to be normally distributed with a mean set to the participant's measured phase shift and a standard deviation of 0.5 h. We estimated the group intrinsic period for this experimental data using two different priors. We considered both a uniform prior ($U(23.5, 25)$) that imposes minimal assumptions on the parameter τ, and, conversely, we considered a normal prior ($N(24.2, 0.28)$) that assumes that the population τ is drawn from the established distribution of healthy adult intrinsic periods.

For all test cases, we completed twelve simulations consisting of four runs from each initial chain value of three chain values (23.8, 24.1, and 24.7 h). We computed the overall average τ value and standard deviation, the credible interval, and the percent of accepted samples for each of the twelve MCMC runs (four runs for each of three initial chain values).

3.4 Results

3.4.1 Structure of illuminance-response curve and τs

The structure of the simulated illuminance-response curve depends on τ. When the illuminance-response curves were simulated with different τ values, a stacked structure of curves was generated where increasing τ values produced larger phase delays (negative phase shifts) compared to curves generated with smaller τ values (Figure 3.2). Additionally, these simulations illustrated the range of phase shift values that are produced by this model over the given range of τ values and light intensities.

3.4.2 Single τ illuminance-response curves

The application of the Metropolis algorithm to the simulated single-τ illuminance-response curves produced average τ values almost exactly equal to the τ value used to generate the single-τ illuminance-response curve data. These curves were simulated with τs equal to

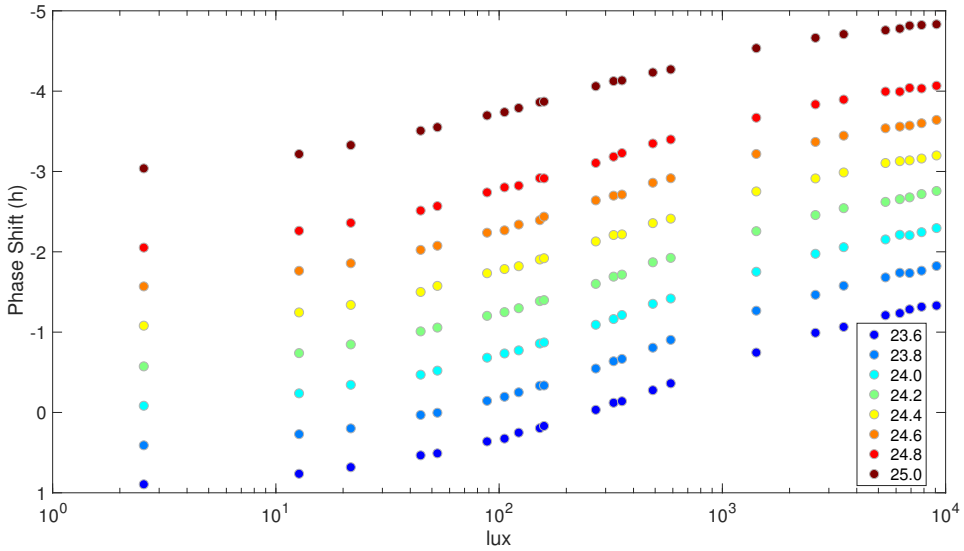

Figure 3.2: Simulated illuminance-response curves for intrinsic period τ varied between 23.6 to 25.0 h. With increasing intrinsic period, the shape of the curve is maintained but the magnitude of the negative phase shifts (phase delays) increases. Additionally, each curve is distinct and does not intersect with any other curves. This structure makes this type of data a good candidate for MCMC methods.

23.7, 24.2, 24.6, and 24.9 h, respectively (Figure 3.3). The means of the runs from three initial chain values (four runs per initial chain value) agree up to two significant figures for each simulated data set and have standard deviations less than 0.05 h (Table 3.1 and Table A.2). Additionally, means from individual runs and the means obtained by averaging over all twelve runs are within 0.01 of the τ value that was used to generate each phase shift data set, and the credible intervals are less than 0.2 h and contain the generative τ values (Table 3.1, Table A.2, and Table A.3). The mean percent of accepted samples ranges from 41% to just over 45% over the initial chain values and all the data sets (Table 3.1 and Table A.4).

3.4.3 Multi-τ illuminance-response curves

Multi-τ illuminance response curves were simulated with τs drawn from $N(23.7, 0.2^2)$, $N(24.2, 0.2^2)$, $N(24.2, 0.4^2)$, and $N(24.6, 0.2^2)$ distributions. The average τ of the posterior

Table 3.1: MCMC estimates of τ for simulated single τ illuminance-response curves generated from τ = 23.7, 24.2, 24.6, and 24.9 h. Average τ values ($\pm$ standard deviations), 95% credible intervals, and percent of accepted samples from twelve MCMC runs (four from each initial chain value) of 10,000 iterations with a 5% burn-in.

τ value used to generate data	Average ($\pm$std) τ of all runs	Average credible interval	Average percent of accepted samples
τ =23.7 h	23.6979 ($\pm$0.0407) h	[23.6190, 23.7780]	43.2167%
τ =24.2 h	24.1967 ($\pm$0.0423) h	[24.1136, 24.2799]	44.7368%
τ =24.6 h	24.5999 ($\pm$0.0433) h	[24.5149, 24.6842]	45.3947%
τ =24.9 h	24.8893 ($\pm$0.0383) h	[24.8096, 24.9554]	41.1833%

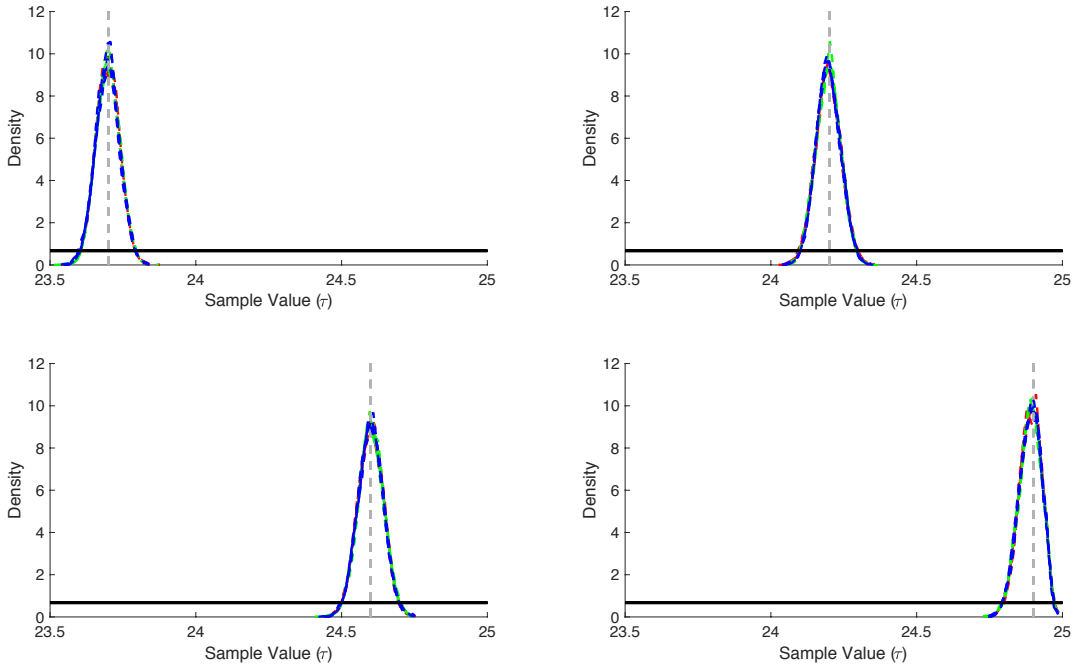

Figure 3.3: Kernel densities of twelve MCMC runs (four from each initial chain value) with synthetic single illuminance-response curve data where τ = 23.7 (A), 24.2 (B), 24.6 (C), and 24.9 h (D). The red (initial chain value is 23.8 h), green (initial chain value is 24.1 h), and blue (initial chain value is 24.7 h) dashed lines are the kernel densities. The gray dotted line indicates the known value that the data was simulated with. The black solid line is the uniform prior.

distribution was almost exactly equal to the mean of the distribution from which the τs were drawn even when the standard deviation in the data was increased. Over twelve runs with three initial chain values (four runs per initial chain value), the means of the samples agree up to two significant figures for each simulated data set (Table A.5). Similarly, we observed agreement in the density plots of the kernel distributions of the runs with a 5% burn-in (Figure 3.4). Furthermore, the overall average means of all of the runs are within 0.02 h of the mean of the distribution of the τs for each data set and have small standard deviations (Table 3.2). The credible intervals generated from the runs are narrow and capture the means of the distributions used to generate the synthetic data (Table 3.2 and Table A.6). However, the standard deviations of the posterior distributions do not correspond to the standard deviations of the distributions from which τs were drawn to simulate the data. For example, when τ values were drawn from $N(24.2, 0.2^2)$ and $N(24.2, 0.4^2)$ distributions, respectively, the average standard deviations of the posteriors were identical and the density plots were very similar (Table 3.2 and Table A.6 and Figure 3.4). The average percent of accepted samples ranges from 42% to 45.5% over the initial chain values and all the data sets (Table 3.2 and Table A.7).

Table 3.2: MCMC estimates of τ for simulated multi-τ illuminance-response curves generated from τs drawn from $N(23.7, 0.2^2)$, $N(24.2, 0.2^2)$, $N(24.2, 0.4^2)$, and $N(24.6, 0.2^2)$. Average τ values ($\pm$standard deviations), 95% credible intervals, and percent of accepted samples from twelve MCMC runs (four from each initial chain value) of 10,000 iterations with a 5% burn-in.

τ distribution data was drawn from	Average ($\pm$std) τ of all runs	Average credible interval	Average percent of accepted samples
$N(23.7, 0.2^2)$	23.6969 ($\pm$0.0407) h	[23.6175, 23.7772]	42.7886%
$N(24.2, 0.2^2)$	24.2121 ($\pm$0.0423) h	[24.1289, 24.2948]	44.1167%
$N(24.2, 0.4^2)$	24.2303 ($\pm$0.0423) h	[24.1482, 24.3144]	43.1763%
$N(24.6, 0.2^2)$	24.6140 ($\pm$0.0435) h	[24.5286, 24.6990]	45.2193%

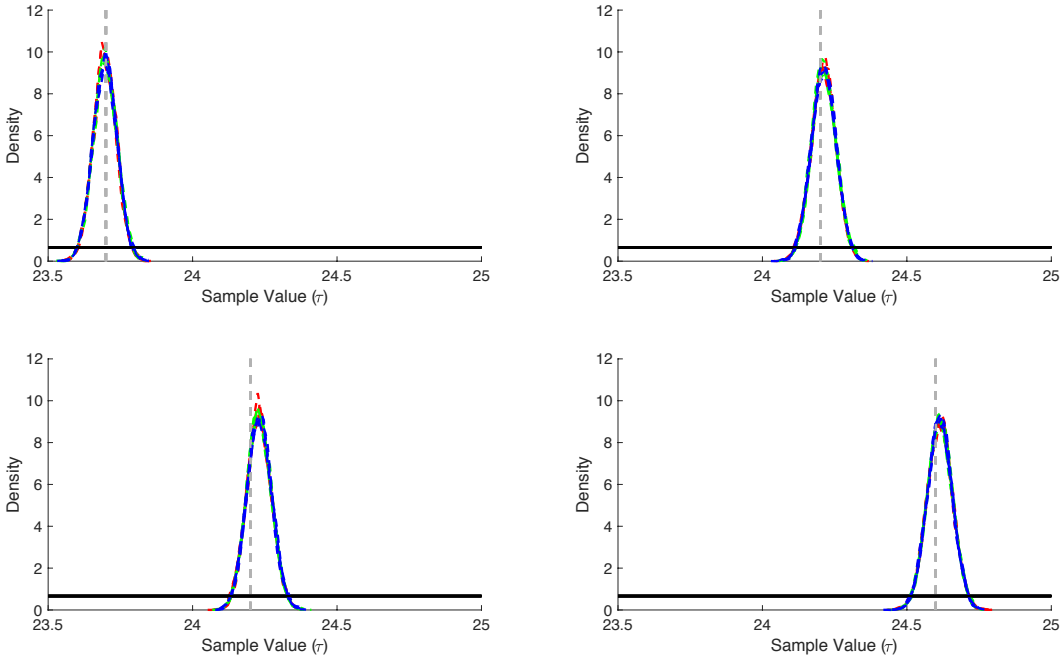

Figure 3.4: Kernel densities of twelve MCMC runs (four from each initial chain value) with synthetic multi- illuminance-response curve data where s were drawn from $N(23.7, 0.2^2)$ (A), $N(24.2, 0.2^2)$ (B), $N(24.2, 0.4^2)$ (C), and $N(24.6, 0.2^2)$ (D) distributions. The red (initial chain value is 23.8 h), green (initial chain value is 24.1 h), and blue (initial chain value is 24.7 h) dashed lines are the kernel densities. The gray dotted line indicates the known mean value that the data was drawn from. The black solid line is the uniform prior.

3.4.4 Experimental illuminance-response curve data

Applying MCMC to the experimental illuminance-response curve data resulted in estimates of a group intrinsic period that was close to the estimated average healthy adult intrinsic period of 24.2 h independent of prior. With uniform priors, estimated mean τ values were 24.27 h for all runs and initial chain values (Table 3.3 and Table A.8 and Figure 3.5). With normal priors, estimated mean τ values were 24.26 h for all runs and initial chain values (Table 3.3 and Table A.8 and Figure 3.6). All of the computed average 95% credible intervals contain 24.2 h (Table 3.3 and Table A.9). The percent of accepted samples was between 42.5% and 44.5% with the uniform prior and between 42% and 44% with the normal prior over twelve runs (Figure 3.5 and Figure 3.6, Table 3.3 and Table A.10). The density plots for the posterior distributions associated with either a uniform or a normal prior were very similar (Figure 3.5 and Figure 3.6).

Table 3.3: MCMC estimates of τ for experimental illuminance-response curve data with a uniform ($U(23.5, 25)$) and a normal ($N(24.2, 0.2^2)$) prior. Average τ values ($\pm$standard deviations), 95% credible intervals, and percent of accepted samples from twelve MCMC runs (four from each initial chain value) of 10,000 iterations with a 5% burn-in.

Prior distribution	Average ($\pm$std) τ of all runs	Average credible interval	Average percent of accepted samples
$U(23.5, 25)$	24.2674 ($\pm$0.0425) h	[24.1833, 24.3506]	43.8632%
$N(24.2, 0.2^2)$	24.2642 ($\pm$0.0414) h	[24.1835, 24.3458]	43.1781%

3.5 Discussion

3.5.1 Intrinsic period affects simulated illuminance-response curves

The intrinsic period of the circadian pacemaker, τ, affects the shape of illuminance-response curves simulated using distinct τ values, and this structure may be exploited to estimate a group τ from illuminance-response curve data. As intrinsic period increases, the magnitude of phase delays increases across light intensities while maintaining a similar curve shape. This produces distinct illuminance-response curves for each τ value with no

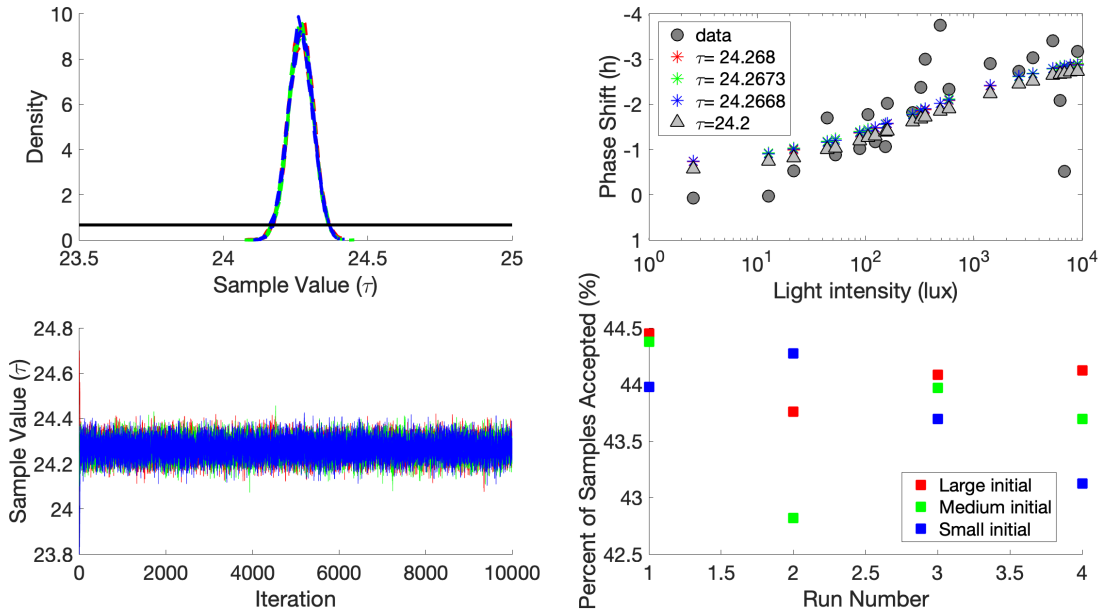

Figure 3.5: (A) Kernel densities of twelve MCMC runs (four from each initial chain value) with experimental illuminance-response curve data. The red (initial chain value is 23.8 h), green (initial chain value is 24.1 h), and blue (initial chain value is 24.7 h) dashed lines are the kernel densities. The black solid line is the uniform prior. (B) The experimental phase shift data, phase shift data generated from average values from each initial chain group, and phase shifts generated with $\tau = 24.2$ h. The red (initial chain value is 23.8 h), green (initial chain value is 24.1 h), and blue (initial chain value is 24.7 h) stars are simulated phase shifts produced when the average τ values from the four MCMC runs is plotted. The experimental phase shift data are dark gray circles and the simulated phase shifts with $\tau = 24.2$ h are light gray triangles. (C) The samples value of each iteration of the Metropolis algorithm for twelve MCMC runs (four from each initial condition). The red (initial chain value is 23.8 h), green (initial chain value is 24.1 h), and blue (initial chain value is 24.7 h) lines are the sample values. (D) The percent of accepted samples from the twelve runs. The red (initial chain value is 23.8 h), green (initial chain value is 24.1 h), and blue (initial chain value is 24.7 h) squares are the percent of accepted samples per run.

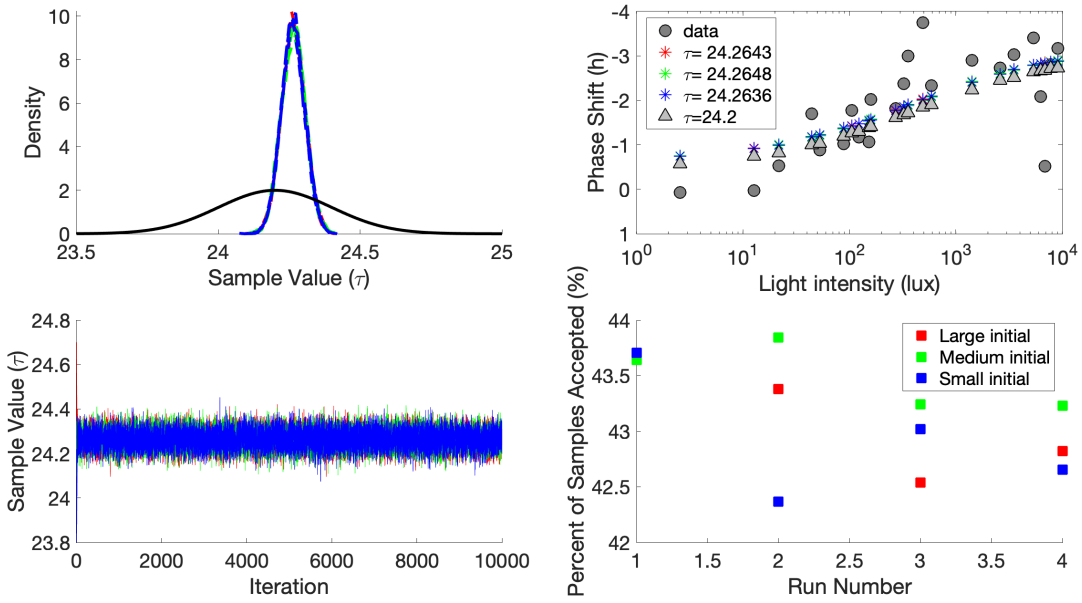

Figure 3.6: (A) Kernel densities of twelve MCMC runs (four from each initial chain value) with experimental illuminance-response curve data. The red (initial chain value is 23.8 h), green (initial chain value is 24.1 h), and blue (initial chain value is 24.7 h) dashed lines are the kernel densities. The black solid line is the normal prior. (B) The experimental phase shift data, phase shift data generated from average values from each initial chain group, and phase shifts generated with $\tau = 24.2$ h. The red (initial chain value is 23.8 h), green (initial chain value is 24.1 h), and blue (initial chain value is 24.7 h) stars are simulated phase shifts produced when the average τ values from the four MCMC runs is plotted. The experimental phase shift data are dark gray circles and the simulated phase shifts with $\tau = 24.2$ h are light gray triangles. (C) The samples value of each iteration of the Metropolis algorithm for twelve MCMC runs (four from each initial condition). The red (initial chain value is 23.8 h), green (initial chain value is 24.1 h), and blue (initial chain value is 24.7 h) lines are the sample values. (D) The percent of accepted samples from the twelve runs. The red (initial chain value is 23.8 h), green (initial chain value is 24.1 h), and blue (initial chain value is 24.7 h) squares are the percent of accepted samples per run

intersections between curves. These features of illuminance-response curves associated with varying τ values demonstrate that this type of data is a good candidate for identifying τ using MCMC parameter estimation.

In practice, illuminance-response curves are generated using data from multiple participants. Therefore, this approach does not provide information about an individual's intrinsic period, but, instead the mean intrinsic period for a group of study participants.

3.5.2 Illuminance-response curve test cases

We validated this methodology by applying the Metropolis algorithm to both single τ and multi-τ Illuminance-response curve synthetic data sets. Simulated phase shift data were generated using a single τ value or collection of τ values drawn from a normal distribution. For both test cases, our method produced mean estimates of the intrinsic period that were very close to the known τ value or mean τ value, respectively. To facilitate comparisons between runs, we reported estimates of τ with six significant figures. However, this is likely beyond the level of precision of τ estimates obtained experimentally using FD protocols [4]. Notably, these results were obtained using an uninformative prior. Although a more informative prior may be preferable when *a priori* information about the parameters is available, our results suggest that it is not necessary to impose assumptions on the prior to obtain accurate estimate for this problem.

The MCMC implementation was robust with respect to a range of implementation metrics. Over multiple trials, estimates of mean intrinsic periods have average standard deviations of less than .045 h, narrow 95% credible intervals, and similar kernel density plots. There was no evidence in any of the metrics that the mean estimates of τ were influenced by the initial chain value or assumptions on the prior. The average percent of accepted samples was between 41% and 46%, an acceptable range for MCMC methods [89]. Overall, these results support the applicability of MCMC methods to accurately estimate the mean intrinsic period of a group of study participants, given appropriate illuminance-response curve data.

3.5.3 Application to experimental data

When applied to the illuminance-response curve generated using 23 healthy adult participants, this method predicted a group intrinsic period of consistent with the mean τ reported for this population [4]. Specifically, the mean τ of 24.18 $\pm$ 0.04h estimated in a healthy young adult population [4] is very close to the group τ of the illuminance-response curve study participants which was estimated to be 24.27 or 24.26h using uniform or normal priors, respectively. The similarity of these estimates of group τ suggests that, for these data, a relatively uninformative prior (like $U(23.5, 25)$) produces similar results compared to a more informative prior (like $N(24.2, 0.2^2)$). Therefore, as discussed in the context of the synthetic data, although a more informative prior may be preferable when *a priori* information about the parameters is available, our results that an uninformative prior may be sufficient. This is an important feature for broader application of the method to illuminance-response data from study populations where there are no previous estimates of the intrinsic period.

As with the synthetic data, all metrics indicated that the MCMC implementation was robust. All of the runs implemented with either a uniform or a normal prior accepted between 41% and 45% of accepted samples. The mean estimates of group τ, percent of accepted samples, and credible intervals were similar across runs and were not affected by initial chain values. Overall, these results suggest that this method applied to illuminance-response curve data can be used to determine a reasonable estimate of the mean intrinsic period of a group of study participants.

3.5.4 Limitations

Mathematical models are powerful tools for interpreting data, making predictions, and informing experimental protocol design. However, models have underlying assumptions that may introduce model dependence in simulation results. The Forger circadian pacemaker model was selected for this study because it includes light processing, it has been fitted to healthy adult data, it has been widely used for many applications, and it includes τ as an

explicit parameter. Furthermore, the model was calibrated using data from populations generally consistent with our study population. However, using MCMC parameter estimation methods with this model to estimate a single parameter may not be appropriate for other demographic populations. For example, differences in light sensitivity as may occur in early childhood [90], adolescence [91], or with age [43] may alter Process L, thereby affecting the relationship between illuminance-response curve data and intrinsic circadian period. In future work, a multi-parameter MCMC approach could be used to investigate the relationship of multiple parameters (e.g., parameters affecting light sensitivity and intrinsic period) to illuminance-response curve data.

Although this method reliably detected the mean τ used to generate the multi-τ simulated illuminance-response curves, the standard deviations of the posterior distributions of τ did not reflect the standard deviations of the τ values used to generate the synthetic data. This suggests that group τ estimates will be robust to individual outliers, however, it also indicates that the posterior distribution does not describe the variability of the intrinsic periods represented within the participant group contributing to the illuminance-response curve data. This limits the interpretation of the group τ for potentially heterogeneous populations.

3.5.5 Conclusions and implications

We have developed a method to estimate the average intrinsic period, τ, of a group of study participants using a mathematical model of the human circadian pacemaker, the Metropolis algorithm, and illuminance-response curve data. We have validated this method using synthetic data and applied it to experimental data from healthy adults. Applying this approach to illuminance-response curve data from other populations, such as children or adults with circadian disorders, who are not good candidates for FD protocols, could contribute to understanding circadian properties in these populations. Furthermore, because illuminance-response curves collectively represent phase shifts from a group of individuals, this analysis yields novel insights about the intrinsic circadian period of the population

using existing data that reflect other circadian features of the individuals. Future work could extend this approach to other types of circadian data including PRCs. Improved understanding of circadian properties of a population may facilitate interpretation of existing data and inform circadian-based interventions ranging from light therapy to school start times.

3.6 Acknowledgements

This study was supported by the National Science Foundation grant DMS 1412571 and the National Institutes of Health grant ROIHD087707

3.7 Declaration of conflicting interests

The author(s) have no potential conflicts of interest with respect to the research, authorship, and/or publication of this article.

CHAPTER 4

PHASE RESPONSE CURVE (PRC) PARAMETER SENSITIVITY AND ADOLESCENT DATA

Paper in preparation.

Nora Stack, MS,* Stephanie Crowley, PhD,× Mary Carskadon, PhD,†,‡ and Cecilia Diniz Behn, PhD*,§, [3]

*Department of Applied Mathematics and Statistics, Colorado School of Mines, Golden, CO, USA, ×Division of Behavioral Sciences, Rush Medical College, Chicago, IL, USA †Sleep for Science Research Laboratory, Department of Psychiatry and Human Behavior, Alpert Medical School of Brown University, Providence, RI, USA, ‡Centre for Sleep Research, University of South Australia, Adelaide, South Australia, Australia and §Division of Endocrinology, Department of Pediatrics, University of Colorado Anschutz Medical Campus, Aurora, CO, USA

4.1 Introduction

Mathematical models of the human circadian pacemaker have been developed based on data from healthy adults. Although circadian pacemakers of other human populations (children, adolescents, the elderly, etc.) have some similar behavior to healthy adults, each population exhibits very unique behavioral characteristics (midday naps, phase delays, difficulty staying asleep, etc.) that mathematical models derived from healthy adult data struggle to describe. Specifically, throughout childhood and adolescence a number of changes to the circadian system have been observed. In early to mid-adolescence, it has been found that adolescents are more sensitive to light [91]. Additionally, adolescents experience a phase delay, meaning that adolescents want to go to bed later and wake up later compared to adults

[3]To whom all correspondence should be addressed: Cecilia Diniz Behn, Department of Applied Mathematics & Statistics, Colorado School of Mines, 1015 14th Street, Golden, CO 80401, USA; e-mail: cdinizbe@mines.edu.

[92] and may have a longer intrinsic circadian period (τ) [34]. This adolescent phase delay and the demands of school, extracurricular activities, and social factors all lead to a lack of sleep during the school week. During the weekends, adolescents then attempt to make up for this school week sleep debt by sleeping more on the weekends (recovery sleep) while also going to bed later [92]. Because adolescents stay up later, sleep longer, and wake up later during the weekend, they are shifting their circadian clocks causing a weekend phase delay. When they then have to switch back to a school day sleep/wake schedule on Sunday night for school early on Monday morning, this forces a circadian shift. This adolescent behavior is often described as "social jet lag" because when teenagers switch from the school week to weekend schedule (or vice versa) they often experience jet lag symptoms. Understanding social jet lag and creating interventions that could minimize the weekend phase delay while also allowing adolescents to get recovery sleep over the weekend could have a drastic effect on individual adolescents as well as societal policies, such as school start time. However, there could still be negative health outcomes associated with weekend recovery sleep [93].

Mathematical models of the circadian pacemaker have been valuable in protocol design but to be the most useful, they need to capture key features of the population whose behavior they are trying to replicate and predict. We conducted a parameter sensitivity analysis to determine how model parameters affected the circadian clock's response to light and identified parameter combinations producing observed adolescent responses from two light protocols from Crowley and Carskadon (2010) which will be described in the Materials and Methods [94]. Their experiment showed that Crowley et al. found that their TYPICAL protocol produced phase shifts of -45±31 minutes and their NAP protocol produced phase shifts of -41±34 minutes [94]. Additionally, we provide predictions of adolescent behavior under two other possible schedule interventions, specifically by simulating the LIGHT protocol used by Crowley and Carskason and their hypothesized NAP and LIGHT protocol. The participants in Experiment 1 (TYPICAL and NAP protocols) did not complete the LIGHT protocol. Crowley and Carskadon found that the LIGHT protocol participants experienced a phase

delay of -38±28 minutes.

4.2 Materials and methods

4.2.1 Experimental data

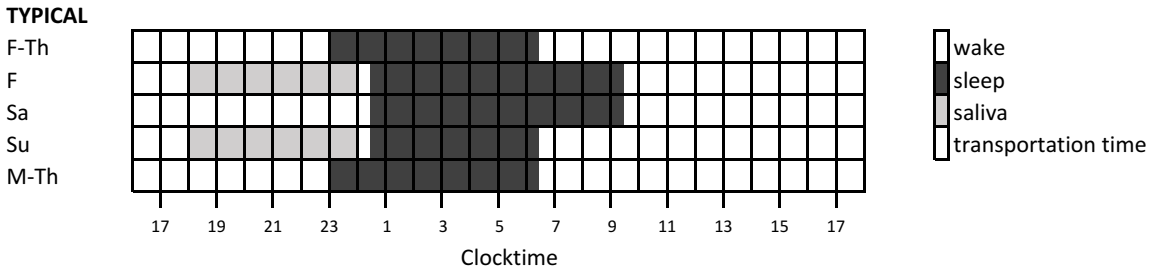

Figure 4.1: TYPICAL protocol used for Experiment 1 and for simulations.

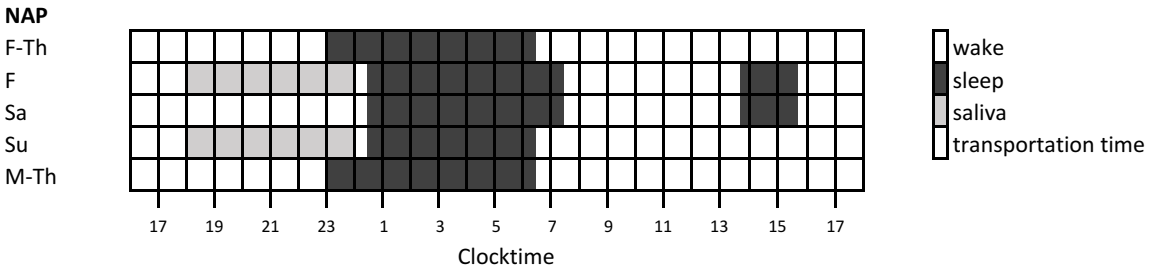

Figure 4.2: NAP protocol used for Experiment 1 and for simulations.

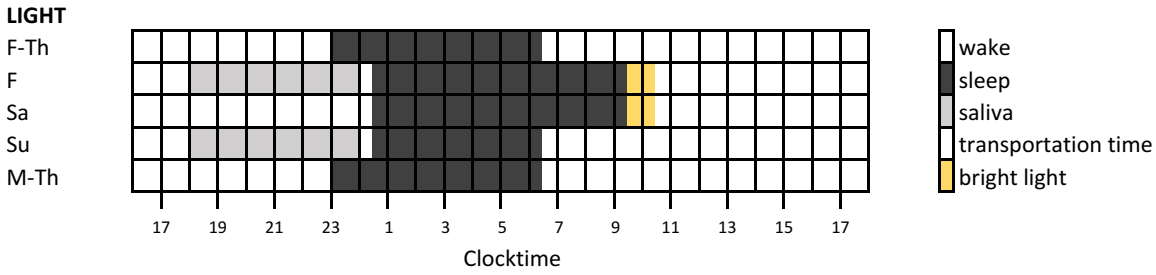

Figure 4.3: LIGHT protocol used for Experiment 2 and for simulations.

In 2010, Crowley and Carskadon conducted two experiments in healthy adolescents. Experiment 1 consisted of a TYPICAL protocol and a NAP protocol where salivary melatonin was used to assess phase shifts [94]. A marker of circadian phase is Dim Light Melatonin

Onset (DLMO) which was computed as occurring after melatonin was above 4 pg/mL. In the TYPICAL protocol, adolescents went to bed at 23:30 and woke up at 6:30 (weekday schedule) for seven days. For the next two days (Friday and Saturday) adolescents went to sleep at 00:30 and woke up at 9:30 for weekend recovery sleep. On Friday night, dim light conditions (<20 lux) are implemented to determine DLMO phase from 18:00 to 0:00. On the tenth day (Sunday), adolescents went to sleep at 00:30 and woke up at 6:30. On Sunday night, dim light conditions (<20 lux) are implemented again to determine DLMO phase from 18:00 to 0:00. For the next four nights, adolescents followed the weekday schedule (Figure 4.1).

The NAP protocol is similar to the TYPICAL protocol except that on the Friday and Saturday night of the protocol, adolescents went to bed at 00:30, woke up at 7:30, and took an afternoon nap from 13:45 to 15:45. On Friday and Sunday nights, DLMO was assessed as in the TYPICAL protocol (Figure 4.2).

Experiment 2 compared the TYPICAL protocol phase shifts from Experiment 1 and the phase shifts that occurred under the LIGHT protocol with different study participants. The LIGHT protocol followed the same light/dark timing as the NAP protocol except on the Saturday and Sunday. On there days is no midday nap and participants woke up at the same time as they did on the TYPICAL weekend. For the first hour they were awake, they experienced bright light. The hypothesized NAP+LIGHT has the same light/dark timing as the NAP protocol but subjects would experience an hour of bright light upon waking (Figure 4.3).

4.2.2 Model equations

The modified van der Pol-based circadian clock model proposed by Forger et al. has two components [14]. Process L describes the effect of light on the system while Process P represents the circadian pacemaker. Light enters the system in Process L and is then filtered into Process P where X is core body temperature and X_c is a complimentary variable.

Process L

$$\alpha(I) = \alpha_0 \left(\frac{I^p}{I_0^p} \right)$$

$$\frac{dn}{dt} = 60[\alpha(I)(1-n) - \beta n]$$

$$\hat{B} = G(1-n)\alpha(I)$$

Sensitivity Modulation

$$B = \hat{B}(1 - 0.4x)(1 - 0.4x_c)$$

Process P

$$\frac{dX}{dt} = \frac{\pi}{12}\left(x_c + B\right)$$

$$\frac{dX_c}{dt} = \frac{\pi}{12}\left[\mu\left(x_c - \frac{4x_c^3}{3}\right) - x\left[\left(\frac{24}{0.99669\tau}\right)^2 + kB\right]\right].$$

Table 4.1: Table of healthy adult parameters for the Forger model.

Parameter	Original Value
α_0	0.05/min
I_0	9500 lux
p	0.5
β	0.0075/min
G	33.75 min
k	0.55
μ	0.23
τ	24.2 h

See Table 4.1 for the original parameter values for the model of a healthy adult. Minimum core body temperature is a marker of circadian phase and can be used to determine the phase shifting effects of light, similarly to DLMO. In the model, minimums of X correspond to minimum core body temperature (CBT_{min}).

4.2.3 Schedules

To determine a range of parameter values that produce model behavior consistent with observations in adolescents, we simulated published experimental protocols, and computed the resulting phase advances and delays, and compared simulated results to observations in adolescents [94]. In previous work,the TYPICAL, NAP, and LIGHT protocols were developed by Crowley and Carskadon and two experiments were conducted. The first experiment consisted of the TYPICAL and the NAP protocol and the second was the TYPICAL and the LIGHT protocol. These protocols were developed to quantify weekend phase delays in adolescents and investigate ways to possibly minimize this delay [94].

For all protocols simulations assume 500 lux of light during waking hours, 20 lux during the time of DLMO assessment, and 3704 lux for bright light exposure in the LIGHT protocol. Phase shifts were computed on Thursday night (Friday morning) and Sunday night (Monday morning) using CBT_{min}.

4.2.4 Assessing parameter sensitivity using Parameters and PRCs

Since the propensity for phase delays and an increased sensitivity to light, particularly in the evenings, are key features of adolescent sleep, we analyzed the role of model parameters as they affect these features.

To assess the propensity for phase delay, one cycle Phase Response Curves (PRCs) were simulated. PRCs were computed based on a protocol described by Jewett and colleagues [39]. A $\sim$ 40 hour constant routine (CR) at 150 lux is followed by 8 hours of darkness at 0 lux. Then light is set to 150 lux except during an $\sim$ 5 hour bright light pulse of 9500 lux that occurs at the same clock time for one day (or cycle). Participants then are in darkness for another 8 hours followed by another $\sim$ 40 hour CR (Fig 2). Phase shifts are calculated as the difference between the CBT_{min} assessed during the first $\sim$ 40 hour CR and the CBT_{min} assessed during the second CR following the bright light pulse. Negative phase shifts indicate phase delays and positive phase shifts indicate phase advances.

The model parameters were varied to examine the effect of changing each parameter on the PRC. The five metrics used were the difference from the baseline PRC of the maximum phase shift, initial phase of maximum phase shift, minimum phase shift, initial phase of minimum phase shift, and difference between the maximum and minimum phase shift (amplitude).

4.2.5 Adolescent data and parameter regimes

From the sensitivity analysis of the PRC, the four parameters that had the greatest overall effect were identified. These Key parameters were then used in simulations of the TYPICAL and NAP protocols. The parameter pairs that produced general behavioral features (phase delay lessened vs. lengthened with the NAP) were examined. Additionally, the subjects from Crowley and Carskadons study were clustered using k-means clustering based on their TYPICAL and NAP phase shifts. Parameter pairs that produced behavior consistent with particular groups of data within 10 minutes of the mean for each cluster were also found. Additionally, analysis of combinations of three parameters were investigated. Furthermore, candidate parameter pairs were identified that produce individual subject behavior. For all parameters except τ, a range of values between $\pm 10\%$ of the baseline parameter value were used. Because $\pm 10\%$ of the intrinsic period, τ, included parameter values outside was set to the reported physiological range of healthy intrinsic periods of τ, we limited the range of τ to 23.5 h to 25 h to reflect physiologically-relevant intrinsic periods [31, 32].

4.2.6 LIGHT protocol and NAP+LIGHT protocol prediction

Simulations for both Experiment 2 and the NAP+LIGHT protocol were run with the same lux levels as described previously. The six candidate parameter pairs for each group that simulated the TYPICAL and NAP behavior closest to the mean of each cluster were used to make predictions about the effectiveness of the LIGHT protocol and the NAP+LIGHT protocol.

4.2.7 Implementation

All simulations were completed using MATLAB (Mathworks, Natick, MA) using the built-in solver **ode45** and the default tolerances. The function **findpeaks** from the Signal Processing Toolbox was used to identify minima and the function **kmeans** was used to determine the number of data clusters.

4.3 Results

4.3.1 Study Demographics

In Experiment 1 there were ten subjects (four boys) between the ages of 15.55-16.66 years (mean ± SD: 16.06±0.369 years). Of the ten participants, eight were White/Caucasian, one participant was Black/African, and one participant was a race not specified (selected other).

4.3.2 PRC parameter sensitivity

To determine the parameter sensitivity of multiple Phase Response Curve (PRC) metrics, the model parameters were varied by ±10% to examine the effect of changing each parameter. The five metrics used were the difference from the baseline PRC of the maximum phase shift, initial phase of maximum phase shift, minimum phase shift, initial phase of minimum phase shift, and difference between the maximum and minimum phase shift. Using these metrics, we identified six parameters that resulted in $> 50\%$ difference from baseline (τ, G, k, p, β, s_2). Of this set, we focused on τ, G, k, and $p.\beta$ and s_2 were eliminated from consideration because the remaining parameters had physiological interpretations and the PRC was more sensitive to them. The remaining four parameters were τ, G, k, p (Figure 4.4). The parameter τ is the intrinsic oscillator period, G is a scaling rate of the increase for the integral of cumulative drive, k is related to amplitude suppression and Aschoff's rule [14–17], and p was derived from the slope of the fitted line of the log-log plot of I (light) and α (the drive rate) values [17].

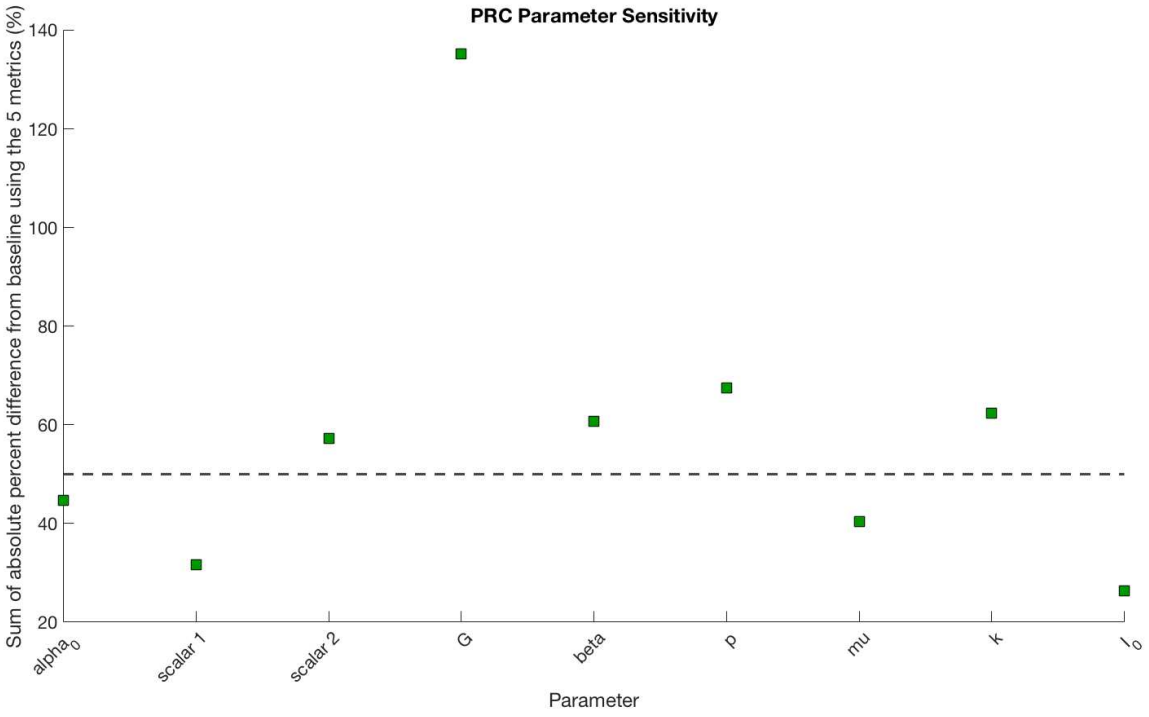

Figure 4.4: The summation over the five sensitivity metrics of the absolute percent differences from baseline. The dashed gray line indicates 50%. Six parameters were $> 50\%$: τ, G, k, p, β, s_2.

4.3.3 Adolescent data and k-means clustering

Using k-means clustering, the ten participants in the TYPICAL and NAP experiment were divided into four groups identified based on the elbow method (Figure B.1, Figure 4.5). We focused on the groups involving at least three participants. For the four subjects in Group 1 (Group N for a positive reaction to the NAP protocol), the weekend phase delay observed under the TYPICAL protocol was lessened by the NAP protocol. Conversely, the weekend phase delay of the three subjects in Group 2 (Group T for a positive reaction to the TYPICAL protocol) increased under the NAP protocol compared to the TYPICAL protocol. For Group N, the TYPICAL protocol produced an average phase delay of -58.5 m ($\pm$ 21.71 m) while the NAP protocol lessened the delay to an average of -11.40 m ($\pm$ 15.21 m). The phase delay produced by the TYPICAL protocol for the Group T subjects was -11.8 m ($\pm$ 16.97 m) and the subjects experienced a phase delay of - 36.20 m ($\pm$10.29 m).

Demographic information about the subjects was also considered to identify potential demographic similarities within the clusters. Sex, age, race, and month of the beginning of the protocol were considered (Figure B.2, Figure B.3, Figure B.4). Group N had two females and two males with a mean age of 15.9103 ($\pm$0.4265) years. Group T had two females and one male with a mean age of 16.3616 ($\pm$0.2825) years. All of the subjects in Group N were white/Caucasian. The male subject in Group T was black/African and the females were white/Caucasian. All subjects in Group T began the protocol in October. Half of the participants in Group N began the protocol in October and the other half began the protocol in January. From the demographic information, no demographic distinctions between Group N and Group T account for the differences in the data.

4.3.4 Parameter pairs and triplets

We varied all the parameters by $\pm$10% of the baseline value (k, μ, p, G I_0, α_0, s_1, s_2, β) or over a physiological range (τ) to define our candidate parameter space. The relative increments of all parameters were identical, so all vectors representing parameter ranges

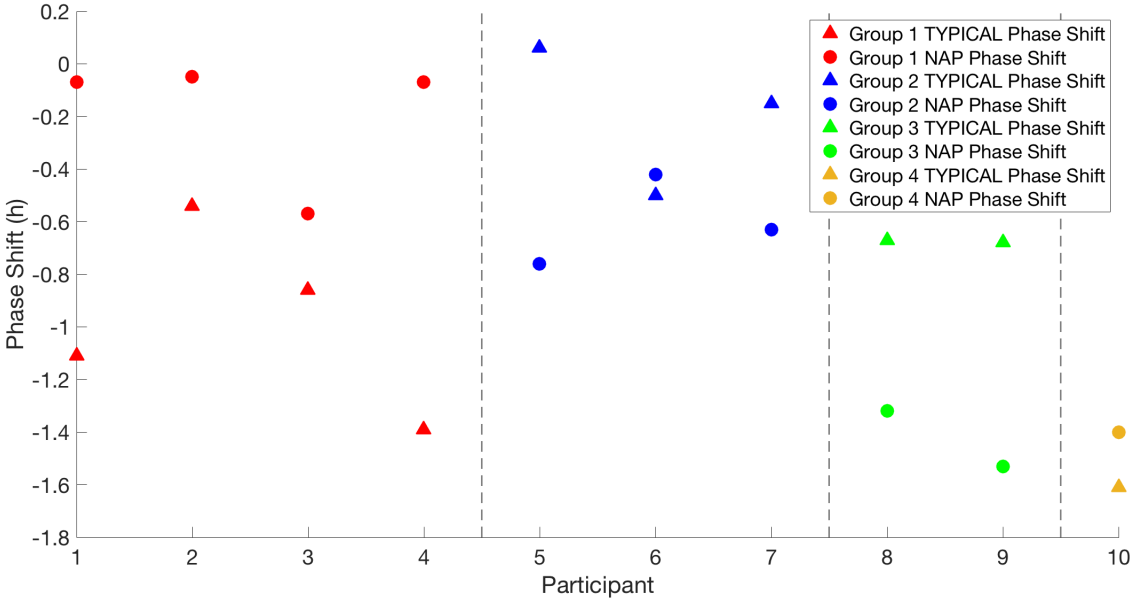

Figure 4.5: K-means clustering of study participants and their phase shifts. Each subject's TYPICAL phase shifts (triangles) and NAP phase shifts (circles) are shown. Participants were clustered into four groups (Group 1: red, Group 2: blue, Group 3: green, Group 4: yellow). The vertical dashed gray lines indicate the separation between different clusters. Two groups have more than three participants.

were are the same length. All 6 pairwise combinations of parameters produced both an increased phase delay with the NAP protocol and a decreased phase delay with the NAP protocol within their ranges. Similarly, all tested parameter pair ranges could simulate both Group N and Group T behavior within ten minutes of the means of the data. Clustering of parameter pairs for both groups was present in the combination of τ and the other three parameters, but when G, k, and p were paired together they failed to produce clustering of eligible parameter pairs for both groups (Figure 4.6). When examining triplets, when τ is on the x-axis similar trends to the pairwise analysis is present (Figure 4.7). Group T behavior is consistently simulated within 10 minutes of the means with τ values near either 24 h or 25 h. By contrast, parameters that simulate Group N behavior consistently lie between the τ values that produce Group T behavior. We also investigated the ability of pairwise changes to parameters to simulate an individual participant's responses to the TYPICAL and NAP protocols with 10 minutes. By contrast with the group behavior, some parameter pairs could not successfully replicate every individual's behavior (Figure 4.8).

4.3.5 LIGHT protocol and NAP and LIGHT protocol prediction

The six candidate parameter pairs that most closely simulated Group 1 behavior were comprised of τ, p, and k (Table 4.2). Using these candidate parameter pairs, we simulated phase shifts under the LIGHT and the NAP+LIGHT protocols. The predicted LIGHT and NAP+LIGHT phase shifts were all smaller than the average TYPICAL phase shifts for Group N. The LIGHT phase delays were all larger than the phase shifts experienced under the NAP protocol. Four of the candidate parameter pairs predicted that the NAP+LIGHT protocol produced phase shifts closer to zero than the average NAP phase shift. One candidate pair produced a phase advance larger than the average nap phase delay.

The predicted LIGHT phase shifts for Group T were close to the average phase shift under the TYPICAL protocol for five of the six candidate pairs (Table 4.3). Three of the candidate parameter pairs predicted that a greater improvement with the NAP and LIGHT protocol. However, the NAP+LIGHT protocol was not predicted to be better than the

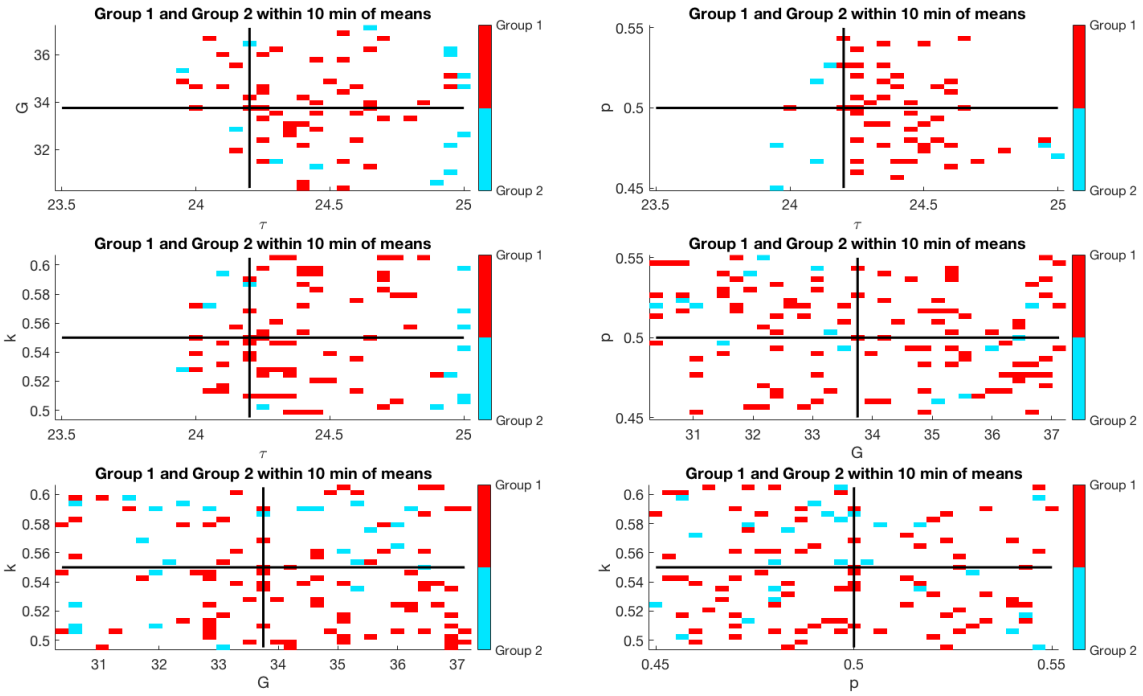

Figure 4.6: Pairs of parameter (τ, G, k, and p) that simulated Group N (Group 1, red) and Group T (Group 2, blue) behavior within 10 minutes of the mean phase shifts of each group. Black lines indicate baseline parameter values.

Table 4.2: The six best candidate pairs that produced the smallest absolute difference between the TYPICAL and NAP phase shift data from Group N (Group 1) and the model simulations. The predicted LIGHT phase shifts and predicted phase shifts from the NAP+LIGHT protocol.

Par 1	Par 2	Abs Difference from TYP & NAP data	Predicted LIGHT PS	Predicted NAP +LIGHT PS
$\tau = 24.2500$	$k = 0.5243$	0.9011 m	-48.6602 m	-13.1921 m
$p = 0.4867$	$k = 0.5060$	1.2137 m	-24.2346 m	-11.2715 m
$p = 0.5433$	$k = 0.5133$	1.8120 m	-29.7473 m	12.1011 m
$p = 0.4833$	$k = 0.5317$	1.9662 m	-33.2132 m	-6.3256 m
$\tau = 24.3000$	$p = 0.5033$	2.1425 m	-35.1048 m	0.2927 m
$\tau = 24.4000$	$k = 0.5977$	2.2540 m	-28.9692 m	-9.0209 m

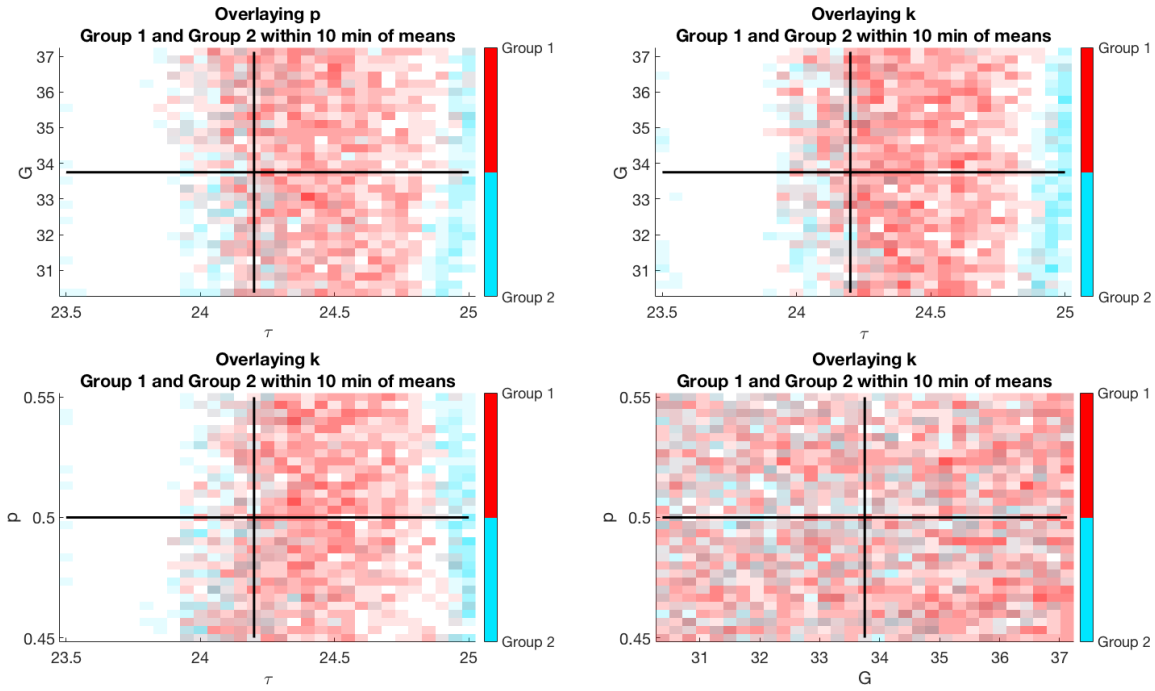

Figure 4.7: Pairs of parameter (τ, G, k, and p) that simulated Group N (Group 1, red) and Group T (Group 2, blue) behavior within 10 minutes of the mean phase shifts of each group. Black lines indicate baseline parameter values. A darker color indicates a parameter pair that produced a group's behavior multiple times with respect to varying a third parameter.

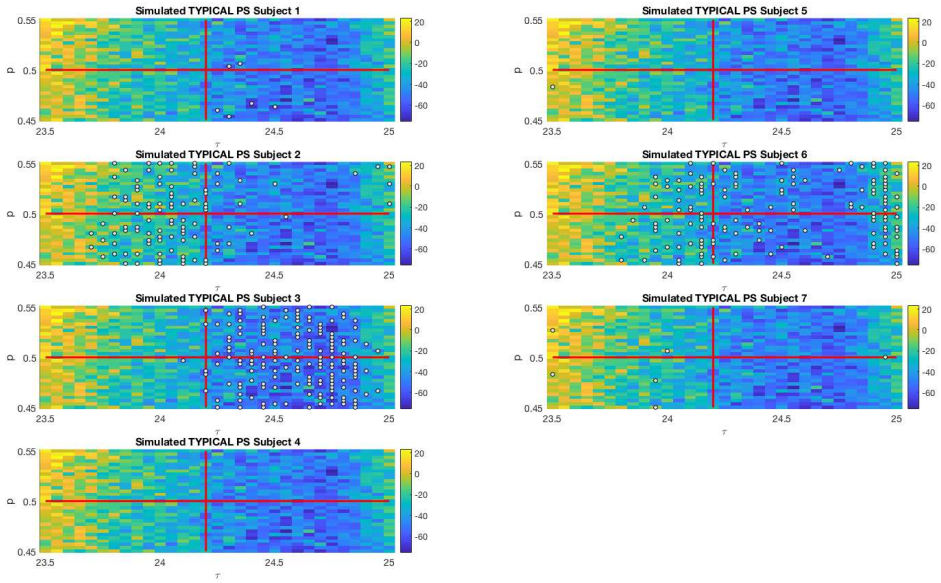

Figure 4.8: Simulations of the TYPICAL protocol varying τ and p. Gray circles indicate parameter pairs that produced behavior within 10 minutes of each subject's phase shift. The red lines indicate baseline parameter values. The color bar indicates the TYPICAL phase shift value.

average NAP protocol alone with any of the candidate pairs.

Table 4.3: The six best candidate pairs that produced the smallest absolute difference between the TYPICAL and NAP phase shift data from Group T (Group 2) and the model simulations. The predicted LIGHT phase shifts and predicted phase shifts from the NAP+LIGHT protocol.

Par 1	Par 2	Abs Difference from TYP & NAP data	Predicted LIGHT PS	Predicted NAP +LIGHT PS
$p = 0.4967$	$k = 0.5830$	2.0082 m	-41.4073 m	-16.0695 m
$\tau = 24.9500$	$G = 32.1750$	2.5989 m	-37.0014 m	-36.8422 m
$p = 0.5300$	$k = 0.5463$	3.5991 m	-65.7860 m	-27.1468 m
$\tau = 25.0000$	$G = 34.6500$	4.0677 m	-37.3976 m	-31.1057 m
$G = 35.5500$	$p = 0.4633$	4.0749 m	-43.5479 m	-15.2145 m
$G = 35.1000$	$k = 0.5610$	4.2670 m	-41.3621 m	-19.2554 m

4.4 Discussion

4.4.1 Identifying parameters

The four parameters that the PRC is most sensitive to are τ, G, k, and p. The parameter that has the most effect on the PRC is τ, the intrinsic oscillator period. In this model, G is a rate parameter for the integral of the cumulative drive while k is related to amplitude suppression and Aschoff's rule [14, 17]. Lastly, the value of p was derived from the slope of the fitted line of a log-log plot of light intensities (I) and α values. The data used to estimate both τ and p were from healthy adults and there has been evidence that adolescents may have a different intrinsic period than adults [34]. From the five metrics, the sum of absolute percent difference from baseline when setting τ equal to 23.5 and 25 was 406.01% whereas all other parameter values had a sum of absolute percent difference less than 150%. The amount of amplitude suppression that adolescents experience is unknown. Similarly, the rate of the cumulative drive is adolescents has not been investigated. These parameters have physical interpretations that may help to identify why the adolescent circadian pacemaker has distinct behavior and characteristics.

4.4.2 Clustering, parameters, and heat maps

There are two groups that include at least three participants: Group N and Group T. These groups experience opposite behavior in Experiment 1. The participants in Group N have a reduction in their weekend phase delay with the NAP protocol while Group T experienced a no distinct improvement or worsened phase delay under the NAP protocol when compared to each participant's phase shifts from the TYPICAL protocol. Group N participants experiences a large average phase delay on the TYPICAL protocol while Group T experienced a small average phase delay for the same protocol. Group N's response was consistent with the response hypothesized by the authors, and this behavior can be replicated within ten minutes of the means of both the TYPICAL and NAP protocols by adult parameter values (-50.0005 minutes and -7.6874 minutes, respectively). However, this response was only observed in a small subset of adolescent participants. There were more candidate parameter pairs over the six parameter combinations that replicated Group N behavior compared to Group T behavior. Group T had fewer candidate parameter pairs.

Although differences in circadian features have been noted between different sexes and races [31–33], the participants in Group N and Group T did not show any clear demographic differences. Group N has two females and two males with a mean age of 15.9103 ($\pm$0.4265 years). Group T has two females and one male and a mean age of 16.3616 ($\pm$0.2825 years). All of the participants in Group N are White/Caucasian. In Group T, both female participants are White/Caucasian and the male participant in Black/African. Additionally, most subjects in Groups N and T began the study in October. Because there were no demographic distinctions between the groups, we suspect that there may be physiological differences in the circadian pacemaker that led to the distinct reactions to the protocols between the two groups.

Interestingly, the τ clustering is similar over the other three parameters. For Group N, candidate parameter pairs are focused between 24 h and 24.9 h while Group T behavior is replicated with either smaller τ values around 24 h or large τ values around 25 h. This

analysis is consistent when the triplets are considered as well. For parameter pairwise combinations that do not include τ, there is some clustering for the pair (G, k) for Group T. Specifically, for k values between 0.58 and 0.6 we see almost a line of potential parameter pairs across the values of G. We do not see clustering behavior with parameter combinations of G, k, and p for Group N.

The response to the TYPICAL and NAP protocols of individual participants in Group N and T were also investigated. For each participant, we identified parameter values that replicated the individual's behavior within 10 minutes. Similar to the group analysis, we found that there were more candidate parameter pairs for individuals in Group N. We also saw similar clustering in individuals in Group N and Group T, respectively. Study participants in Group N tended to have candidate parameter pairs in one distinct cluster while some Group T subjects have two clusters. Unlike the group analysis to simulate an individuals behavior there were parameter combinations that produced no viable candidate pairs.

4.4.3 Prediction

The best candidate pairs for Group N and Group T yielded very different predictions under Experiment 2 and the proposed NAP & LIGHT protocol. The average of LIGHT phase shift predictions for Group N and Group T were -33.3216 ($\pm$ 8.3995) m and -44.4170 ($\pm$ 10.7707), respectively. While the average phase shifts under the NAP and LIGHT protocol were -4.5694 ($\pm$ 9.4203) m for Group N and -24.2723 ($\pm$ 8.8029) m for Group T. For Group N, the combination of the NAP+LIGHT protocol lessens the average phase delay better than the NAP protocol while the average phase shift of the LIGHT protocol is predicted to not be able to reduce the weekend phase delay better than the NAP protocol. The average phase shift under NAP+LIGHT protocol was predicted to be an improvement in phase delay for Group T, however it was still larger than the delay experienced under the TYPICAL protocol. The LIGHT protocol also produced an average phase shift that was larger than the phase shift experienced under the NAP protocol. These predictions suggest that for some adolescents the NAP+LIGHT protocol will be effective in mitigating social

jet lag in adolescents but for other adolescents a midday NAP is the best way to combat a weekend phase delay.

The best candidate parameter pairs to simulate Group N behavior do not contain any parameter changes to G. The intrinsic period, τ, is in three candidate pairs and in every case, τ is larger than the average adult's intrinsic period of 24.2 h. For Group T, when τ is in two of the six best candidate pairs. In both cases, τ is significantly larger than 24.2 h and larger than the τ values in the best candidate pairs of Group N. This distinction as well as the clustering from the pairs and triplets analysis may indicate that between Group N and Group T, τ may be a parameter that is distinctly different between the groups.

When Experiment 2 was conducted, Crowley and Carskadon found a phase delay of -38 ($\pm$ 28) m in different adolescent subjects. The observed phase delay was almost identical to the average phase delay over the twelve candidate pairs from Group N and Group T of -38.8693 ($\pm$ 10.8801) m. This agreement was an interesting discovery that demonstrated the similarities between the predictions for Group N and Group T subjects and the subjects in Experiment 2.

4.4.4 Conclusions

These results demonstrate that inter-individual differences in properties of the circadian system may drastically affect responses to different schedules which has implications for possible interventions to minimize "social jet." Furthermore, these results provide insights into the underlying reasons for differences in adolescent responses under the same protocols and predict responses in different groups to potential methods to minimize social jet lag.

CHAPTER 5

CONCLUSIONS AND FUTURE WORK

This chapter describes two extensions of work that was previously discussed in Chapters 3 and 4. The chapter will conclude with a summary of the completed work from Chapters 2, 3, and 4.

5.1 Future Work: Estimating Human Intrinsic Periods with Phase Response Curves (PRCs)

5.1.1 Introduction

An extension of the work in Chapter 3 is to implement MCMC parameter estimation algorithms on Phase Response Curve (PRC) data. There are many different types of PRCs that have been completed and therefore numerous datasets [39, 40, 44, 46–48]. These preliminary results demonstrate that this approach has shown promise as a way to extract information about intrinsic periods from synthetic PRC data.

5.1.2 Methods

5.1.2.1 Forger Model and MCMC Implementation

To estimate average intrinsic period in a group of study participants using PRC data a methodology similar to that of Chapter 3 was implemented. The same mathematical model by Forger and colleagues was implemented [14]. Additionally, the MCMC framework is as described in Chapter 3. Simulations were completed with runs of 5,000 iterations from the initial chain values of τ =24.1 h. No burn-in was considered for this analysis.

5.1.2.2 Phase Response Curve Protocol

The PRC protocol was adapted from the PRCs derived by Jewett and colleagues [39]. For two weeks prior to the in-lab portion of the protocol a consistent light:dark (LD) schedule was maintained. This schedule was 16 h of light (150 lux) and 8 h of darkness (0 lux)

from midnight to 0800. Once the in-lab portion begins, an ∼40 h constant routine (CR) is simulated at 10 lux. Following the CR, there is an 8 h period of darkness (0 lux) followed by just over 5 h at 150 lux, then just under 6 h of bright light at 9500 lux. After the bright light exposure, there is another 5.1 h at 150 lux followed by an 8 h period of darkness. There is then another ∼ 40 h constant routine, after which the protocol ends (Figure 5.1).

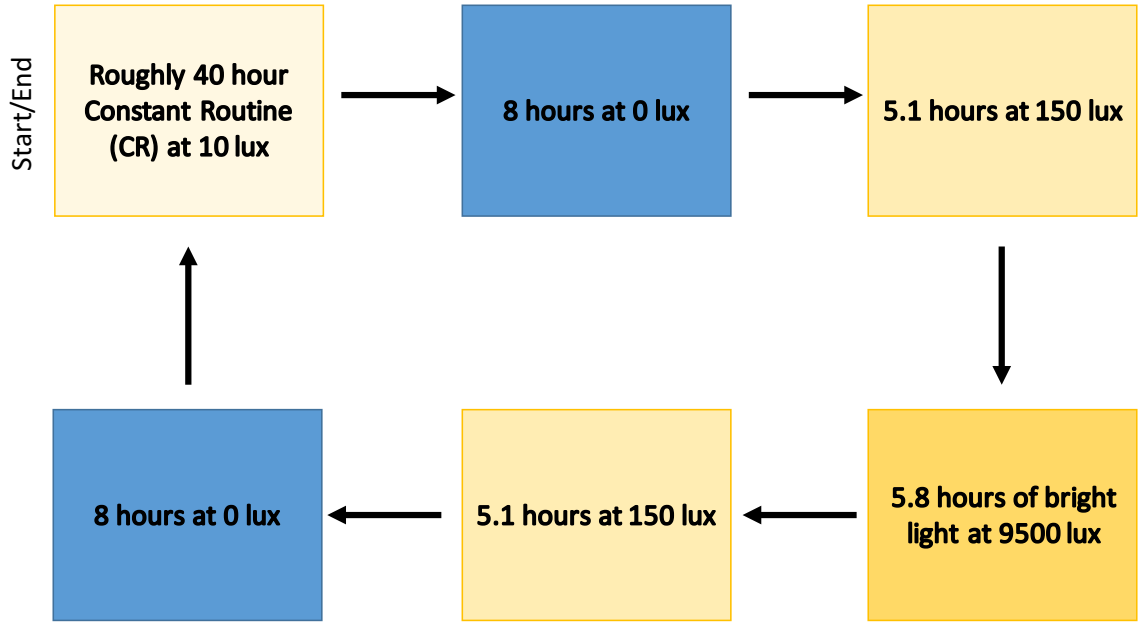

Figure 5.1: Schematic of the PRC protocol and simulation implementation used for parameter estimation of τ.

5.1.2.3 Synthetic PRC Data

Synthetic phase shift data was produced from known τ values. We considered two different types of synthetic data: single τ PRC data and multi-τ PRC data. Single τ PRC data were generated with one τ value. This case is useful as a simple test case but is not realistic because every data point is generated from the same intrinsic period value. Conversely, multi-τ data is generated with τ values drawn from known distributions. Preliminary results will be presented for synthetic single τ data with τ =23.7, 24.2, and 24.6 h and multi-τ data generated with τs drawn from $N(24.2, 0.15^2)$.

For single τ PRCs, data points were assumed to each be normally distributed with 0.2 h standard deviation. The multi-τ data points were also assumed to each be normally distributed with 0.5 h standard deviation.

5.1.3 Preliminary Results and Discussion

5.1.3.1 Structure of PRC

When the PRC protocol is simulated with increasing τ values the shape of the curve is maintained but the curves are shifted down (Figure 5.2). Larger τ values produce large negative phase shifts (phase delays) and smaller positive phase shifts (phase advances). Therefore PRCs with different τ values are distinct from each other. This structure suggests that PRC data may work well with MCMC parameter estimation.

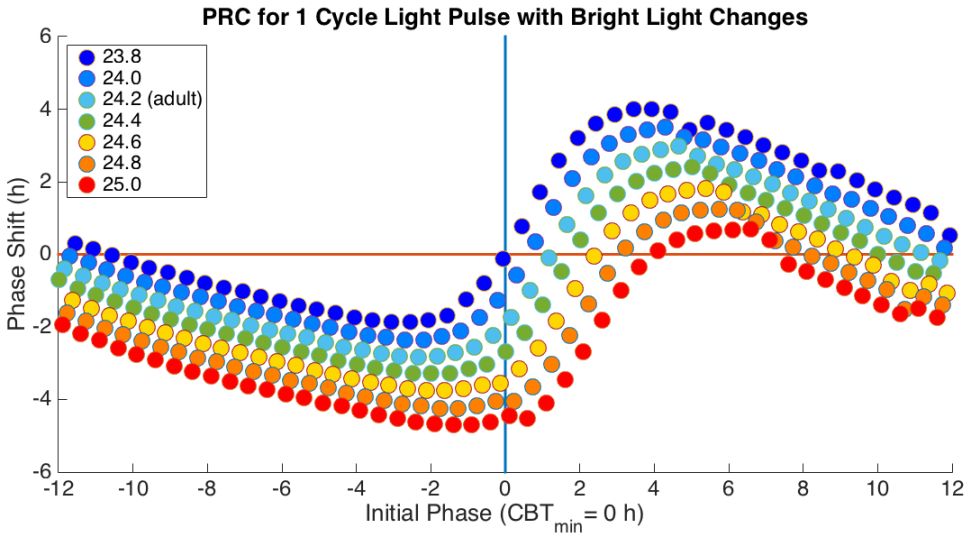

Figure 5.2: Simulated PRC curves with varying values of the intrinsic period τ. With increasing τ values, the shape of the PRC is maintained but the curves are shifted down, therefore increasing phase delays (negative phase shifts) and decreasing phase advances (positive phase shifts).

5.1.3.2 Synthetic Data

Single τ PRC data was generated from τ =23.7, 24.2, 24.6 h (Figure 5.3). Means produced from the four MCMC runs are very close to the true τ values (Table 5.1). For τ =24.6, the

mean is larger than the true value and there is a more deviation in the kernel densities.

Mutli-τ PRC data was generated from $N(24.2, 0.15^2)$ (Figure 5.4). There is good agreement between the MCMC runs. When the means from the MCMC runs are compared to the true τ mean, there is a difference of less than 0.05 h (Figure 5.4). The mean intrinsic period of the four runs was 24.1692 h.

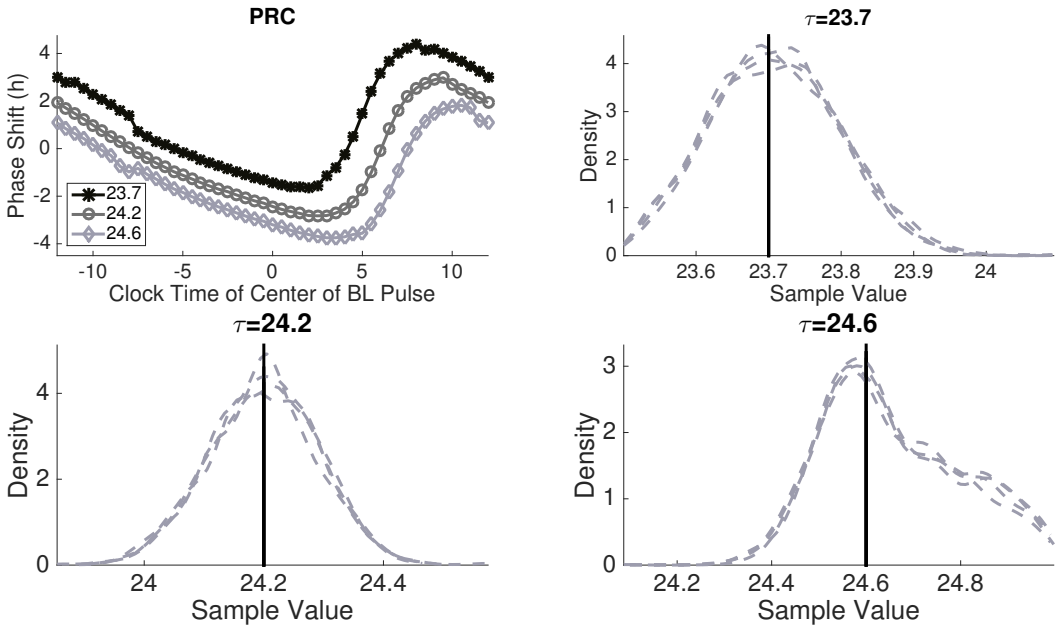

Figure 5.3: Synthetic PRC data and kernel densities of four MCMC runs. (A) Synthetic single τ PRCs for $\tau = 23.7$ (black stars), 24.2 (gray circles), 24.6 h (light gray diamonds). (B-D) Kernel densities of four MCMC runs from the initial chain value $\tau = 24.1$ h (dashed gray lines). Black solid lines indicated the τ value that was used to generate the synthetic single τ PRC.

Table 5.1: MCMC estimates of τ from single τ PRC data. Mean estimates of the average intrinsic period from four MCMC runs starting from the initial chain value $\tau = 24.1$ h.

τ used to generate PRC data	Average of all runs
τ =23.7 h	23.7085 h
τ =24.2 h	24.1997 h
τ =24.6 h	24.6574 h

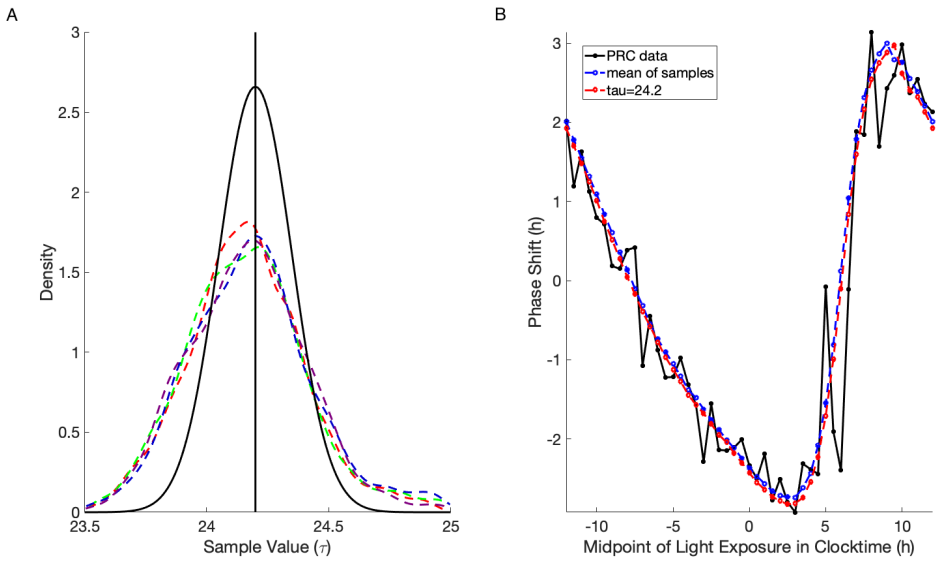

Figure 5.4: (A) Kernel densities of four MCMC runs with τs drawn from $N(24.2, 0.15^2)$. The dashed lines indicate densities from MCMC runs. The black vertical line denotes τ=24.2 and the black curve is the $N(24.2, 0.15^2)$ distribution. (B) Synthetic multi-τ PRC data ($N(24.2, 0.15^2)$) used for runs (black), PRC data generated with the mean of four run (blue), and simulated PRC data generated from τ =24.2 h (red). The mean of the four runs was 24.1692 h.

5.1.4 Future Directions for PRC and MCMC Parameter Estimation

There are ways that we can improve our implementation of the Metropolis algorithm in the future. For example, we can increase the number of iterations per run, incorporating burn-in, and start runs from different initial chain values.

The results from single τ and multi-τ synthentic data indicate that MCMC parameter estimation has promise in estimating average group intrinsic period. In the future, we would like to continue to explore this application of MCMC parameter estimation to PRCs. The next step is to continue to fine tune the application of the Metropolis algorithm. Then we would like to validate the approach on experimental PRC data to estimate the average intrinsic periods of a group of study participants. An additional extension of the current work would be to include initial phase (timing of light relative to an individual's CBT_{min}) in the statistical analysis. Exploiting the underlying relationship between τ and PRCs could produce more information about populations who have completed PRC protocols but not forced desynchrony protocols.

5.2 Future Work: Active Subspace Analysis of a Human Circadian Pacemaker Model

5.2.1 Introduction

To gain new information about the global parameter sensitivity of a widely used phenomenological human circadian pacemaker model we used active subspace analysis [95, 96]. In collaboration with Paul Diaz, MS[4], we identified the main quantity of interest (QoI) to be average amplitude; under multiple lighting conditions, we seek to determine what parameters were the most and least influential on the QoI. With this new understanding about the underlying dynamics of the parameters of the model, we hope to establish a framework to identify parameters that influence behavior from various populations and identify parameters with minimal effect on the QoI.

[4]Department of Aerospace Engineering, University of Colorado Boulder, Boulder, CO, USA

5.2.2 Methods

5.2.2.1 Circadian Pacemaker Model

For this analysis, we will be using the Forger model described in Chapters 3 and 4 [14]. This model is part of a family of phenomenological circadian pacemaker models based on modified van der Pol oscillators with two components Process L for light and Process P for the pacemaker [14, 14, 15]. Time dependent light enters the model as I in Process L [14, 17]. The effect of light is captured in the sensitivity modulation function that is incorporated into Process P [14].

5.2.2.2 Active Subspace Analysis

Active subspace analysis was completed using the framework established by Constantine [95] and Constantine and Diaz [96]. Let $\mathbf{x} = [x_1, \ldots, x_m]^T$ be the model parameters and $f(\mathbf{x})$ be a scalar-valued quantity of interest (QoI). For this analysis the parameter ranges must be scaled to be in $[-1, 1]$. Thus $f(\mathbf{x})$ is defined on an m-dimensional hypercube such that $\mathbf{x} = [x_1, ..., x_m]^T \in [-1, 1]^m$ where the uniform density function is $\rho(\mathbf{x}) = 2^{-m}$ for $\mathbf{x} \in [-1, 1]^m$ and zero elsewhere. To determine an active subspace the eigenpairs of the following $m \times m$ matrix are needed

$$\mathbf{C} = \int \nabla f(\mathbf{x}) \nabla f(\mathbf{x})^T \rho(\mathbf{x}) d\mathbf{x} = \mathbf{W} \Lambda \mathbf{W}^T$$

where $\mathbf{W} = [\mathbf{w_1}, ..., \mathbf{w_m}]$ is the orthogonal matrix of eigenvalues and the diagonals of Λ are the eigenvalues of C in decreasing order. The eigenvalues and eigenvectors satisfy

$$\lambda_i = \mathbf{w}_i^T \mathbf{C} \mathbf{w}_i = \int (\nabla f(\mathbf{x})^T \mathbf{w}_i)^2 \rho(\mathbf{x}) d\mathbf{x}.$$

According to the above equation, an eigenvalue, λ_i, is equal to zero if and only if f is constant along the direction $\mathbf{w}_i$. If this is the case, then the parameter space dimension can be reduced for further parameter studies.

Suppose that there is a sufficiently large gap between λ_n and λ_{n+1} for some $n < m$. Then Λ and $\mathbf{W}$ can be partitioned such that

$$\Lambda = \begin{bmatrix} \Lambda_1 & \\ & \Lambda_2 \end{bmatrix}$$

and $\mathbf{W} = [\mathbf{W}_1, \mathbf{W}_2]$ where Λ_1 contains the first n eigenvalues and $\mathbf{W}_1$ contains the corresponding first n eigenvectors. The n-dimensional active subspace is defined as the column-span of $\mathbf{W}_1$.

To estimate the matrix $\mathbf{C}$, a Monte Carlo approach is used. For $i = 1, ..., M$, each sample $\mathbf{x}_i$ is drawn according to $\rho(\mathbf{x})$ and the following is computed:

$$C \approx \hat{C} = \frac{1}{M} \sum_{i=1}^{M} \nabla f_i \nabla f_i^T = \hat{\mathbf{W}} \hat{\Lambda} \hat{\mathbf{W}}^T.$$

Finite difference approximations were used to calculate $\nabla f(\mathbf{x})$. For this approximation, M=10000 independent samples were used.

To measure the sensitivity of a QoI to parameters, the activity score

$$\alpha_{act}(n) = \sum_{j=1}^{n} \lambda_j w_j^2,$$

where $n \in [1, m]$, is used. When $n = m$, the activity score is a measure of global sensitivity that can be interpreted as a truncation of a derivative based sensitivity metric defined by Sobol' and Kucherenko [96, 97].

5.2.2.3 Parameter Ranges

Original parameter values were determined through multiple iterations of the family circadian pacemaker model based on modified van der Pol oscillators [14, 15, 17]. The parameter ranges for active subspace analysis were chosen to reflect the intuition and meaning of the parameter while not overly restricting parameters to fit adult data (Table 5.2). Parameter ranges for α_0, β, μ, and τ were determined based on data while ranges for G, k, p were determined from simulations.

α_0 and β: The drive rate (α_0) and the backwards regeneration constant (*beta*) values were determined from adult data in the model by Kronauer and colleagues. Parameter ranges for α_0 and β were identified from the ranges considered by Kronauer et al. [17].

$\underline{p}$: In the Kronauer et al. model, the value of p was the slope of the fitted line to a log-log plot of I and $\alpha(I)$ using adult data [17]. The interpretation of this relationship between $\alpha(I)$ and I is that $\alpha(I) = I^{0.5}$. Thus we determined a range of values for p so that I has a smaller effect on α ($p = .25$) and I has a larger effect on α ($p = .75$).

$\underline{G}$: In the derivation of the family of models by Kronauer and colleagues, G was determined based on the α_0 and β values that were fit using adult data [17]. Since we did not want to rely on adult data to determine parameter ranges, the range of G values was determined so that G still has an effect on the drive of the pacemaker $\hat{B}$ ($G > 0$); the prompt response of the model to light is lessened with smaller G values and increased with larger G values.

$\underline{k}$: The parameter k was initially added to the family of models to incorporate Aschoff's rule which states that increasing light intensities shorten the period of the model [16]. We chose the parameter range of k to begin at 0.4 and go to 0.7 so that we incorporate Aschoff's rule but span a range of values to investigate the effects of reducing ($k = 0.4$) and increasing ($k = 0.7$) the effect of bright light on the oscillation period from the standard k value.

$\underline{\mu}$: The stiffness of the oscillator, μ was originally chosen to be $<< 1$ [17]. The experimental range was determined was to be between 0.005 and 0.42 [14, 98, 99].

$\underline{\tau}$: The final parameter that was considered for this analysis is the intrinsic period τ [14, 17]. The range of τ values was selected to reflect the range of known intrinsic period that have been found in subjects [31, 32].

$\underline{I_0}$: The last parameter of the model is I_0, the typical bright light stimulus [17]. This parameter was not varied since 9500 lux is the standard bright light stimulus in the lab and is independent of human physiology.

5.2.2.4 Light Conditions and Quantity of Interest

The Quantity of Interest (QoI) chosen for this model is the average oscillation amplitude and we consider how it changes under various lighting conditions. The first condition considered was complete darkness for 40 days. After 30 days, the average period and average amplitude are assessed. This lighting condition means that the only parameters playing a

Table 5.2: Table of Forger model parameter original parameter values and parameter ranges used for active subspace analysis.

Parameter	Original Value	Parameter Range
α_0	0.05/min	[0.03, 0.13]
p	0.5	[0.25, 0.75]
β	0.0075/min	[0.004, 0.013]
G	33.75 min	[10, 50]
k	0.55	[0.4, 0.7]
μ	0.23	[0.005, 0.42]
τ	24.2 h	[23.5, 25.0]

role are in Process P (μ and τ). This light protocol was used to ensure that the implementation of the algorithm and the ODE solver specifics (tolerances, time step, etc.) were performing as expected. All other simulations were run with a 30 day entrainment period with a consistent light:dark (L:D) schedule of 16 hours of light and 8 hours of darkness from midnight to 0800 at 0 lux and 150 lux at all other times. After the 30 day period, the model then simulated the experimental period where the light intensity is kept constant for 10 days. During this time, the period and amplitude of the oscillations were assessed. The experimental lux values were 10, 500, and 9500 lux. This range of values was selected to test a variety of different lighting conditions that represent dim light (10 lux), daily light exposure (500 lux), and brighter light intensities (9500 lux). The average amplitude was calculated as the mean of $\sqrt{X^2 + X_c^2}$ [16].

5.2.2.5 Implementation

Model equations were implemented and solved numerically in MATLAB (Mathworks, Natick, MA). The built-in MATLAB solver **ode45** with the small tolerances. The relative tolerance was set to $1e^{-10}$ and an absolute tolerance set to $1e^{-11}$. Additionally, all simulations have the same timestep (1/3600 h=1 s) to ensure that the adaptive ode solver did not compare metrics with different timesteps and therefore introduce computational error. Finite differences were used to compute gradients. To reduce computation time, the built-in

MATLAB Parallel Computing Toolbox function **parfor** was used to calculate gradients with respect to each parameter.

5.2.3 Preliminary Results and Discussion

5.2.3.1 Complete Darkness Conditions

The model was simulated for 40 days at 0 lux. During the last ten days, average amplitude was calculated. Because the light intensity during the entire protocol was set to zero, the effects of α_0, p, β, k, and G in Process L were anticipated to have no influence on average period and average amplitude. Active subspace analysis revealed that average amplitude was affected by only the oscillator stiffness μ (Figure 5.5).

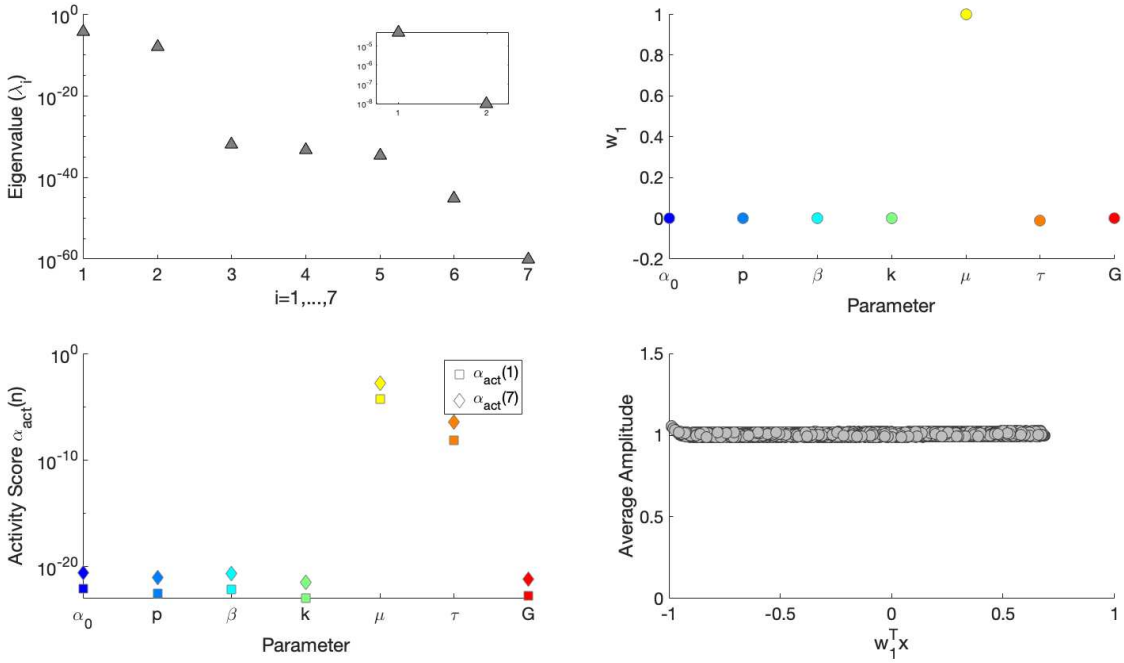

Figure 5.5: Analysis for average amplitude under 0 lux conditions using active subspace analysis. (Top Left) Eigenvalues of $\hat{C}$ with M=2000. Eigenvalues indicate a 1-dimensional active subspace. (Top Right) Components of the first eigenvector $\mathbf{w}_1$. The parameter corresponding to the greatest change in average amplitude is μ. (Bottom Left) The activity scores with $n = 1$ ($\alpha_{act}(1)$) and $n = 7$ ($\alpha_{act}(7)$). The activity score with n=7 is a global sensitivity metric. (Bottom Right) The first eigenvalue multiplied by the samples and the average amplitude.

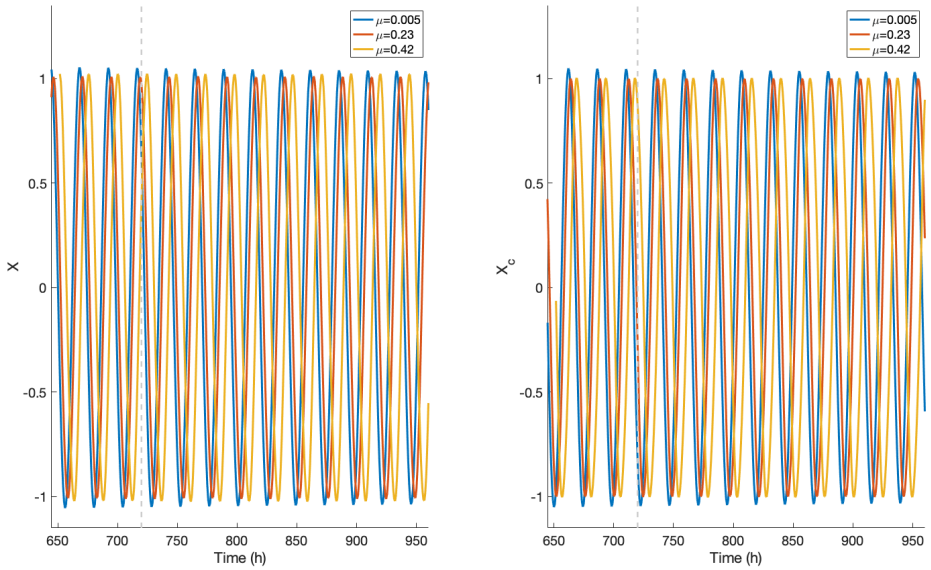

Figure 5.6: The minimum (blue), baseline (red), and maximum (yellow) μ values considered for this analysis under constant darkness conditions. The vertical gray dashed line indicates 720 hours.

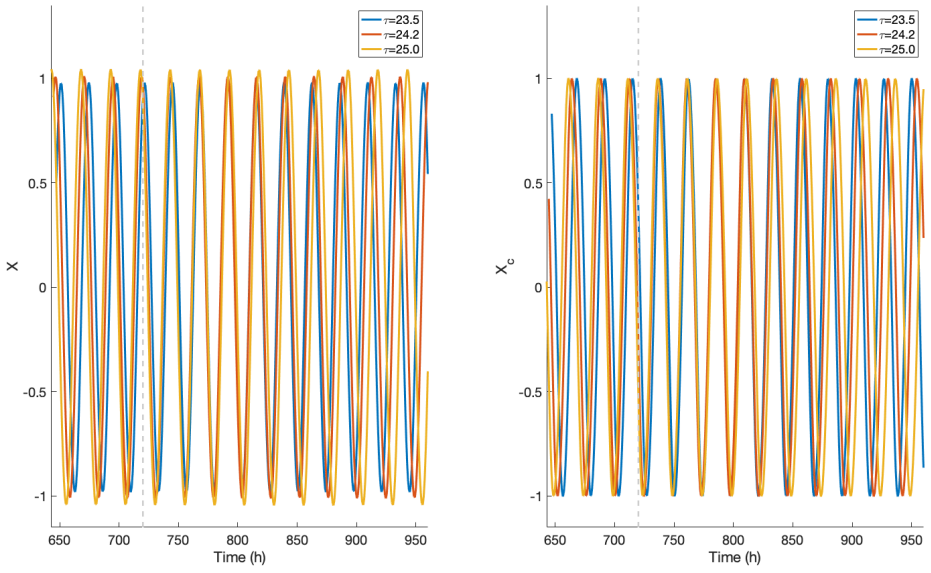

Figure 5.7: The minimum (blue), baseline (red), and maximum (yellow) τ values considered for this analysis under constant darkness conditions. The vertical gray dashed line indicates 720 hours.

When the model is run with the light intensity I set to zero for all time, the equations $\alpha(t)$, $\hat{B}$, and B equal zero. The differential equation $\frac{dn}{dt}$ is equal to $60 * (\beta n)$ which decays to an equilibrium value. Since $B = 0$, in equation $\frac{dX_c}{dt}$ the value of k will have no effect on the system since it is multiplied by B. Thus we expected α_0, p, β, G, and k to have no effect ($\lambda = 0$) on our QoIs. As anticipated, active subspace analysis of the model produced only μ and τ as parameters that the QoIs were sensitive to. If the minimum, baseline, and maximum values of μ are considered, there are distinct changes in the amplitude of X (Figure 5.6 and Figure 5.7). Similarly, the minimum, baseline, and maximum values of τ produce little variation in the amplitude of X_c. Therefore, the conclusion that μ is the parameter that the QoI was most sensitive is in line with expectations.

5.2.3.2 10 and 500 lux Conditions

Average amplitude was assessed for 10 days after a 30 day entrainment period. Under constant dim light conditions (10 lux), the parameter that the QoI is most sensitive to is μ Figure 5.8. However, for this light protocol we see additional parameters associated with larger activity scores and less of a difference in global sensitivity of the QoI compared to the constant darkness protocol. As the constant light is increased to 500 lux, there is a less defined gap between eigenvalues Figure 5.9. When examining the activity scores the parameters α_0, p, β, and τ are all of the same order while μ and G are larger. The parameter k is the parameter that average amplitude is least sensitive to.

When comparing the constant 10 lux to the constant 500 lux light exposure, the global parameter sensitivity of average amplitude changes but for both light schedules. However, μ, the oscillator stiffness, is the parameter that average amplitude was the most sensitive to for both protocols.

5.2.4 Future Directions for the Active Subspace Analysis

These results have shown promise in determining global parameter sensitivity related to average oscillation amplitude of the Forger model. Additionally, this work provides a

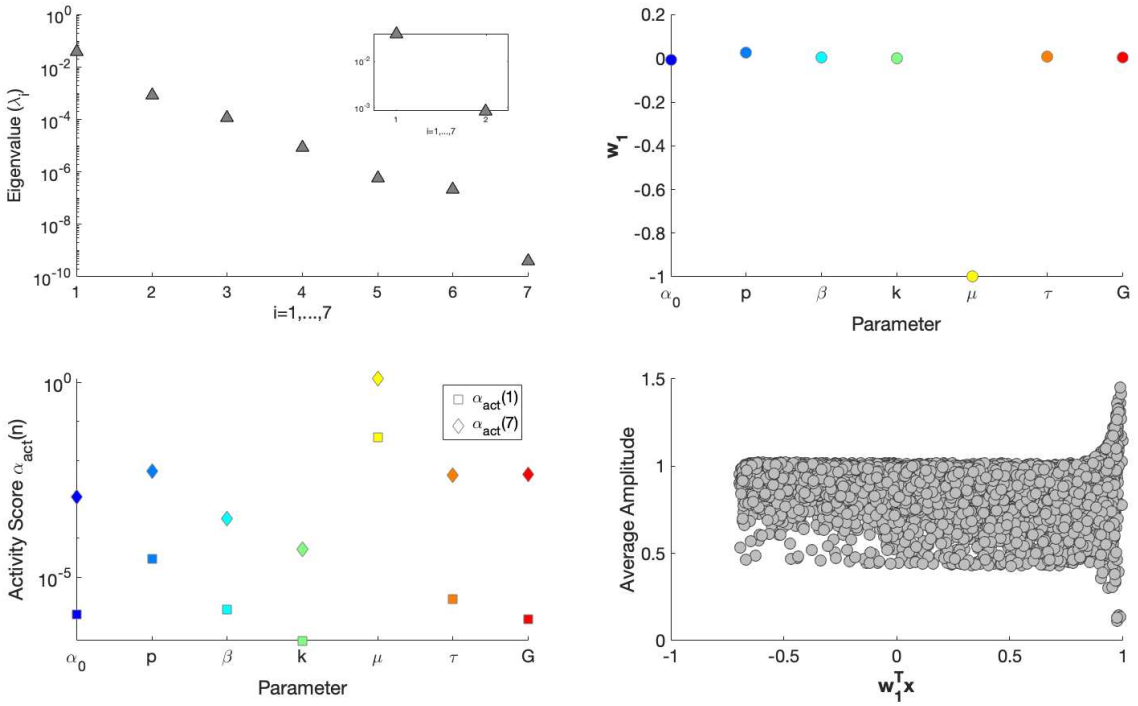

Figure 5.8: Analysis for average amplitude under 10 lux conditions using active subspace analysis. (Top Left) Eigenvalues of $\hat{C}$ with M=2000. (Top Right) Components of the first eigenvector $\mathbf{w}_1$. (Bottom Left) The activity scores with $n = 1$ ($\alpha_{act}(1)$) and $n = 7$ ($\alpha_{act}(7)$). (Bottom Right) The first eigenvalue multiplied by the samples and the average amplitude.

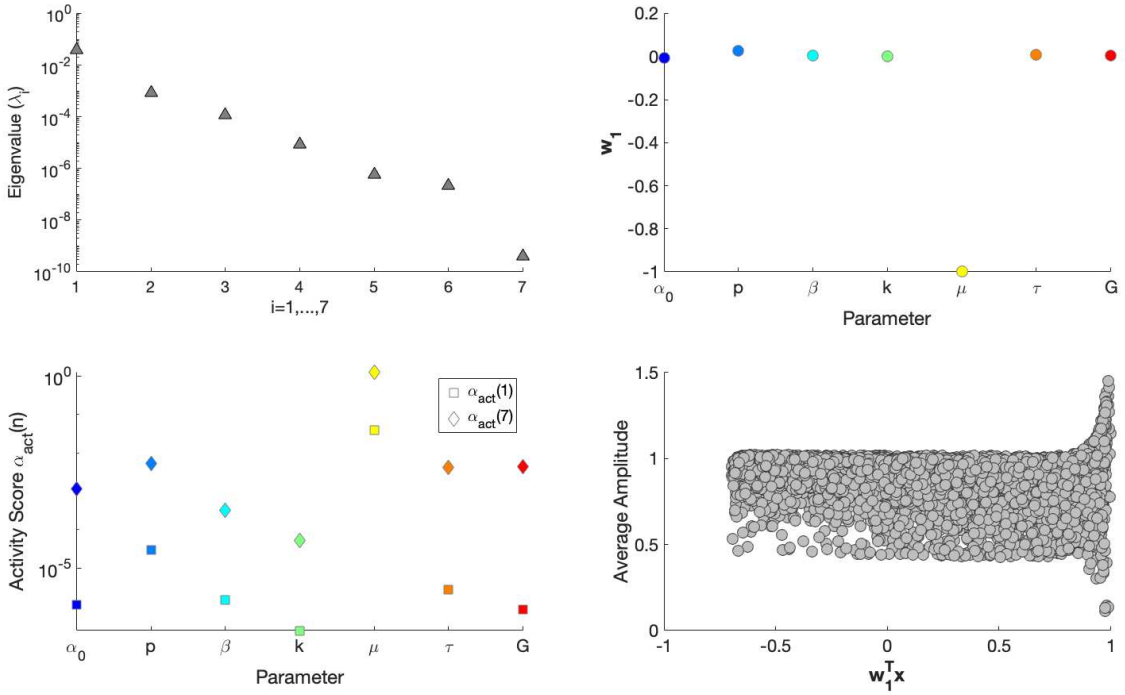

Figure 5.9: Analysis for average amplitude under 500 lux conditions using active subspace analysis. (Top Left) Eigenvalues of $\hat{C}$ with M=2000. (Top Right) Components of the first eigenvector $\mathbf{w}_1$. (Bottom Left) The activity scores with $n = 1$ ($\alpha_{act}(1)$) and $n = 7$ ($\alpha_{act}(7)$). (Bottom Right) The first eigenvalue multiplied by the samples and the average amplitude.

framework for future active subspace analyses with circadian pacemaker models.

In the future, we would like to do a similar analysis with different QoIs to determine how features of the oscillator are differentially affected by parameters. Specifically, we would like to examine average oscillation period and Phase Response Curve (PRC) metrics such as maximum phase shift, minimum phase shift, and amplitude to understand which parameters period and PRCs are most sensitive to. Further, we hope that our results can help to inform researchers about what parameters may be influencing behavior that they have seen in the lab. Therefore, our future work will provide insight into what parameters may need to be changed to model behavior in populations with circadian features are not simulated by a healthy adult circadian pacemaker model, as seen in the adolescent's response to the NAP protocol in Chapter 4. Additionally, this work has the potential for providing mechanistic insights regarding atypical circadian behavior.

5.3 Summary of Work

The common theme of this thesis revolves around the inherent variability in human circadian pacemakers. This work focused on applications of human circadian pacemaker models to optimize experimental protocol design, gain more information from existing circadian data, and determine the sensitivity of multiple circadian metrics to model parameters. Many techniques were used to complete this work including mathematical modeling, Markov chain Monte Carlo (MCMC) methods, and parameter sensitivity analysis. This thesis highlights the utility of mathematical circadian pacemaker models in the field of biological rhythms in order to gain insights into multiple areas of interest.

In Chapter 2 we showed how a mathematical model of the circadian pacemaker was used to optimize ultradian forced desynchrony protocols. We considered light:dark cycle duration, light intensity, phase onset, and study duration in our analysis. Additionally, we considered a range of intrinsic periods to optimize the protocol implementation for all known intrinsic periods. These recommendations can be used to optimize future ultradian forced desynchrony protocol implementations and provide estimates of potential error in existing

studies.

The next chapter demonstrated how mathematical models and existing data can be used to learn more information about average group intrinsic period. We applied a MCMC algorithm to illuminance-response curve data to estimate the average group intrinsic period of a study's participants. First, this methodology was applied to synthetic illuminance-response curve data where the intrinsic period or periods were known. Next, we estimated the average group intrinsic period from experimental data. This work established a framework for estimating the average group intrinsic period from illuminance-response curve data.

The fourth chapter was focused on the parameter sensitivity analysis of a circadian pacemaker model and applying those insights to adolescent data. First we determined the parameters to which PRCs were most sensitive. We then clustered adolescent data using k-means clustering. Once the clusters were established, two groups contained at least three subjects. These two clusters had opposite reactions to the NAP protocol. Using the insights from the parameter sensitivity analysis, parameter pairs and triples that simulated each group's behavior were identified. Finally, using the best candidate parameter pairs, we made predictions about each group's response to different light protocols.

Two extensions of these projects were presented. We showed preliminary results for estimating group intrinsic periods using Phase Response Curves as well as active subspace analysis of the Forger model with respect average amplitude under different lighting conditions.

In the future, the methods and ideas of this thesis may help researchers learn new information. In particular, MCMC methods were applied to illuminance-response curve data with the intention of being able to apply them to forthcoming illuminance-response curve data in young children from our collaborator Monique LeBourgeois. With these methods, novel insights into group intrinsic periods of young children may be learned.

REFERENCES CITED

[1] C. B. Saper, T. E. Scammell, and Jun Lu. Hypothalamic regulation of sleep and circadian rhythms. *Nature*, 437:1257–1263, 2005.

[2] Jun Lu, D. Sherman, M. Devor, and C. B. Saper. A putative flipflop switch for control of rem sleep. *Nature*, 441:589–594, 2006.

[3] A.A. Borbély. A two process model of sleep regulation. *Human Neurobiology*, 1(3): 195–204, 2006.

[4] C. A. Czeisler, J. F. Duffy, T. L. Shanahan, E. N. Brown, J. F. Mitchell, D. W. Rimmer, J. M. Ronda, E. J. Silva, J. S. Allan, J. S. Emens, D.J. Dijk, and R. E. Kronauer. Stability, precision, and near-24-hour period of the human circadian pacemaker. *Science*, 284(5423):2177–2181, 1999.

[5] National Sleep Foundation. Sleep drive and your body clock. `https://sleepfoundation.org/sleep-topics/sleep-drive-and-your-body-clock` [Accessed: 18 October 2016], 2016.

[6] National Institutes of Health: National Institute of General Medical Sciences. Circadian rhythms. `https://www.nigms.nih.gov/education/pages/factsheet_circadianrhythms.aspx` [Accessed: 28 March 2019], 2017.

[7] O. M. Buxton, C. W. Lee, M. L'Hermite-Balriaux, F. W. Turek, and E. Van Cauter. Exercise elicits fhase shifts and acute alterations of melatonin that vary with circadian phase. *American Journal of Physiology - Regulatory, Integrative and Comparative Physiology*, 284(3):R714–R724, 2003.

[8] Howard Hughes Medical Institute. The human suprachiasmatic nucleus. `http://www.hhmi.org/biointeractive/human-suprachiasmatic-nucleus` [Accessed: 17 November 2016], 2016.

[9] M. E. Jewett, D. W. Rimmer, J. F. Duffy, E. B. Klerman, R. E. Kronauer, and C. A. Czeisler. Human circadian pacemaker is sensitive to light throughout subjective day without evidence of transients. *Am J Physiol*, 273(2017):1–13, 1997.

[10] S. Daan, D.G. Beersma, and A.A. Borbely. Timing of human sleep: Recovery gated by a circadian pacemaker. *Am. J. Physiol.*, 246:R161–R178, 1984.

[11] D. Gonze. Modeling circadian clocks: From equations to oscillations. *Central European Journal of Biology*, 6(5):699–71, 2011.

[12] E.R. Breslow , A. J. K. Phillips, J. M.Huang, M. A. St. Hilaire, and E. B. Klerman. A mathematical model of the circadian phase-shifting effects of exogenous melatonin. *Journal of Biological Rhythms*, 28(1):7989, 2013.

[13] A. Goldbeter. A model for circadian oscillations in the drosophila period protein (per). *Proc bio Sci*, 261(1362):319–324, 1995.

[14] D.B Forger, M.E. Jewett, and R.E. Kronauer. A simpler model of the human circadian pacemaker. *Journal of Biological Rhythms*, 14(6):532–537, 1999.

[15] M. E. Jewett, D. B. Forger, and R. E. Kronauer. Revised limit cycle oscillator model of human circadian pacemaker. *Journal of Biological Rhythms*, 14(6):493–499, 1999.

[16] M. E. Jewett and R. E. Kronauer. Refinement of a limit cycle oscillator model of the effects of light on the human circadian pacemaker. *Journal of Theoretical Biology*, 192: 455–465, 1998.

[17] R.E. Kronauer, D.B. Forger , and M.E. Jewett. Quantifying human circadian pacemaker response to brief, extended, and repeated light stimuli over the phototopic range. *Journal of Biological Rhythms*, 14(6):501–515, 1999.

[18] A.A. Borbely. A two process model of sleep regulation. *Hum Neurobiol*, 1:195–204, 1982.

[19] M. D. Belle, C. O. Diekman, D. B. Forger, and H. D. Piggins. Daily electrical silencing in the mammalian circadian clock. *Science*, 326(5950):281–284, 2009.

[20] A. L. Hodgkin and A. F. Huxley. A quantitative description of membrane current and its application to conduction and excitation in nerve. *The Journal of Physiology*, 117: 500–544, 1952.

[21] C. O. Diekman, M. D. C. Belle, R. P. Irwin, C. N. Allen,H. D. Piggins, and D.B. Forger. Causes and consequences of hyperexcitation in central clock neurons. *PLOS Computational Biology*, 9(8):1–11, 2013.

[22] B. C. Goodwin. Oscillatory behavior in enzymatic control processes. *Advances in Enzyme Regulation*, 3:425–428, 1965.

[23] D.B. Forger and C.S. Peskin. A detailed predictive model of the mammalian circadian clock. *Proc Natl Acad Sci U.S.A.*, 100(25):14806–14811, 2003.

[24] K. M. Hannay. *Macroscopic Models and Phase Resetting of Coupled Biological Oscillators*. PhD thesis, University of Michigan, 500 S State St, Ann Arbor, MI 48109, 2017.

[25] R. Kronauer, C. Czeisler, S. F. Pilato, M. Moore-Ede, and E. D. Weitzman. Mathematical model of the human circadian system with two interacting oscillators. *The American Journal of Physiology*, 242(1):R3–17, 1982.

[26] R. E. Kronauer. A quantitative model for the effects of light on the amplitude and phase of the deep circadian pacemaker, based on human data. In J. Horne, editor, *Sleep '90, Proceedings of the Tenth European Congress on Sleep Research*, pages 306–309, Dusseldorf, 1990. Pontenagel Press.

[27] E.B. Klerman, D.J. Dijk, R.E. Kronauer, and C.A. Czeisler. Simulations of light effects on the human circadian pacemaker: implications for assessment of intrinsic period. *American Journal of Physilogy*, 270(1 Pt 2):R271–R282, 1996.

[28] J. Aschoff. Exogenous and endogenous components in circadian rhythms. *Cold Spring Harb Symp Quant Biol*, 25:11–28, 1960.

[29] Casey O Diekman and Amitabha Bose. Reentrainment of the circadian pacemaker during jet lag: East-west asymmetry and the effects of north-south travel. *Journal of theoretical biology*, 437:261–285, 2018.

[30] R. A. Wever. *The Circadian System of Man: Results of Experiments Under Temporal Isolation*. Springer-Verlag New York, New York, 1 edition, 1979. ISBN 978-1-4612-6142-1.

[31] M. R. Smith, H. J. Burgess, L. F. Fogg, and C. I. Eastman. Racial differences in the human endogenous circadian period. *PLOS ONE*, 4(6):1–6, 2009.

[32] J.F. Duffy, S. W. Cain, A.M. Chang, A. J. K. Phillips, M. Y. Mnch, C. Gronfier, J. K. Wyatt, D.J. Dijk, K. P. Wright, Jr., and C. A. Czeisler. Sex difference in the near-24-hour intrinsic period of the human circadian timing system. *Proc Natl Acad Sci U S A.*, 108(Suppl. 3):15602–15608, 2011.

[33] C. I. Eastman, T. A. Molina, M. E. Dziepak, and M. R. Smith. Blacks (african americans) have shorter free-running circadian periods than whites (caucasian americans). *Chronobiology International*, 29(8):1072–1077, 2012.

[34] M. A. Carskadon, S. E. Labyak, C. Acebo, and R. Seifer. Intrinsic circadian period of adolescent humans measured in conditions of forced desynchrony. *Neuroscience Letters*, 260:129–132, 1999.

[35] S. J. Crowley and C. I. Eastman. Free-running circadian period in adolescents and adults. *Journal of Sleep Research*, 27(5), 2018.

[36] G. Micic, N. Lovato, M Gradisar, H. J. Burgess, S. A. Ferguson, and L. Lack. Circadian melatonin and temperature taus in delayed sleep-wake phase disorder and non-24- hour sleep-wake rhythm disorder patients: an ultradian constant routine study. *Journal of Biological Rhythms*, 31(4):387–405, 2016.

[37] H.J. Burgess and C.I. Eastman. Human tau in an ultradian light-dark cycle. *Journal of Biological Rhythms*, 23(4):374–376, 2008.

[38] S. J. Crowley and C. I. Eastman. Human adolescent phase response curves to bright white light. *Journal of Biological Rhythms*, 32(4):334–344, 2017.

[39] M. E. Jewett, R. E., Kronauer,, and C. A. Czeisler. Phase-amplitude resetting of the human circadian pacemaker via bright light: A further analysis. *Journal of Biological Rhythms*, 9(3-4):295–314, 1994.

[40] S. B. S. Khalsa, M. E. Jewett, C. Cajochen, and C. A. Czeisler. A phase response curve to single bright light pulses in human subjects. *The Journal of Physiology*, 549 (3):945–952, 2003.

[41] J. M. Zeitzer, D.-J. Dijk, R. E. Kronauer, E. N. Brown, and C. A. Czeisler. Sensitivity of the human circadian pacemaker to nocturnal light: melatonin phase resetting and suppression. *The Journal of Physiology*, 526(3):695–702, 2000.

[42] J. M. Zeitzer, S. B. S. Khalsa, D. B. Boivin, J. F. Duffy, T. L. Shanahan, R. E., Kronauer,, and C. A. Czeisler. Temporal dynamics of late-night photic stimulation of the human circadian timing system. *American Journal of Physiology-Regulatory, Integrative and Comparative Physiology*, 289(3):R839–R844, 2005.

[43] J.F. Duffy, J. M. Zeitzer, and C. A. Czeisler. Decreased sensitivity to phase-delaying effects of moderate intensity light in older subjects. *Neurobiology of Aging*, 28(5):799–807, 2007.

[44] D. S.Minors, J. M.Waterhouse, A. Wirz-Justice. A human phase-response curve to light. *Neuroscience Letters*, 133(1):36–40, 1991.

[45] S.W. Lockley, G.C. Brainard GC, and C. A. Czeisler. High sensitivity of the human circadian melatonin rhythm to resetting by short wavelength light. *J Clin Endocrinol Metab.*, 88(9):4502–5, 2003.

[46] C. A. Czeisler, R. E. Kronauer, J. S. Allan, J. F. Duffy, M. E. Jewett, E. N. Brown, and J. M. Ronda. Bright light induction of strong (type 0) resetting of the human circadian pacemaker. *Science*, 244(4910):1328–1333, 1989.

[47] M. A. St Hilaire, J. J. Gooley, S. B. S. Khalsa, R. E. Kronauer, C. A. Czeisler, and S. W. Lockley. Human phase response curve to a 1 h pulse of bright white light. *The Journal of Physiology*, 590(13):3035–3045, 2012.

[48] M. Rü ger, M. A. St Hilaire, G. C. Brainard, S. B. S. Khalsa, R. E. Kronauer, C. A. Czeisler, and S. W. Lockley. Human phase response curve to a single 6.5 h pulse of short wavelength light. *The Journal of Physiology*, 591(1):353–363, 2012.

[49] A. J. Lewy, V. K. Bauer, S. Ahmed, K. H. Thomas, N. L. Cutler, C. M. Singer, M. T. Moffit, and R. L. Sack. The human phase response curve (prc) to melatonin is about 12 hours out of phase with the prc to light. *Chronobiol Int*, 15(1):71–83, 1998.

[50] H. J. Burgess, V. L. Revell, and C. I. Eastman. A three pulse phase response curve to three milligrams of melatonin in humans. *The Journal of Physiology*, 586(2):639–647, 2008.

[51] H. J. Burgess, V. L. Revell, T.A. Molina, and C. I. Eastman. Human phase response curves to three days of daily melatonin: 0.5 mg versus 3.0 mg. *J Clin Endocrinol Metab*, 95(7):3325–3331, 2010.

[52] N. Stack, D. Barker, M. Carskadon, and C. Diniz Behn. A model-based approach to optimizing ultradian forced desynchrony protocols for human circadian research. *Journal of Biological Rhythms*, 32(5):485–498, 2017. doi: 10.1177/0748730417730488.

[53] J. F. Duffy and K. P. Wright Jr. Entrainment of the human circadian system by light. *Journal of Biological Rhythms*, 20(4):326–338, 2005.

[54] F.A. Scheer, K. P. Wright Jr., R.E. Kronauer, and C. A. Czeisler. Plasticity of the intrinsic period of the human circadian timing system. *PLoS One*, 2(8):e721, 2007.

[55] J.F. Duffy and C. A. Czeisler. Age-related change in the relationship between circadian period, circadian phase, and diurnal preference in humans. *Neurosci Lett*, 318(3):117–120, 2002.

[56] S. S. Campbell and P. J. Murphy. Delayed sleep phase disorder in temporal isolation. *Sleep*, 30(9):1225–1228, 2007.

[57] S. Sahar and P. Sassone-Corsi. Metabolism and cancer: the circadian clock connection. *Nat Rev Cancer*, 9(12):886–896, 2009.

[58] C. M. Depner, E. R. Stothard, and K. P. Wright Jr. Metabolic consequences of sleep and circadian disorders. *Curr Diab Rep*, 14(7):507, 2014.

[59] B. J. Altman. Cancer clocks out for lunch: disruption of circadian rhythm and metabolic oscillation in cancer. *Front Cell Dev Biol*, 4:64, 2016.

[60] K. K. Truong, M. T. Lam, M. A. Grandner, C. S. Sassoon, and A. Malhotra. Timing matters: circadian rhythm in sepsis, obstructive lung disease, obstructive sleep apnea, and cancer. *Ann Am Thorac Soc*, 13(7):1144–1154, 2016.

[61] U. Albrecht. The circadian clock, metabolism and obesity. *Obes Rev*, 18(Supp 1):25–33, 2017.

[62] C.J. Madrid-Navarro, R. Sanchez-Galvez, A. Martinez-Nicolas, R. Marina, J.A. Garcia, J.A. Madrid, and M.A. Rol. Disruption of circadian rhythms and delirium, sleep impairment and sepsis in critically ill patients. potential therapeutic implications for increased light-dark contrast and melatonin therapy in an icu environment. *Curr Pharm Des*, 21(24):3453–3468, 2015.

[63] H. K. Ritchie, E. R. Stothard, and K. P. Wright. Entrainment of the human circadian clock to the light-dark cycle and its impact on patients in the icu and nursing home settings. *Curr Pharm Des*, 21(24):3438–3442, 2015.

[64] M.A. Carskadon, A.R. Wolfson, C. Acebo, O. Tzischinsky, and R. Seifer. Adoelscent sleep patterns, circadian timing, and sleepiness at a transition to early school days. *SLEEP*, 21(8):871–881, 1998.

[65] J. A. Owens, K. Belon, and P. Moss. Impact of delaying school start time on adolescent sleep, mood, and behavior. *Arch Pediatr Adolesc Med*, 164(7):608–614, 2010.

[66] J. Aschoff. Circadian rhythms in man. *Science*, 148(3676):1427–1432, 1965.

[67] J. K. Wyatt, A. Ritz-De Cecco, C. A. Czeisler, and D. J. Dijk. Circadian temperature and melatonin rhythms, sleep, and neurobehavioral function in humans living on a 20-h day. *Am J Physiol*, 277(4 Pt. 2):R1152–R1163, 1999.

[68] D. B. Boivin, J. F. Duffy, R. E. Kronauer, and C. A. Czeisler. Dose-response relationships for resetting of human circadian clock by light. *Nature*, 379(6565):540–542, 1996.

[69] K. P. Wright Jr., R. J. Hughes, R. E. Kronauer, D. J. Dijk, and C. A. Czeisler. Intrinsic near-24-h pacemaker period determines limits of circadian entrainment to a weak synchronizer in humans. *Ann Am Thorac Soc*, 98(24):14027–14032, 2001.

[70] J. J. Gooley, S. M. Rajaratnam, G. C. Brainard, R. E. Kronauer, C. A. Czeisler, and S. W. Lockley. Spectral responses of the human circadian system depend on the irradiance and duration of exposure to light. *Sci Transl Med*, 2(31):31ra33, 2010.

[71] S. B. Khalsa, D. A. Conroy, J. F. Duffy, C. A. Czeisler, and D. J. Dijk. Sleep- and circadian-dependent modulation of rem density. *J Sleep Res*, 11(1):53–59, 2015.

[72] K. P. Wright Jr., J. T. Hull, and C. A. Czeisler. Relationship between alertness, performance, and body temperature in humans. *Am J Physiol Regul Integr Comp Physiol*, 283(6):R1370–R1377, 2002.

[73] K.M. Koorengevel, D.G. Beersma, J. A. den Boer, and R. H. van den Hoofdakker. A forced desynchrony study of circadian pacemaker characteristics in seasonal affective disorder. *Journal of Biological Rhythms*, 17(5):463–475, 2002.

[74] D. F. Kripke, S. D. Youngstedt, J. A. Elliott, A. Tuunainen, K. M. Rex, R. L. Hauger, and M. R. Marler. Circadian phase in adults of contrasting ages. *Chronobiol Int*, 22(4): 695–709, 2005.

[75] V. L. Revell, T. A. Molina, and C. I. Eastman. Human phase response curve to intermittent blue light using a commercially available device. *J Physiol*, 590(19):4859– 4868, 2012.

[76] C. I. Eastman, C. Suh, V. A. Tomaka, and S. J. Crowley. Circadian rhythm phase shifts and endogenous free- running circadian period differ between african- americans and european-americans. *Sci Rep*, 5:8381, 2015.

[77] P. Achermann P and H. Kunz. Modeling circadian rhythm generation in the suprachiasmatic nucleus with locally coupled self-sustained oscillators: phase shifts and phase response curves. *Journal of Biological Rhythms*, 14(6):460–468, 1999.

[78] J. S. Takahashi, D. K. Welsh and S. A. Kay. Suprachiasmatic nucleus: cell autonomy and network properties. *Annu Rev Physiol*, 72:551–577, 2010.

[79] C. I. Eastman, V. A. Tomaka, and S. J. Crowley. Circadian rhythms of european and african-americans after a large delay of sleep as in jet lag and night work. *Sci Rep*, 6: 36716, 2015.

[80] J. J. Gooley. Treatment of circadian rhythm sleep disorders with light. *Ann Acad Med Singapore*, 37(8):669–676, 2008.

[81] C. P. Landrigan, C. A. Czeisler, L. K. Barger, N. T. Ayas, J. M. Rothschild, S. W. Lockley. Errata: Quantifying human circadian pacemaker response to brief, extended, and repeated light stimuli over the photopic ranges. *The Joint Commission Journal on Quality and Patient Safety*, 33(11):19–29, 2007.

[82] M. A. Carskadon, C. Acebo, and O. G. Jenni. Regulation of adolescent sleep: implications for behavior. *Ann N Y Acad Sci*, 1021:276–291, 2004.

[83] F. Danner and B. Phillips. Adolescent sleep, school start times, and teen motor vehicle crashes. *J Clin Sleep Med*, 4(6):533–535, 2008.

[84] G. P. Dunster, L. de la Iglesia, M. Ben-Hamo, C. Nave, J. G. Fleischer, S. Panda, and H. O. de la Iglesia. Sleepmore in seattle: Later school start times are associated with more sleep and better performance in high school students. *Sci Adv*, 4(12):eaau6200, 2018.

[85] O. M Buxton, S. A. Frank, M. L'Hermite-Baleriaux, R. Leproult, F. W. Turek, and E. Van Cauter. Roles of intensity and duration of nocturnal exercise in causing phase delays of human circadian rhythms. *Am J Physiol*, 273(3 Pt. 1):E536–542, 1997.

[86] Phillips, P. Y. Chen, A. J and P. A. Robinson. Probing the mechanisms of chronotype using quantitative modeling. *Journal of Biological Rhythms*, 25(3):217–227, 2010.

[87] M. Fleshner, V. Booth, D. B. Forger, and C. G. Diniz Behn. Circadian regulation of sleep-wake behaviour in nocturnal rats requires multiple signals from suprachiasmatic nucleus. *Philos Trans A Math Phys Eng Sci*, 369(1952):3855–3883, 2011.

[88] R. Kronauer, D. B. Forger, and M. E. Jewett. Errata: Quantifying human circadian pacemaker response to brief, extended, and repeated light stimuli over the photopic ranges. *Journal of Biological Rhythms*, 15(2):184–186, 2000.

[89] S. Banerjee, B. Carlin, and A. Gelfand. *Hierarchical Modeling and Analysis for Spatial Data*. Chapman and Hall, Washington, D.C., 1 edition, 2003. ISBN 158488410X.

[90] S. Higuchi, Y. Nagafuchi, S. I. Lee, and T. Harada. Influence of light at night on melatonin suppression in children. *J Clin Endocrinol Metab*, 99(9):3298–3303, 2014.

[91] S. J. Crowley, S. W. Cain, A. C. Burns, C. Acebo, and M. A. Carskadon. Increased sensitivity of the circadian system to light in early/mid-puberty. *J Clin Endocrinol Metab*, 100(11):4067–4073, 2015.

[92] S.J. Crowley, C. Acebo, and M.A. Carskadon. Sleep, circadian rhythms, and delayed phase in adolescence. *Sleep Medicine*, 8(6):602–612, 2007.

[93] C. M. Depner, E. L. Melanson, R. H. Eckel, J. K. Snell-Bergeon, L. Perreault, B. C.Bergman, J. A. Higgins, M. K. Guerin, E. R. Stothard, S. J. Morton, and K. P. Wright Jr. Ad libitum weekend recovery sleep fails to prevent metabolic dysregulation during a repeating pattern of insufficient sleep and weekend recovery sleep. *Current Biology*, 29(6):957–967.e4, 2019.

[94] S. Crowley and M. Carskadon. Modifications to weekend recovery sleep delay circadian phase in older adolescents. *Chronobiology International*, 27(7):1469–1492, 2010.

[95] P. G. Constantine. *Active Subspaces: Emerging Ideas for Dimension Reduction in Parameter Studies*. SIAM-Society for Industrial and Applied Mathematics, Philadelphia, 2015. ISBN 9781611973853.

[96] P. G. Constantine and P. Diaz. Global sensitivity metrics from active subspaces. *Reliability Engineering and System Safety*, 162:1–13, 2017.

[97] I. Sobol' and S. Kucherenko. Derivative based global sensitivity measures and their link with global sensitivity indices. *Math Comput Simul*, 79(10):3009–3017, 2009.

[98] E. N. Brown, Y. Choe, and C. A. Czeisler. Statistical analysis of human core-temperature rhythms with differential equation methods. *Bio Rhy Res*, 10:372, 1995.

[99] A. Gundel and M. Spencer. A circadian oscillator model based on empirical data. *Journal of Biological Rhythms*, 14:516–523, 1999.

APPENDIX A

SUPPLEMENTAL TABLES

Table A.1: Table of Forger model parameters and original parameter values.

Parameter	Original Value
α_0	0.05/min
p	0.5
β	0.0075/min
G	33.75 min
k	0.55
μ	0.23
τ	24.2 h

Table A.2: MCMC estimates of τ for simulated single illuminance-response curves generated from τ = 23.7, 24.2, 24.6, and 24.9 h. Average τ values (±standard deviations) from four runs from each initial chain value (τ = 23.9, 24.1, and 24.7 h) and all runs. Each run was 10,000 iterations with a 5% burn-in.

τ value used to generate data	Initial Chain Value: τ= 23.8 h	Initial Chain Value: τ= 24.1 h	Initial Chain Value: τ= 24.7 h	Average of all runs
τ =23.7 h	23.6972 (±0.0408) h	23.6984 (±0.0405) h	23.6981 (±0.0409) h	23.6979 (±0.0407) h
τ =24.2 h	24.1967 (±0.0417) h	24.1970 (±0.0420) h	24.1966 (±0.0433) h	24.1967 (±0.0423) h
τ =24.6 h	24.5996 (±0.0433) h	24.6005 (±0.0433) h	24.5996 (±0.0433) h	24.5999 (±0.0433) h
τ =24.9 h	24.8891 (±0.0382) h	24.8891 (±0.0387) h	24.8897 (±0.0381) h	24.8893 (±0.0383) h

Table A.3: MCMC estimates of τ for simulated single illuminance-response curves generated from τ = 23.7, 24.2, 24.6, and 24.9 h. Average 95% credible intervals of τ from four runs from each initial chain value (τ = 23.9, 24.1, and 24.7 h) and all runs. Each run was 10,000 iterations with a 5% burn-in.

τ value used to generate data	Initial Chain Value: τ= 23.8 h	Initial Chain Value: τ= 24.1 h	Initial Chain Value: τ= 24.7 h	Average of all runs
τ =23.7 h	[23.6163, 23.7771]	[23.6214, 23.7785]	[23.6193, 23.7785]	[23.6190, 23.7780]
τ =24.2 h	[24.1157, 24.2797]	[24.1140, 24.2785]	[24.1110, 24.2815]	[24.1136, 24.2799]
τ =24.6 h	[24.5146, 24.6847]	[24.5156, 24.6851]	[24.5145, 24.6828]	[24.5149, 24.6842]
τ =24.9 h	[24.8090, 24.9542]	[24.8089, 24.9562]	[24.8109, 24.9559]	[24.8096, 24.9554]

Table A.4: MCMC estimates of τ for simulated single illuminance-response curves generated from τ = 23.7, 24.2, 24.6, and 24.9 h. Average percent of accepted samples from four runs from each initial chain value (τ = 23.9, 24.1, and 24.7 h) and all runs. Each run was 10,000 iterations with a 5% burn-in.

τ value used to generate data	Initial Chain Value: τ= 23.8 h	Initial Chain Value: τ= 24.1 h	Initial Chain Value: τ= 24.7 h	Average of all runs
τ =23.7 h	42.9658%	43.3105%	43.3737%	43.2167%
τ =24.2 h	44.4711%	45.0974%	44.6421%	44.7368%
τ =24.6 h	45.8105%	45.3711%	45.0026%	45.3947%
τ =24.9 h	41.1079%	41.3000%	41.1421%	41.1833%

Table A.5: MCMC estimates of τ for simulated multi-τ illuminance-response curves generated from τs drawn from $N(23.7, 0.2^2)$, $N(24.2, 0.2^2)$, $N(24.2, 0.4^2)$, and $N(24.6, 0.2^2)$. Average τ values ($\pm$standard deviations) from four runs from each initial chain value (τ = 23.9, 24.1, and 24.7 h) and all runs. Each run was 10,000 iterations with a 5% burn-in.

τ distribution data was drawn from	Initial Chain Value: τ= 23.8 h	Initial Chain Value: τ= 24.1 h	Initial Chain Value: τ= 24.7 h	Average of all runs
$N(23.7, 0.2^2)$	23.6970 ($\pm$0.0412) h	23.6974 ($\pm$0.0409) h	23.6963 ($\pm$0.0399) h	23.6969 ($\pm$0.0407) h
$N(24.2, 0.2^2)$	24.2122 ($\pm$0.0425) h	24.2127 ($\pm$0.0421) h	24.2114 ($\pm$0.0422) h	24.2121 ($\pm$0.0423) h
$N(24.2, 0.4^2)$	24.2310 ($\pm$0.0426) h	24.2301 ($\pm$0.0421) h	24.2298 ($\pm$0.0421) h	24.2303 ($\pm$0.0423) h
$N(24.6, 0.2^2)$	24.6140 ($\pm$0.0433) h	24.6141 ($\pm$0.0435) h	24.6138 ($\pm$0.0438) h	24.6140 ($\pm$0.0435) h

Table A.6: MCMC estimates of τ for simulated multi-τ illuminance-response curves generated from τs drawn from $N(23.7, 0.2^2)$, $N(24.2, 0.2^2)$, $N(24.2, 0.4^2)$, and $N(24.6, 0.2^2)$. Average 95% credible intervals of τ from four runs from each initial chain value (τ = 23.9, 24.1, and 24.7 h) and all runs. Each run was 10,000 iterations with a 5% burn-in.

τ distribution data was drawn from	Initial Chain Value: τ= 23.8 h	Initial Chain Value: τ= 24.1 h	Initial Chain Value: τ= 24.7 h	Average of all runs
$N(23.7, 0.2^2)$	[23.6171, 23.7779]	[23.6164, 23.7781]	[23.6190, 23.7757]	[23.6175, 23.7772]
$N(24.2, 0.2^2)$	[24.1286, 24.2947]	[24.1314, 24.2966]	[24.1267, 24.2930]	[24.1289, 24.2948]
$N(24.2, 0.4^2)$	[24.1486, 24.3157]	[24.1486, 24.3137]	[24.1475, 24.3137]	[24.1482, 24.3144]
$N(24.6, 0.2^2)$	[24.5286, 24.6986]	[24.5297, 24.6995]	[24.5277, 24.6990]	[24.5286, 24.6990]

Table A.7: MCMC estimates of τ for simulated multi-τ illuminance-response curves generated from τs drawn from $N(23.7, 0.2^2)$, $N(24.2, 0.2^2)$, $N(24.2, 0.4^2)$, and $N(24.6, 0.2^2)$. Average percent of accepted samples from four runs from each initial chain value (τ = 23.9, 24.1, and 24.7 h) and all runs. Each run was 10,000 iterations with a 5% burn-in.

τ distribution data was drawn from	Initial Chain Value: τ= 23.8 h	Initial Chain Value: τ= 24.1 h	Initial Chain Value: τ= 24.7 h	Average of all runs
$N(23.7, 0.2^2)$	43.0158%	42.7789%	42.5711%	42.7886%
$N(24.2, 0.2^2)$	44.1947%	44.1237%	44.0316%	44.1167%
$N(24.2, 0.4^2)$	43.5921%	42.7895%	43.1474%	43.1763%
$N(24.6, 0.2^2)$	45.2263%	45.4526%	44.9789%	45.2193%

Table A.8: MCMC estimates of τ for experimental illuminance-response curve data with a uniform ($U(23.5, 25.0)$) and a normal ($N(24.2, 0.2^2)$) prior. Average τ values ($\pm$standard deviations) from four runs from each initial chain value (τ = 23.9, 24.1, and 24.7 h) and all runs. Each run was 10,000 iterations with a 5% burn-in.

Prior distribution	Initial Chain Value: τ= 23.8 h	Initial Chain Value: τ= 24.1 h	Initial Chain Value: τ= 24.7 h	Average of all runs
$U(23.5, 25.0)$	24.2668 ($\pm$0.0427) h	24.2673 ($\pm$0.0420) h	24.2680 ($\pm$0.0430) h	24.2674 ($\pm$0.0425) h
$N(24.2, 0.2^2)$	24.2636 ($\pm$0.0410) h	24.2648 ($\pm$0.0418) h	24.2643 ($\pm$0.0413) h	24.2642 ($\pm$0.0414) h

Table A.9: MCMC estimates of τ for experimental illuminance-response curve data with a uniform ($U(23.5, 25.0)$) and a normal ($N(24.2, 0.2^2)$) prior. Average 95% credible intervals of τ from four runs from each initial chain value (τ = 23.9, 24.1, and 24.7 h) and all runs. Each run was 10,000 iterations with a 5% burn-in.

Prior distribution	Initial Chain Value: τ= 23.8 h	Initial Chain Value: τ= 24.1 h	Initial Chain Value: τ= 24.7 h	Average of all runs
$U(23.5, 25.0)$	[24.1823, 24.3506]	[24.1832, 24.3490]	[24.1845, 24.3521]	[24.1833, 24.3506]
$N(24.2, 0.2^2)$	[24.1833, 24.3447]	[24.1845, 24.3469]	[24.1828, 24.3458]	[24.1835, 24.3458]

Table A.10: MCMC estimates of τ for experimental illuminance-response curve data with a uniform ($U(23.5, 25.0)$) and a normal ($N(24.2, 0.2^2)$) prior. Average percent of accepted samples from four runs from each initial chain value (τ = 23.9, 24.1, and 24.7 h) and all runs. Each run was 10,000 iterations with a 5% burn-in.

Prior distribution	Initial Chain Value: τ= 23.8 h	Initial Chain Value: τ= 24.1 h	Initial Chain Value: τ= 24.7 h	Average of all runs
$U(23.5, 25.0)$	43.7684%	43.7158%	44.1053%	43.8632%
$N(24.2, 0.2^2)$	42.9368%	43.4895%	43.1079%	43.1781%

APPENDIX B

SUPPLEMENTAL FIGURES

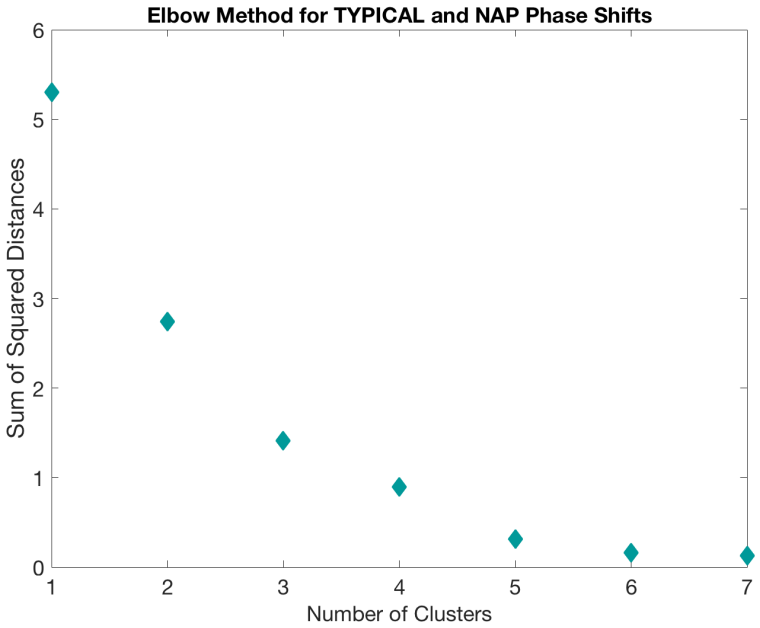

Figure B.1: Elbow analysis for k-means clustering. The number of clusters is plotted with the sum of squared distances. Four clusters were chosen for this analysis.

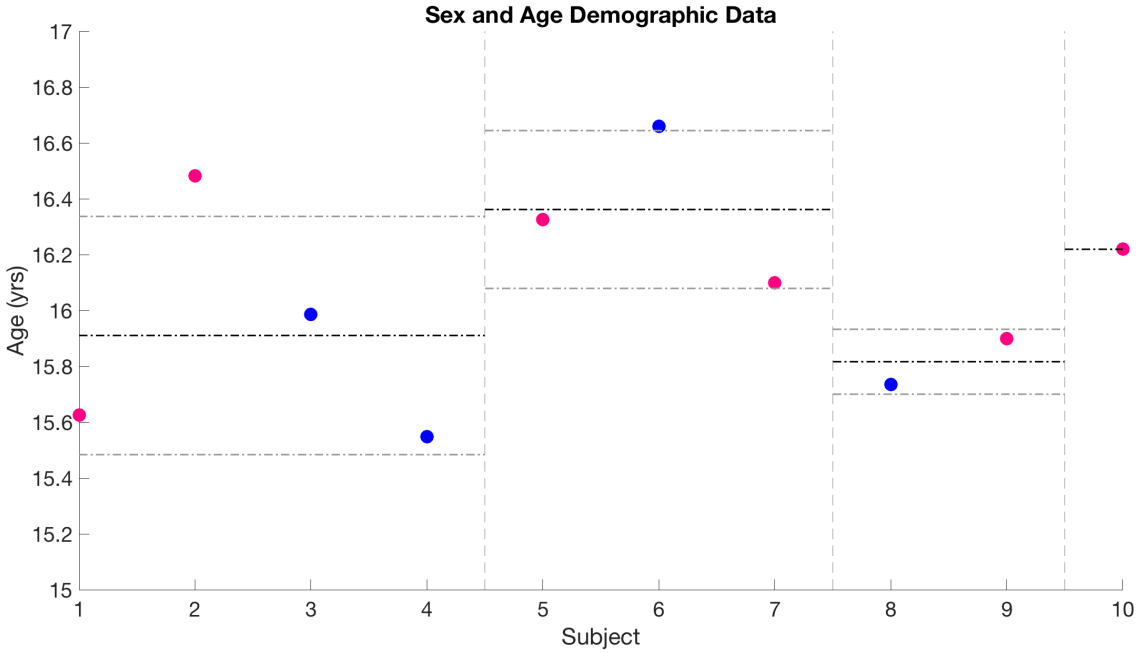

Figure B.2: Sex and age demographic data of the Crowley and Carskadon study participants [94]. Pink circles represent female subjects and blue circles represent male subjects. The vertical dashed gray lines indicate the separation between different clusters. Black dashed dot lines indicate mean age within the cluster and gray dashed dot lines indicate ± the standard deviation. Group N (subjects 1-4) had a mean age of 15.9103 (±0.4265) years and Group T (subjects 5-7) had a mean age of 16.3616 (±0.2825) years.

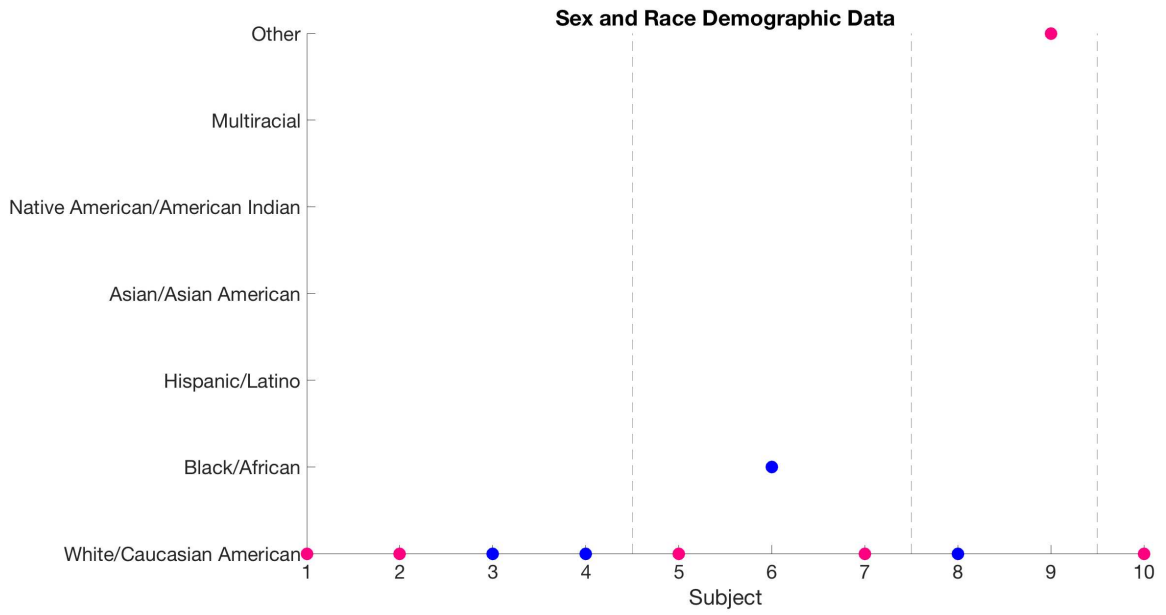

Figure B.3: Sex and race demographic data of the Crowley and Carskadon study participants [94]. Pink circles represent female subjects and blue circles represent male subjects. The vertical dashed gray lines indicate the separation between different clusters. Group N (subjects 1-4) are all white/caucasian. In Group T, subjects 5 and 7 are white/caucasian and subject 6 is black/African.

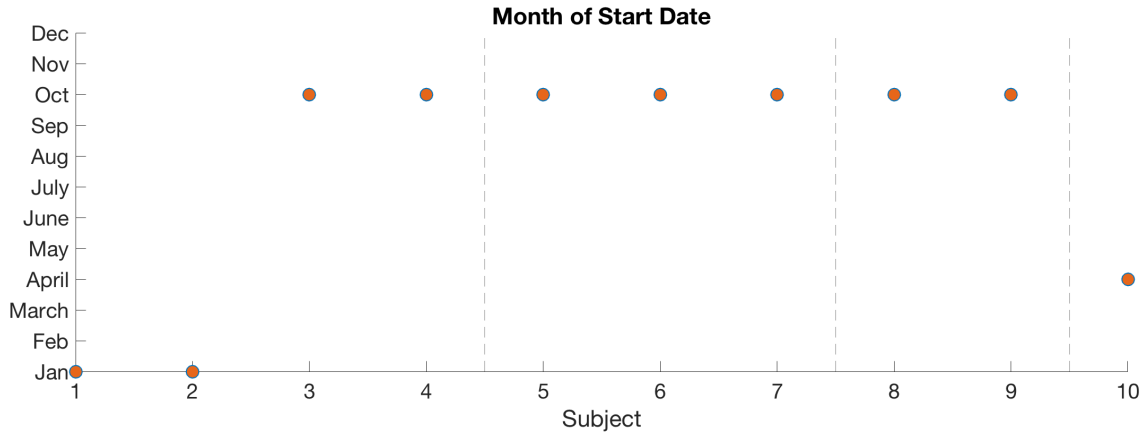

Figure B.4: The month of the start date of the study for each of the Crowley and Carskadon study participants [94]. The vertical dashed gray lines indicate the separation between different clusters. In Group T (subjects 5-7), all subjects began the study in October. Two participants in Group N (subjects 1-2) began in January while the other two subjects began the study in October (subjects 3-4).